NASA-CR-168,026

NASA CR - 168026

NASA-CR-168026
19830010731

A PHENOMENOLOGICAL MODEL FOR ORIFIED HOLLOW CATHODES

PREPARED FOR

LEWIS RESEARCH CENTER

NATIONAL AERONAUTICS AND SPACE ADMINISTRATION

GRANT NGR-06-002-112

by

Daniel E. Siegfried

LIBRARY COPY

FEB 15 1983

LANGLEY RESEARCH CENTER
LIBRARY, NASA
HAMPTON, VIRGINIA

Approved by

Paul J. Wilbur

December 1982

Department of Mechanical Engineering
Colorado State University
Fort Collins, Colorado

NF01876

1 Report No	2 Government Accession No	3 Recipient's Catalog No
NASA CR 168026		

4 Title and Subtitle	5 Report Date
A PHENOMENOLOGICAL MODEL FOR ORIFICED HOLLOW CATHODES	Dec. 1982
	6 Performing Organization Code
7 Author(s) Daniel E. Siegfried and Paul J. Wilbur	8 Performing Organization Report No
	10 Work Unit No
9 Performing Organization Name and Address Department of Mechanical Engineering Colorado State University Fort Collins, Colorado 80523	11 Contract or Grant No NGR-06-002-112
	13 Type of Report and Period Covered Dec. 1, 1981 - Dec. 1, 1982
12 Sponsoring Agency Name and Address National Aeronautics and Space Administration Washington, D.C. 20546	14 Sponsoring Agency Code

15 Supplementary Notes Grant Monitor - William Kerslake, NASA Lewis Research Center, Cleveland, Ohio 44135. This report is a reproduction of the Ph. D. Dissertation of Daniel E. Siegfried. It is submitted to the sponsor and to the distribution list in this form both as a presentation of the technical material, and as an indication of the academic program supported by the grant.

16 Abstract

An experimental investigation is described which used a special quartz tube hollow cathode to provide detailed information about the operating conditions within a mercury orificed hollow cathode. A summary of the results of this investigation including insert temperature profiles, cathode current distributions, plasma property profiles, and internal pressure-mass flow rate data are presented. A phenomenological model is developed based on these results. This model is shown to provide a useful qualitative description of the electron emission and plasma production processes taking place within the cathode. By defining an idealized ion production region within which most of the plasma processes are concentrated, this phenomenological model is expressed analytically as a simple set of equations which relate cathode dimensions and specifiable operating conditions, such as mass flow rate and discharge current, to such important parameters as emission surface temperature and internal plasma properties. The following summary indicates the key aspects of the analytical model.

- The model accounts for electrons produced in the ion production region both by surface emission and by volume ionization.
- Field-enhanced thermionic emission is determined to be the dominant surface emission process producing ~70% of the total discharge current.
- Insert surface and plasma volume energy balances are used to predict plasma density and plasma potential in the ion production region.
- The energy exchange mean free path for primary electrons is used as a criterion for determining the length (L_e) of this region.
- An ion production region aspect ratio (D/L_e) of two is suggested as a design criterion for minimizing keeper voltage.
- An empirical relation is used to estimate cathode internal pressure (a necessary input to the model) from the discharge current and cathode orifice diameter.

The agreement between predictions of the model and the experimental results indicates that our understanding of the important physical processes for these devices is correct.

17 Key Words (Suggested by Author(s))	18 Distribution Statement
Electrostatic Thruster Hollow Cathode	Unclassified - Unlimited

19 Security Classif (of this report)	20 Security Classif (of this page)	21 No of Pages	22 Price*
Unclassified	Unclassified	164	

* For sale by the National Technical Information Service, Springfield Virginia 22161

NASA-C-168 (Rev 10-75)

N83-19002#

TABLE OF CONTENTS

Chapter	Page
I. INTRODUCTION	1
Background	2
Ion Thruster Applications	4
Hollow Cathode Research	6
Overview	12
II. PRELIMINARY EXPERIMENTS	14
Apparatus and Procedure	14
Cathode	14
Insert Construction	19
Segmented Insert	21
Pressure Measurements	21
Throttle Valve	22
Temperature Measurements	23
Plasma Property Measurements	23
Results	24
Typical Hollow Cathode Conditions	34
III. MODEL OF INTERNAL PLASMA PROCESSES	37
Phenomenological Model	37
Neutral Gas Density	41
The Internal Plasma	44
Collisional Processes	45
Excited State Densities and the Primary Electron Mean Free Path	52
Energy Balances	62
IV. SURFACE EMISSION PROCESSES	75
Simple Thermionic Emission	75
Field-Enhanced Thermionic Emission	76
Field Emission	81
Photoelectric Emission	82
Secondary Emission	85
Surface Work Function and the Emission Mechanism	91
V. SUMMARY OF MODEL	101

TABLE OF CONTENTS (continued)

Chapter | Page

VI. COMPARISON WITH EXPERIMENT..... 106

Current Accounting..... 106
Ion Currents..... 110
Ion Production Region..... 114
Predictions of the Model..... 116
The Orifice Region..... 126

VII. CONCLUSIONS..... 133
Future Work..... 135

REFERENCES..... 138

APPENDIX A. Probe Analysis..... 141

APPENDIX B. Determination of Primary Electron Inelastic Mean Free Path and Density..... 149

APPENDIX C. Thermal Losses from Emission Surface..... 152

APPENDIX D. Determination of the Work Function of an Emitting Patch..... 155

LIST OF TABLES

Table		Page
I.	Typical Cathode Conditions	35
II.	Energy Exchange Mean Free Paths and Collision Frequencies	46
III.	Excited State Densities for Operating Conditions Given in Table I	61
IV.	Summary of Equations Used in Model	102
V.	List of Symbols and Units	104
VI.	Cathode Current Accounting	109
VII.	Calculated Ion and Electron Currents to Insert	109

LIST OF FIGURES

Figure		Page
1.	Hollow Cathode Test Configuration	15
2a.	View of Downstream Side of Orifice Plate/Valve Assembly	17
2b.	Detail of Segmented Insert	17
2c.	Detail of Spherical Probe	17
3a.	Effect of Discharge Current on Hollow Cathode Current Distribution	26
3b.	Effect of Internal Pressure on Hollow Cathode Current Distribution	26
4a.	Effect of Orifice Area on Insert Temperature Profile	27
4b.	Effect of Total Discharge Current on Maximum Insert Temperature	27
4c.	Effect of Internal Pressure on Maximum Insert Temperature	27
5a.	Plasma Density Profile	30
5b.	Plasma Potential Profile	30
5c.	Electron Temperature Profile	30
6.	Internal Pressure - Flow Rate Correlation	33
7.	Schematic of Ion Production Region	38
8.	Ion Production Region Reaction Schematic	54
9.	Effect of Total Neutral Atom Density on Primary Electron, Inelastic Mean Free Path	56
10.	Apparatus for In-Situ Measurement of Patch Work Function	94
11.	Comparison of Surface Work Function With and Without Discharge Present	96

LIST OF FIGURES (continued)

Figure Page

12. Test Cathode for Current Accounting..... 108

13. Typical Voltage-Current Characteristic for a Cathode Surface.. 112

14a. Effect of Total Discharge Current on Plasma Densities..... 115

14b. Effect of Internal Pressure on Plasma Densities..... 115

15. Comparison of Emission Length with Primary Electron, Energy Exchange Mean Free Path..... 117

16a. Effect of Discharge Current on Calculated and Measured Emission Surface Temperatures..... 120

16b. Effect of Internal Pressure on Calculated and Measured Emission Surface Temperatures..... 120

17a. Effect of Discharge Current on Calculated and Measured Plasma Densities..... 121

17b. Effect of Internal Pressure on Calculated and Measured Plasma Densities..... 121

18a. Effect of Discharge Current on Calculated and Measured Plasma Potentials..... 122

18b. Effect of Internal Pressure on Calculated and Measured Plasma Potentials..... 122

A.1 Typical Langmuir Probe, Current-Voltage Characteristic..... 142

C.1 Thermal Power Loss for Tantalum Foil Insert Segment..... 153

D.1 Patch Current-Voltage Characteristic..... 156

I. INTRODUCTION

Operating in an arc discharge mode, hollow cathodes are capable of providing large electron currents (> 1A), efficiently (< 50V potential drop), for very long time periods (1000's of hours). These operating characteristics give hollow cathodes significant advantages over other types of electron sources and have led to their use in a wide variety of plasma discharge devices. In addition, the cathode is itself a plasma discharge device forming a dense, highly ionized internal plasma during operation. Because of its advantages as an electron source and its unique properties as a plasma source, the hollow cathode has been the subject of a considerable amount of research since its first appearance more than fifty years ago. Though this research has improved our understanding of cathode physical processes and has led to a number of analytical models, there have remained areas of disagreement regarding key aspects of cathode operation and none of the models has proven to be wholly satisfactory as a predictive, self consistent description of hollow cathode operation.

The present study deals specifically with cylindrical, orificed hollow cathodes of the type used in mercury ion thrusters. The study has two basic objectives. The first is to provide a better understanding of the physical phenomena underlying orificed hollow cathode operation. This aspect of the study is based on an experimental investigation which included detailed measurements of plasma properties, surface temperature, and current density profiles within the cathode.

These measurements were undertaken to identity the location and mechanism for various electron production processes within the cathode and to determine the effect of cathode operating parameters on these processes. The second objective is to develop an analytical model which describes these processes and which can be used to predict important cathode operating parameters such as emission surface temperature and discharge voltage.

Though these studies are concerned with orificed hollow cathodes, much of the research involving the more common open-channel, (non-orificed) hollow cathode has proven applicable to the orificed cathodes. In turn, many of the physical processes and much of the analysis of the present study should also be applicable to other hollow cathode configurations, including the open-channel cathode. Before presenting the results of the present study, it will be useful to provide, by way of background, a brief general discussion of hollow cathodes, the impetus for this study, and its relation to previous research on hollow cathodes.

Background

The operation of hollow cathodes falls into two distinct regimes: hollow cathode glow discharges (low currents, $I < 1A$ with high cathode potential drops, $V_c > 100V$) and hollow cathode arcs (high currents, $I > 1A$ with low poential drops, $V_c < 100V$). The various emission and excitation processes underlying operation in these two regimes are considerably different and require different experimental and theoretical methods. Consequently, research on hollow cathodes is generally divided into investigations dealing with either the arc or the

glow discharge regime. The orificed hollow cathodes used in ion thrusters operate in the arc regime. The present study and the research which will be reviewed in this section deal with cathodes operating in this arc regime.

The obvious defining characteristic of the hollow cathode is that the electrode, usually a refractory metal, forms a hollow cavity with walls at cathode potential and an opening which faces the anode side of the discharge. During operation a plasma discharge is established which extends into this cavity. The interaction of this internal plasma with the cathode cavity surface is an essential feature of the operation of the device. Free electrons are produced within the cavity both by surface processes, such as thermionic and various secondary emission processes, as well as by volume ionization of the working gas. The ions, photons, and metastable species produced in the volume processes return to the walls of the cavity providing the heating necessary to control the emission process and make the discharge self-sustaining. It is the combination of electrode geometry and the efficient confinement of the internal plasma discharge which is responsible for the unique characteristics of the hollow cathode arc discharge. These characteristics - high current capacity, relatively low power requirement, long lifetime, and a very dense internal plasma - have made hollow cathodes attractive for a variety of applications. Besides their application as an electron source in ion thrusters, cathodes have also been used as plasma sources for research work and as spectral light sources. They have received application in devices such as gas lasers, neutral beam injectors for fusion research, plasma jets, and thermionic converters. Since the motivation for the present work is based on their

application to ion thrusters, the present discussion will focus on that application. Readers interested in other applications are referred to papers by Krishnan [1] and by Delcroix and Trindade [2], which include discussions of the history and various other applications of hollow cathodes.

Ion Thruster Applications

Ion thrusters, because they are capable of a high specific impulse, have significant advantages over chemical rockets for missions requiring large characteristic velocities. However, because the ion thruster is an inherently low thrust density device, a typical mission of interest for this type of propulsion system requires reliable operation of the thruster for time periods on the order of 10,000 hours. Moreover, the overall performance of the propulsion system is very sensitive to thruster electrical efficiency because of its effect on powerplant mass. These requirements mean that thruster components such as the cathode, need to be efficient, reliable, and durable.

Electron bombardment ion sources require cathodes both to supply electrons to the main discharge chamber and to neutralize the ion beam. Orificed, hollow cathodes were developed from the more common open-channel cathode specifically to meet the needs of this application. Open-channel cathodes, in order to operate in a normal arc regime, require an unsuitably large gas flow rate for thruster applications, so an orifice plate was added to restrict the gas flow. In addition, an insert containing a low work function chemical mix was incorporated into the cathode design to aid in starting and to improve performance. Because of the lack of understanding of the physical processes taking

place within the cathode, the development of these orificed cathodes was more or less a cut and try affair. Even simple changes in cathode design or operating requirements require extensive experimental re-evaluation followed by lifetime testing. Such programs are both expensive and time consuming. For this reason, it is desireable to understand hollow cathode physics and to have a model which can predict cathode performance given cathode dimensions and operating conditions (discharge current and propellant flow rate).

For thruster applications, cathode lifetimes and cathode power and propellant requirements are important considerations. The cathode lifetime is most sensitive to the operating temperature of the low work function insert because the insert temperature determines the depletion rate of the low work function impregnant. The power required to operate the cathode is proportional to the plasma potential just downstream of the cathode orifice. (This is approximately the same as the voltage required to operate the small sustainer anode known as a keeper). This voltage is important for two reasons. First, it is a measure of the electrical efficiency of the cathode, and therefore, affects overall thruster efficiency. Second, it affects the plasma potential in the thruster discharge chamber which determines the ion energies, and thereby, affects the ion sputter rate of critical components in the discharge chamber. Finally, the propellant flow rate, particularly that through the neutralizer cathode, affects the overall propellant utilization of the thruster system and also affects the insert temperature and cathode plasma potential. A useful model, therefore, would be one which could predict, for a given cathode, the insert operating temperature and plasma potential downstream of the cathode

orifice for a prescribed cathode current and propellant flow rate. The development of such a model is one of the objectives of the present study.

Hollow Cathode Research

The long term goal of hollow cathode research has been a thorough understanding of the physical phenomena involved in hollow cathode operation and, ultimately, the development of an analytical model to predict cathode performance. This has proven exceedingly difficult for two important reasons. First, plasma diagnostics and other measurements within the cathode are difficult. This is because the cathodes are relatively small (a few millimeters diameter typically), operate at high temperature (+1000°C), and sustain a very dense, internal discharge. Second, the processes taking place inside the cathode are very complex. It is possible for electrons to be produced by any combination of five surface emission processes: simple thermionic, field-enhanced thermionic (Schottky effect), field, photo electric, and secondary emission (including ions and excited states); as well as by the volume ionization process which sustains the internal discharge. These processes are coupled together in a complex way and they are also coupled with the gasdynamics affecting the flow through the cathode. In spite of the considerable amount of research done on hollow cathodes, the emission and plasma production processes have continued to be the center of vigorous discussion. At this point it will be useful to review briefly that hollow cathode research which is pertinent to the present study. It will be helpful here to discriminate between research which deals specifically with orificed hollow cathodes and that of a more general

nature dealing with hollow cathode arcs, including open-channel cathodes.

Orificed, hollow cathode research has been directed mainly at specific applications. The early work on these devices was for ion thruster applications, while more recently there has been considerable interest in orificed hollow cathodes for use in neutral beam injectors for fusion research. Soon after the orificed hollow cathode's initial development [3,4] in the mid 1960's, it was apparent that performance criteria for thruster applications could be met without fully understanding the physics of the device. Because of this and because of the difficulty in making measurements within the cathode, many of the early studies were parametric in nature, concerned mostly with the development of a reliable device. However, there was also an interest in understanding the physics of the device and the early studies produced numerous theories for operation of the cathode. However, lacking the necessary experimental data, it was difficult to answer even the basic questions of where and how the electrons were produced. For example, various investigators [4,5,6] involved in these early studies were able to provide arguments in support of each of the five emission mechanisms discussed earlier, either singly or in combination with one another. Most of these studies concluded that the emission takes place predominantly from the wall of the cathode orifice. It has only been since measurements of plasma properties [7], surface temperatures [8,9] and currents [9,10] in the cathode interior have been attempted that this view of the emission process has begun to change. These more recent studies, which include data from the cathode interior, suggest that emission takes place mostly from the cathode interior surfaces and

that the predominant surface emission process is probably thermionic in nature. Even as this view was becoming widely accepted, other studies provided convincing arguments supporting the earlier theories or suggesting entirely new ones.

Bessling [11] concluded on the basis of an experimental study using two cathodes having orifice plates made of materials with different work functions (tantalum and thoriated-tungsten) that electron emission is from the orifice surface and is due to a combination of field-enhanced thermionic emission and pure field emission at surface irregularities. This experimental evidence was based largely on photomicrographs of the orifice surface before and after operation. While these data could be open to other interpretations, his detailed analytical model did agree well with this evidence.

A study that arrives at a totally different conclusion is one by Krishnan [1] involving the large diameter argon hollow cathodes used in magnetoplasmadynamic arcjets. Although these are not orificed cathodes, this research is mentioned here because it was partly motivated by an interest in identifying fundamental physical processes which might also be applicable to the small diameter, ion thruster cathodes. The idea was that the large diameter cathodes used in the arcjet would allow detailed internal plasma diagnostics which could not be done on smaller cathodes. Krishnan concluded from his experiments that it is possible for photoelectric emission to play an important role in hollow cathodes and that the surface emission will locate itself one diameter upstream of the exit plane when the mean free path for energy exchange of the emitted electrons is approximately equal to the cathode diameter. As Krishnan admitted, it is not clear that the results for these large

pulsed cathodes are applicable to the smaller, steady-state, orificed, cathodes used in ion thrusters. It does suggest, however, that photo electric emission is a process that should be considered. This discussion serves to highlight the diverse nature of the theories that have been proposed regarding orificed hollow cathodes and to emphasize the commonly held opinion that detailed data from the cathode interior are critical to understanding hollow cathode physical processes.

In addition to orificed hollow cathode research, which has been concerned mostly with cathodes for a specific application, there is a large body of research which is related to the broader topic of hollow cathode arcs. Much of the hollow cathode arc research, particularly that carried out in France in recent years by Delcroix and his colleagues, is of a more general nature in the sense that it is not directed at a specific application. While the literature on hollow cathode arcs deals with a wide variety of hollow cathode configurations, the most common is the tubular, open-channel hollow cathode. As with orificed hollow cathodes, these cathodes require a minimum gas flow through the tube in order to establish a hollow cathode arc discharge. Though there are obvious and significant differences in the gas flow patterns between an open-channel and an orificed hollow cathode, the research on open-channel cathodes is of interest because the electron and plasma production processes are expected to be similar for both types of cathodes. Research on open-channel, hollow cathodes has, until recent years, been in the same situation as that on orificed hollow cathodes and for the same reasons. It has been hampered by the lack of experimental data from the cathode interior and by the complexity of the internal processes. As with orificed hollow cathodes, this situation

has changed in recent years as experimental data [12] have become available for the cathode interior. The considerable amount of information on hollow cathode arc research is reviewed in an excellent survey article by Delcroix and Trindade [2]. Since publication of the survey article, Ferreira and Delcroix [13] have published what is certainly the best attempt to date to construct a comprehensive and self-consistent theory for the open-channel, hollow cathode arc. Their model agrees well with the available experimental data and will probably replace the earlier theoretical work covered in the review article. Our discussion will, therefore, focus on this recent theory.

The model proposed by Ferreira and Delcroix provides a detailed analytical description of the basic physical phenomena involved in the operation of open-channel, hollow cathodes. These phenomena include the gas flow through the cathode, the surface emission process, the formation of the internal plasma by the wall emitted electrons, the radial transport of ions and electrons, the axial transport of Maxwellian electrons and their kinetic energy, and the energy balance at the cathode wall. In describing the formation of the internal plasma the model uses a method proposed by Allis [13] to determine the mean number of excitations and ionizations produced per primary (surface emitted) electron. This method uses a "gain function" to account for the collisional degradation in velocity space of the primary electrons. Using this analysis, the authors calculate that, for argon, each primary electron yields on the average one additional electron due to ionization. This means that the volume and surface processes share equally in the total discharge current. They assume that field-enhanced thermionic emission is the dominant surface emission process.

To the extent that this model correlates with the available experimental data, it appears to represent a reasonable description of the important hollow cathode physical processes. The theory, however, does not account for the possibility of other surface emission processes and the degree of correlation between theory and experiment is not sufficient to rule them out. Indeed, in the test case used for comparison, the model could account for only 9A out of the 15A measured discharge current. In addition, there is no direct experimental evidence supporting the assumption that field-enhanced thermionic emission is the dominant emission process for this type of cathode.

In spite of its detailed analytical formulation, the model proposed by Ferreira and Delcroix is not a predicitive one. The model cannot predict the location or extent of the cathode emission region or explain its observed dependence on gas flow rate and discharge current. In addition, the authors rely on an experimentally determined emitting surface temperature profile as input to the model in order to obtain a comparison of theory with experiment. Using such a profile as input is, of course, unsatisfactory for a predictive model both because the temperature profile is usually not known and because the results are extremely sensitive to these temperatures.

It is evident that a better understanding of the surface emission processes and the related plasma production processes which determine the location and extent of the emission region is critical to the development of a predictive, self-consistent model describing hollow cathode operation. The ability to make detailed measurements within the cathode of operating parameters such as surface temperatures, current

densities, and plasma properties will clearly be a critical factor in improving our understanding of these processes.

Overview

This thesis is organized in the following manner. Chapter II describes the apparatus and special test cathodes used in the experiments with the emphasis on the type of measurements which it was possible to make and the type of data which were collected. This chapter is meant to provide an overview of the preliminary experimental work, including a summary of important results, as a background and physically grounded reference for the discussion of the model which follows. Chapter III discusses the model beginning with a phenomenological description of the physical processes taking place within the cathode. Each of the important physical processes related to formation of the internal plasma discharge is then discussed in detail based on the experimental results presented in Chapter I. A simple, analytical model is proposed to describe these processes. Chapter IV addresses the question of the surface emission mechanism, investigating each of the possible processes to determine their relative importance. This chapter concludes with the description of an experiment designed to test the resulting hypothesis that field-enhanced thermionic emission is the dominant surface emission process. Chapter V presents, in summary form, the analytical relationships which comprise the model and the major assumptions on which they are based. It also includes a list of symbols and units used in the model. Chapter VI describes an experiment designed to account for all of the possible current components which make up the total discharge current. The results of this experiment are

used to test a number of important assumptions regarding the extent of the internal active region, the flux of ions leaving the region, and the energy balance used for predicting the plasma density in the region. The results of calculations based on the proposed model are presented for the conditions used in the experiment and compared with the available experimental data. Finally, two experiments are described which provide some insight into processes taking place in the orifice region. Chapter VII summarizes the key results of this investigation and suggests some areas for future research which could provide additional insight into the operation of these devices.

All equations presented in this paper are in MKS units except for a few empirical expressions where the units are clearly indicated. Plasma potentials, surface work functions and excitation energies are expressed in volts or electron volts, as appropriate. Important or frequently used symbols are listed in Table V of Chapter V. Other symbols are defined in the text at the point where they are used.

II. PRELIMINARY EXPERIMENTS

The model which will be presented in Chapter III is a direct outgrowth of a series of experiments aimed specifically at identifying the electron production processes and their location within the cathode. The experiments which provided this information used a specially designed cathode and mounting fixture which facilitated making measurements which previously had not been attempted. This chapter will describe the cathode and related equipment, the type of measurements it was possible to make, and the procedures used in making them. It will also present a summary of certain key results of these experiments. The purpose here is to present, as background for Chapter III, those results which provide the physical understanding on which the model is based. Additional experiments and more detailed results will be presented in subsequent chapters to verify certain assumptions of the model and to test its accuracy.

Apparatus and Procedure

Cathode

In order to isolate the insert electrically and to provide for direct visual observation of the insert, a special cathode was constructed using a quartz body tube in the manner suggested by Fig. 1. The cathode consisted of a quartz tube 6.3 mm OD x 4.0 mm ID covered on the downstream end with an orifice place. The end of the quartz tube and the back of the orifice plate were both ground flat to facilitate a good seal between them. The plate was held tight against the tube by a

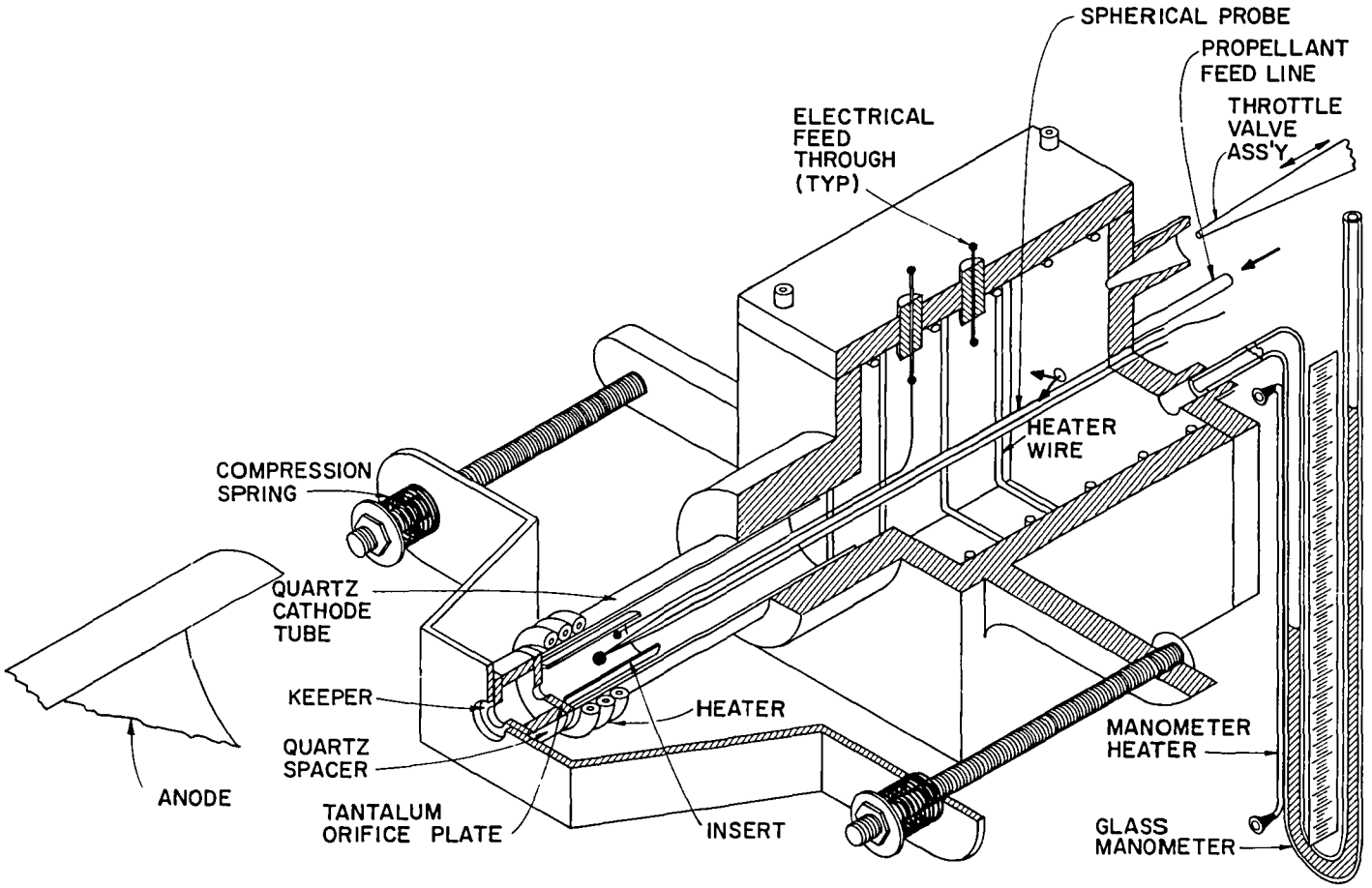

Figure 1. Hollow Cathode Test Configuration

tensioning device which also acted as the keeper electrode. This electrode had an orifice diameter of 3.6 mm and was separated from the orifice plate by a 2.5 mm thick quartz spacer as shown in Fig. 1. Although preliminary testing was conducted using the orifice plate shown in the figure, most of the data were collected using the orifice plate/valve assembly shown in Fig. 2a. This assembly facilitated rapid in vacuo variations of the orifice size. It consisted of a tantalum body and sliding orifice plate. The body was ground flat on both sides and had a 1.6 mm diameter orifice. The tantalum orifice slide, also ground smooth and flat, had three orifices with diameters of 0.51, 0.79, and 1.0 mm drilled through it. A pair of leaf springs held the slide in contact with the downstream side of the body. By moving the slide to match different size orifices with the body hole, one could change the cathode orifice diameter quickly without the necessity of opening the bell jar and exposing the insert to the atmosphere. During cathode operation the orifice diameter was changed incrementally by turning off the discharge and moving the slide to change from one diameter orifice to another. It was also possible, by moving through a short distance, to change the orifice area continuously without having to shut off the discharge. For some tests this latter mode of operation was preferred.

The quartz tube was covered on the outside by a wire heater wrapped in a serpentine pattern, which was in turn covered on both its interior and exterior surfaces by a tantalum foil radiation shield. The heater covered ~ 75% of the perimeter of the quartz tubing leaving a longitudinal gap along one side of the cathode through which the insert could be viewed. The insert, which was 3.9 mm in diameter,

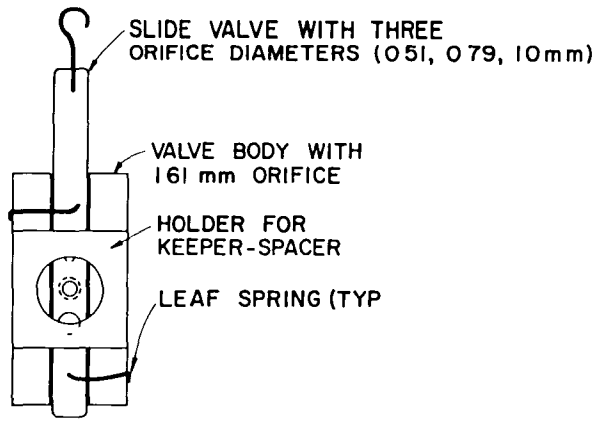

Figure 2a. View of Downstream Side of Orifice Plate/Valve Assembly

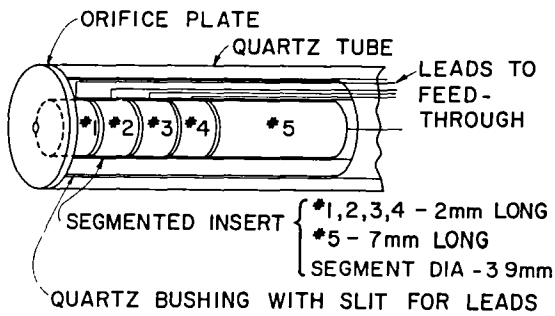

Figure 2b. Detail of Segmented Insert

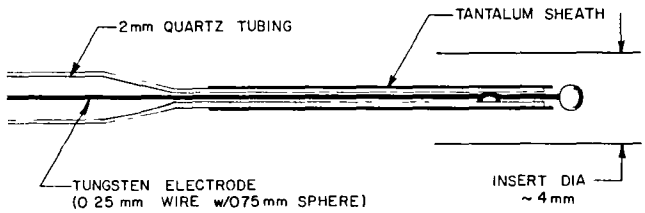

Figure 2c. Detail of Spherical Probe

was constructed of 0.025 mm tantalum foil coated with the chemical R-500;* and was placed in the quartz body in such a way that it presented a single layer thickness in the viewing direction. Its construction will be discussed in greater detail below. The cathode assembly was mounted in the support structure shown in Fig. 1. The stainless steel support structure shown in Fig. 1 included a plenum chamber with removable covers on both the top and the upstream end. The inside of the chamber was fitted with a wire heater to prevent mercury condensation. The top cover was fitted with five electrical feedthroughs which could be used to make electrical connections to the inside of the cathode such as the one to the insert shown in Fig. 1. The rear plate contained a tapered hole which was used as a throttle valve seat and another straight hole which accepted the pressure tap of a U-tube monometer. The needle of the throttle valve was made of a piece of tapered quartz tubing which could be moved axially to vent a portion of the mercury propellant into the bell jar. This allowed rapid adjustment of the pressure in the plenum chamber without requiring an adjustment of the mercury vaporizer heater. The rear plate also contained a feed through aligned on the cathode axis which allowed insertion of a movable Langmuir probe into the insert region of the cathode.

Since the purpose of these experiments was to investigate basic cathode phenomena, the experiments were conducted by operating the cathode in a vacuum bell jar rather than a thruster. Discharge coupling was to an axially-mounted, cylindrical anode 6 cm in diameter and 8 cm

---

* A double carbonate mixture - (Ba/Sr) CO_3 manufactured by the J.R. Baker Chemical Co., Phillipsburg, New Jersey.

long, made from perforated stainless steel sheet. The bell jar pressure was in the 10^{-3} to 10^{-4} Torr range during the tests. When there was no mercury flow, as was the case during insert conditioning, the bell jar pressure would drop to $\sim 10^{-6}$ Torr.

The results presented here will use as a parameter the total discharge current I_D, which is the sum of the keeper current I_K, and the anode current I_A. It was found that, for a given emission current, the keeper current I_K had (over the range of interest for thruster application) a negligible effect on major cathode parameters such as insert temperature and the internal pressure. For all tests the keeper current was, therefore, held constant at 0.3 A.

Insert Construction

Earlier testing showed that insert temperatures were very dependent on operating history and exposure to the atmosphere. This was found to be particularly important with a single layer, foil insert which did not contain a significant amount of R-500 which could be released after the original surface was depleted or contaiminated. Since the surface work function of the insert is critically important in determining insert temperatures as well as keeper and discharge voltages, considerable care was taken in the fabrication and conditioning of the inserts. Inserts were constructed of 0.025 mm tantalum foil 15 mm long and ~ 1.75 times the perimeter of the 3.9 mm diameter mandrel around which they were wrapped. The flat foil was first cleaned with chlorothene and then with acetone. The three quarter turn section which would be two layers thick in the final insert was coated with R-500. This was done to provide a reservoir of R-500 thereby extending the useful lifetime of the insert. The foil was then wrapped around the mandrel and both free edges were

spot welded. The inside diameter of the insert and the upstream side of the orifice plate were then coated with R-500. The insert was assembled in the cathode with the one quarter circumference section, which was a single layer thick, positioned where it could be viewed directly. The downstream edge of the insert was positioned ~0.5 mm from the orifice plate. The insert was conditioned by allowing the cathode assembly to warm up overnight with the cathode tube heater operating at ~850°C and the mounting structure heaters at operating temperature. The cathode was started and allowed to operate at 2 to 3 A emission current until the insert temperatures had stabilized. This required 4 to 5 hours of operation. On initial startup it was found that the insert would operate cold (no visible radiation) or would have a small hot region along or near the downstream edge. During the breakin period the temperature profile would change to what was considered the normal operating condition for this insert, a condition that will be shown later in the results. Between operating periods the cathode was maintained in a vacuum environment with the mechanical pump. If the bell jar was opened, it was kept open for as short a period as possible. After the initial break in, the cathode warmup time was a few hours and the cathode was generally allowed to run for an additional couple of hours before data were collected. These precautions were sufficient to insure that insert temperatures at a given operating condition could be reproduced to within ±25°C during different runs and within ±10°C during a single run using the same insert. Temperature variations somewhat greater than this were observed between cathodes using different inserts.

Segmented Insert

A special, segmented insert was constructed in order to determine more precisely where the emission takes place on the insert and to correlate this with the insert surface temperature at that location. An insert was first constructed in the manner described previously, and then it was cut into four 2 mm long sections and one 7 mm long section. Each section was connected with a lead wire to a separate feed through on the top cover of the cathode mounting structure. A sketch of this segmented insert is shown in Fig. 2b. The segments were separated by ~0.3 mm, and the emission current for each segment was monitored separately. The conditioning procedure and precautions mentioned above in regard to the continuous insert were also followed with this segmented one.

Pressure Measurements

The stagnation pressure in the plenum chamber supporting the quartz cathode was sensed by a U-tube manometer (Fig. 1) filled with Dow Corning 705 diffusion pump fluid. This fluid has a vapor point at 0.5 Torr of 245°C compared to 108°C for mercury. The heater on the high pressure side of the manometer maintained that column at a temperature which prevented mercury condensation without causing the diffusion pump fluid to boil. The manometer was contained completely within the bell jar and thus provided direct measurement of the pressure difference between the bell jar and the plenum chamber. The manometer had a pressure range of 24 cm of fluid which was equivalent to 13.2 Torr.

The fluid levels in the manometer could easily be read to within ±0.5 mm, which for the low specific gravity indicating fluid was equivalent to 0.038 Torr. Because of this the precision of the pressure

data is considered to be very good. However, the heater on the high pressure column of the manometer causes that column to be at a higher temperature than the low pressure column. This significantly affects the fluid density of the high pressure column. The results presented in this report are corrected for this effect. The uncertainty associated with this correction is estimated to be 0.25 Torr although errors as high as 1 Torr are considered possible. Unfortunately the greatest absolute error occurs at low pressures when the two column heights are nearly equal, resulting in what could be substantial relative error at these pressures.

Throttle Valve

In order to determine whether the throttle valve could be used to adjust the internal pressure and, therefore, the flow rate through the cathode orifice rapidly without adverse experimental effects, the following experiment was conducted. The cathode was operated at a constant emission current for four different flow rates into the plenum chamber while the internal cathode pressure was maintained at a constant value by adjusting the throttle valve. Flow into the plenum chamber at each operating condition was set by adjusting the vaporizer heater current. The test was performed on three occasions and included operation with two different orifice diameters and operation at two different emission currents. In all cases, it was found that, for a constant emission current and constant internal pressure, the insert temperatures remained essentially constant regardless of the flow rate into the plenum chamber. The results of this experiment indicated that the internal pressure and, therefore, the flow through the cathode orifice can be varied using either the throttle valve or the vaporizer

heater and that either method gives the same results for measurements made within the cathode. It should be pointed out that the total mass flow into the plenum chamber does affect the bell jar pressure; and, as expected, changes in total flow rate were found to have a small effect on the discharge and the keeper voltages.

Temperature Measurements

Insert surface temperatures were measured using a micro-optical pyrometer. This method of temperature measurement is influenced by both the emissivity of the radiating surface and the transmissivity of the quartz tube and glass bell jar. These effects were accounted for by calibrating the pyrometer against a platinum/platinum-rhodium thermocouple. The calibration was carried out for a sample of the tantalum foil used in making the inserts. The material sample was spot welded to a section of swaged heater wire and the thermocouple was attached to the surface of the sample. This sample/heater assembly was then inserted into a quartz tube and the whole apparatus was placed in the bell jar. The surface temperature of the sample was then measured at various heater powers using both the thermocouple and the micro-optical pyrometer. Insert surface temperatures measured during the experiments were corrected based on the calibration curves resulting from these tests.

Plasma Property Measurements

Plasma properties in the insert region were determined using a Langmuir probe with a 0.75 mm diameter spherical electrode. Details of the probe are shown in Fig. 2c. The tungsten sphere used as an electrode was formed on the end of 0.25 mm tungsten wire by striking a DC arc between the wire and a graphite electrode in a helium atmosphere.

The body of the probe was formed by drawing 2 mm diameter quartz tubing as shown in Fig. 2c. A layer of 0.025 mm thick tantalum foil covered the necked down portion of the quartz tube. This provided thermal protection from the intense plasma discharge and acted as a shield to minimize sputter coating of the insulator end. Because of the density of the plasma in the insert region ($\sim 10^{14}$ cm^{-3}), it is not possible to bias such a probe near plasma potential without burning up the probe and/or significantly perturbing the discharge. Plasma properties were, therefore, estimated from the ion saturation portion of the probe trace obtained by biasing the probe from cathode potential to potentials slightly above floating potential. The method of recording and analyzing the probe traces is discussed in detail in Appendix A. Actually, any cathode surface which can be shown to be non-emitting and can be electrically isolated from surrounding surfaces can also be used to estimate average plasma properties adjacent to itself. The method of analysis is the same as that used for the probe. Such surfaces were used in a number of experiments for estimating average plasma densities.

Results

Using the apparatus and procedures discussed above, axial profiles of insert temperature, insert current and plasma properties were collected over a wide range of cathode operating conditions. These operating conditions included total discharge currents ranging from 0.3 to 7.3 A, orifice diameters of 0.51, 0.79, and 1.00 mm, and mass flow rates ranging from 90 to 450 mA. These results are presented in detail in earlier publications [7,9] so only those results will be summarized

here which are necessary for the development of the model which is to follow.

The objective of the experiments described above was to identify the electron emission region and determine the plasma properties in that region. The results showed that under normal operating conditions approximately 87% of the total discharge current comes from the insert and that the electron emission is normally localized to a region two millimeters long at the downstream end of the insert. The orifice plate accounts for most of the remainder of the current. This is shown in Fig. 3a where the fraction of emission current from various surfaces is plotted as a function of discharge current for a cathode with 0.79 mm diameter orifice operating with a segmented insert at an internal cathode pressure of 6.7 Torr. Figure 3a shows that for this moderate pressure, the emission current distribution of the cathode is, at least within the resolution of the 2 mm long insert segments, essentially independent of discharge current. Figure 3b shows the effect of internal cathode pressure on the emission current distribution of the same cathode operating at a discharge current of 7.3 A. At pressures above ~4 Torr the current is distributed in essentially the same way as indicated in Fig. 3a. However, as the pressure is decreased below ~4 Torr, the emission current region extends upstream involving more of the insert surface.

As expected, the highest insert temperature was found to correspond to the location of the emission region with temperatures on the order of 1000^{0}C being typical for an emission current of a few amperes. A typical insert temperture profile is shown in Fig. 4a for a cathode having a continuous insert operating at a discharge current of 3.3 A and

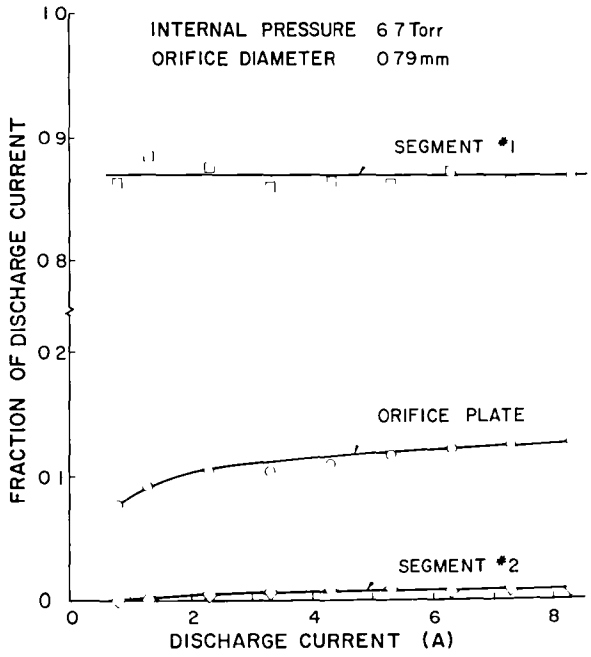

Figure 3a. Effect of Discharge Current on Hollow Cathode Current Distribution

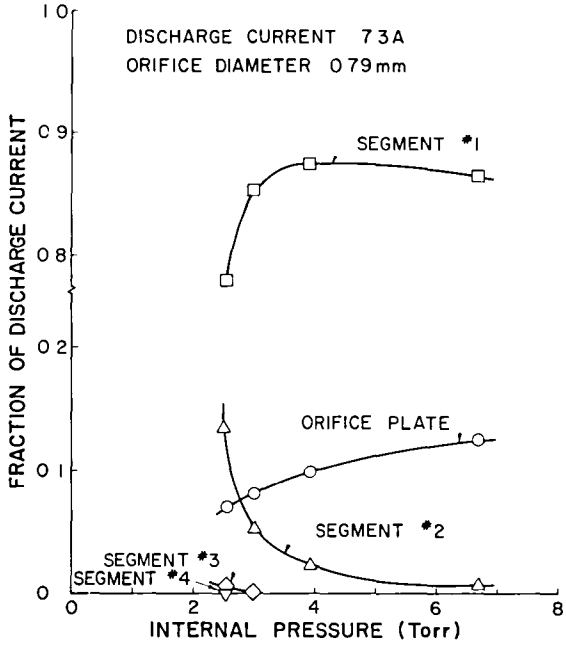

Figure 3b. Effect of Internal Pressure on Hollow Cathode Current Distribution

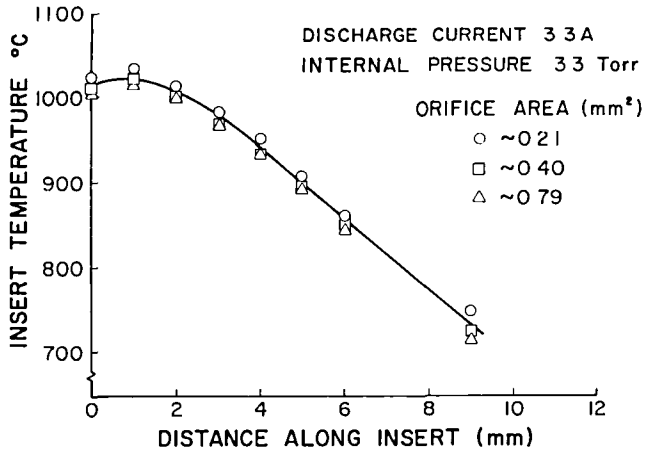

Figure 4a. Effect of Orifice Area on Insert Temperature Profile

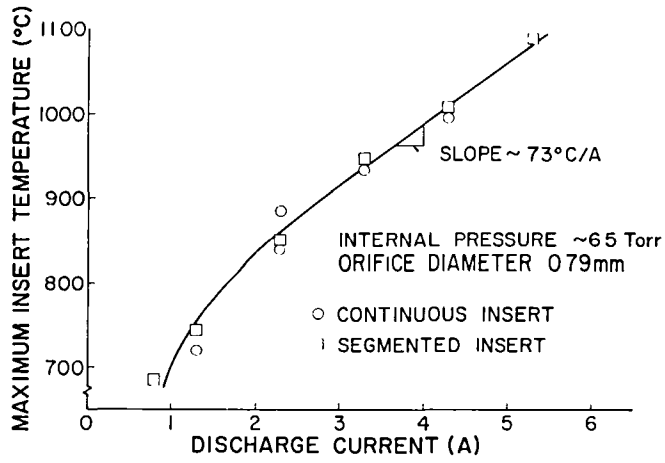

Figure 4b. Effect of Total Discharge Current on Maximum Insert Temperature

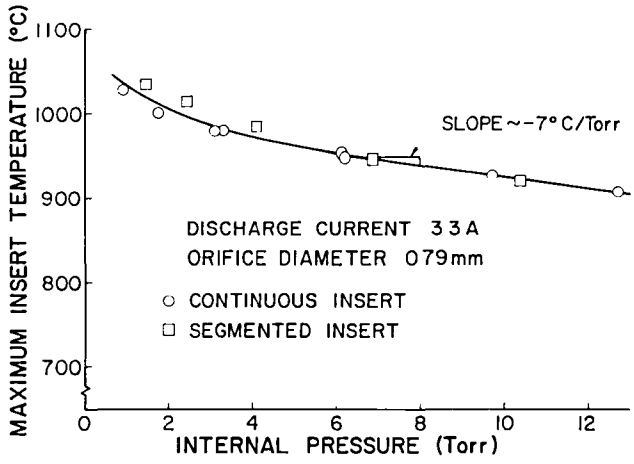

Figure 4c. Fffect of Internal Pressure on Maximum Insert Temperature

an internal pressure of 3.3 Torr. For this pressure, the current distribution results indicate that the emission region should cover ~2 mm of the insert. This agrees with the results of Fig. 4a which show that the highest insert temperature occurs on the downstream end of the insert. The temperature is fairly uniform over the downstream two millimeters of the insert and drops off rapidly in the upstream direction. The effect of discharge current and internal pressure on the maximum insert temperature are shown in Figs. 4b and 4c for a cathode with a 0.79 mm diameter orifice. Data shown for both the continuous and the segmented insert are seen to follow essentially the same curve which suggests that segmenting the insert did not substantially alter its thermal and emissive characteristics. The important result of Fig. 4b is that the maximum insert temperature substantially increases with increases in discharge current when the internal pressure is held constant. This increase was found to be consistent with thermionic types of emission. The simultaneous measurement of current and emission surface temperature in these experiments provided sufficient information to allow calculation of an average, effective thermionic work function for the emissive surface. Values of 1.7 to 2.0 eV were found to be typical. A work function of this magnitude is reasonable for the coated insert used in the tests [14]. Figure 4c shows that the maximum insert temperature decreases when the internal pressures is increased at a constant discharge current.

Typical plasma conditions found in the region adjacent to the emitting portion of the insert were a plasma density of a few times 10^{14} cm^{-3}, a plasma potential of ~9 volts, and an electron temperature of ~0.7 eV. Profiles of the plasma properties measured on the axis

inside the cathode are shown in Fig. 5 for a cathode with a 0.76 mm diameter orifice and a segmented insert. Figure 5a is a semi-log plot of the plasma density profiles for the cathode operating at an internal pressure of 4.6 Torr for discharge currents of 1.3, 2.3, and 3.3 amperes. It is seen that the density increases with increasing discharge current. Other data (not shown) indicate that adjacent to the emission region the plasma density increases with increases in internal cathode pressure as well. Figure 5a indicates that near the orifice the plasma density is on the order of 10^{14} cm $^{-3}$ and falls off exponentially in the upstream direction. The density curves show no distinct inflection point but do tend to flatten near the orifice. It is significant that insert temperature measurements indicated that the emission for this particular test was taking place mainly from the downstream (0 to 1 mm) half of the segment. This is considered the probable reason that the density curves do not exhibit a clearly defined plateau near their downstream end (0 to 2 mm). Figures 5b and 5c show the plasa potential and electron temperature for the same test for discharge currents from 1.3 to 3.3 A and internal pressures from 0.9 to 7.1 Torr. The circles represent the average of the data for the given location while the bars indicate the range of the data for that location. At the one millimeter position, which is adjacent to the insert emission region, the plasma potential and electron temperature are respectively 8.7 V and 0.71 eV. The results in Figs. 5b and 5c are presented in terms of the average values of the parameters because there was no clear correlation with either current or pressure for these results, except for the electron temperature which showed a very slight tendency to decrease with increasing pressure. It should also be

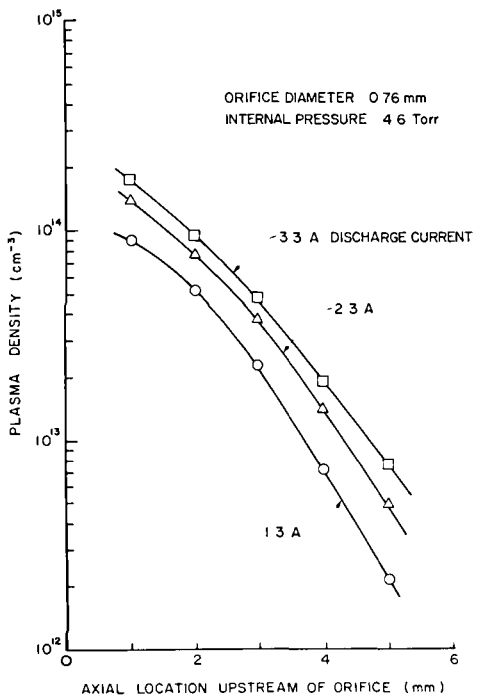

Figure 5a. Plasma Density Profile

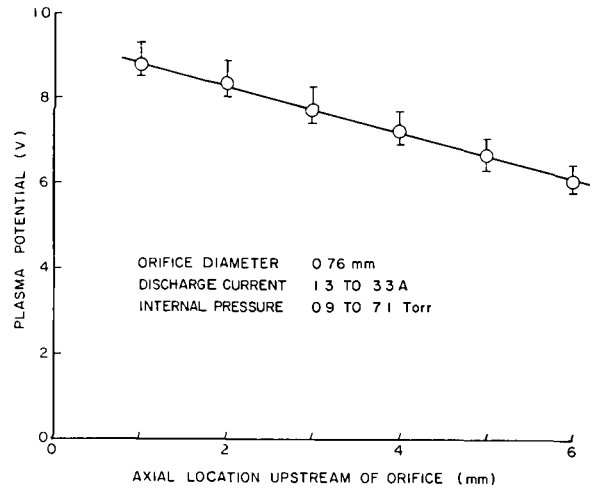

Figure 5b. Plasma Potential Profile

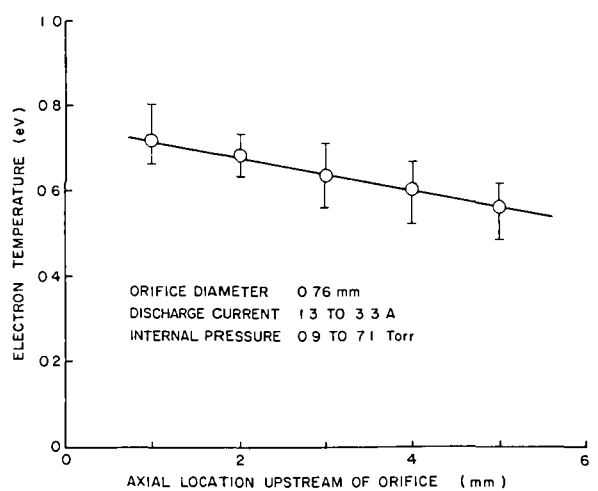

Figure 5c. Electron Temperature Profile

mentioned here that all of the plasma properties were found to increase significantly when the insert work function increased due to either contamination or depletion.

The results of these experiments showed that the orifice diameter and mass flow rate are important in determining the internal cathode processes only to the extent that they determine the internal cathode pressure. More specifically, insert temperatures were found to be independent of orifice diameter and mass flow rate so long as the internal pressure was constant. This can be seen in Fig. 4a where the insert temperature date for a pressure of 3.3 Torr and current of 3.3 A are plotted for three different orifice open areas. Both the magnitudes of the insert temperatures and the insert temperature profiles were relatively insensitive to the almost four-fold change in orifice area (and corresponding change in mass flow rate) as long as the emission current and internal pressure were held constant. The internal cathode processes were found to be essentially independent of orifice diameter and mass flow rate for an operation at a given internal pressure, while the internal pressure was found to be an important parameter affecting not only the emitting length of the insert but also the maximum insert temperature (Figs. 3b and 4c). It is for this reason that the internal cathode pressure rather than the mass flow rate was used as a parameter in the data collected for the experiments discussed above. However, mass flow rate is the parameter normally controlled during cathode operation; so it is necessary to have some means of relating internal cathode pressure to mass flow rate. In order to do this, the stagnation pressure in the plenum chamber immediately upstream of the cathode was measured with the manometer for a range of emission currents, orifice

diameters, and mass flow rates. The throttle valve was closed during these tests. The results of these measurements are shown in Fig. 6 where the parameter $P_o/(\dot{m}/d_o^2)$ is plotted as a function of total discharge current I_D. Here P_o is the stagnation pressure in Torr, $\dot{m}$ is the mass flow rate in milliamps equivalent, and d_o is the orifice diameter in millimeters. The three symbols in Fig. 6 represent the three orifice sizes tested, while the bar on the symbol represents the range of the data for that particular orifice diameter when the mass flow rate was varied from ~ 90 to 450 mA. The least squares fit of the data to a straight line with the equation

$$P_o/(\dot{m}/d_o^2) = (13.7 + 7.82 I_D) \times 10^{-3} \ (\mathrm{Torr \cdot mm^2/mA}) \qquad (1)$$

is reasonably good. It is believed that the length of the orifice channel has some effect on the pressure. The effect of this parameter is not explicitly accounted for by the empirical correlation represented by Eq. 1. However, for normal cathode dimensions and operating conditions this equation is believed to be accurate to within ± 30% for orificed cathodes operating on mercury.

It is noteworthy that both the theory of free molecular flow and the theory of continuum, choked flow predict that the pressure mass flow relation takes the form

$$P_o/(\dot{m}/d_o^2) = C\sqrt{T/M} \qquad (2)$$

where, T is the gas stagnation temperature at the orifice and M is the atomic weight of the gas. The parameter C is a constant of proportionality which is different for the two cases (free molecular and continuum). The gas temperature for the no discharge case ($I_D = 0$) was

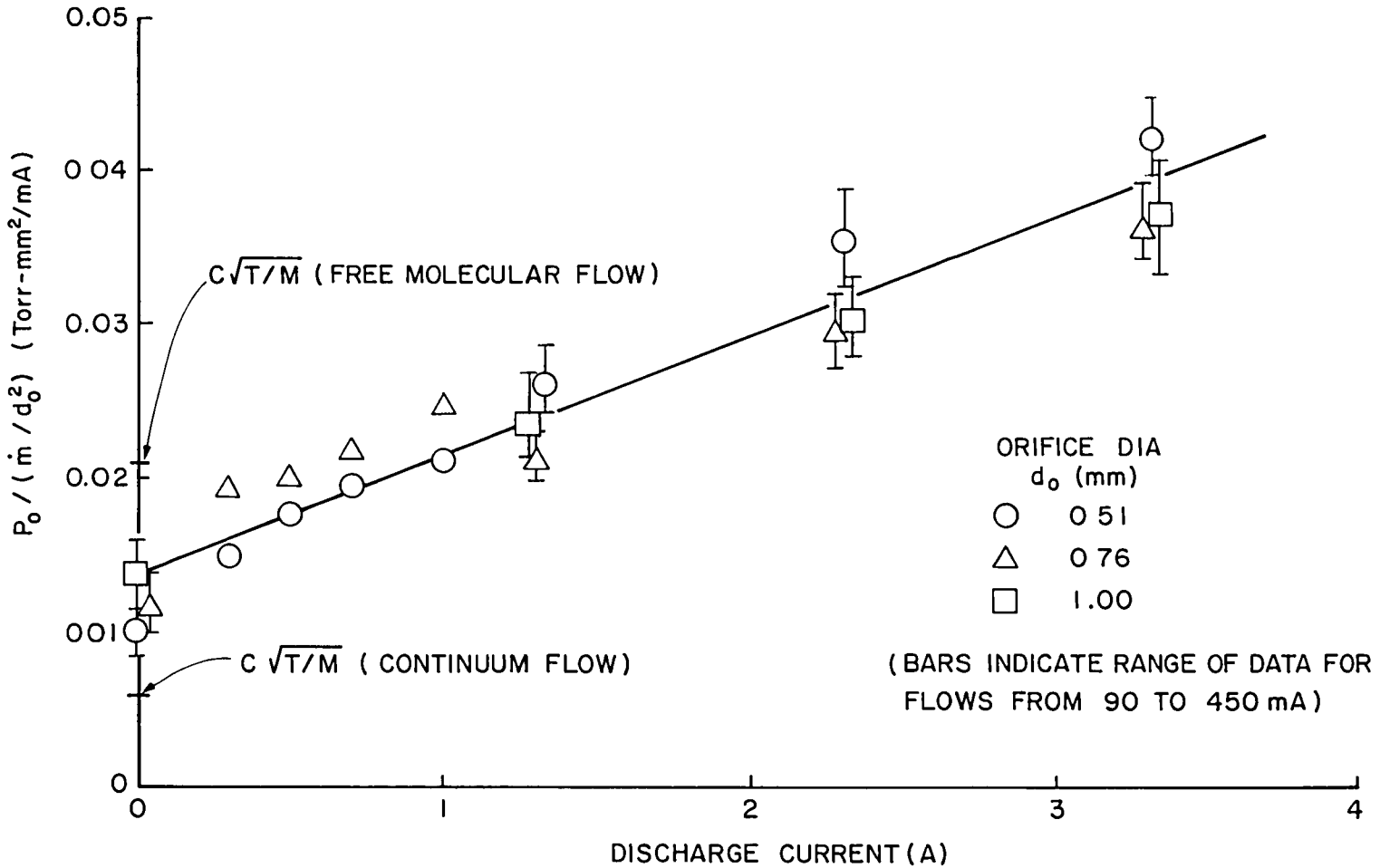

Figure 6. Internal Pressure - Flow Rate Correlation

estimated on the basis of the plenum and cathode wall temperatures to be ~ 425°C. The value of $C\sqrt{T/M}$ based on this temperature is plotted on the vertical axis for the two flow cases. Clearly, the hollow cathode flow is in the transition region between these two types of flow for the no discharge case. In the presence of the internal discharge, additional complications are added due to the heating effect of the discharge and the influence of electrical forces on the charged particles of the plasma. These effects, which presumably cause the ratio $P_o/(\dot{m}/d_o^2)$ to increase with temperature, will be discussed in more detail in subsequent chapters.

Typical Hollow Cathode Conditions

It will be useful in the following chapters to have available a set of parameters typical of hollow cathode operating conditions for use in discussions and examples. Based on the results of the experiments discussed above the conditions in Table I are selected.

Table I

Typical Cathode Conditions

Discharge Current:	$I_D = 3.3A$
Orifice Diameter:	$d_o = 0.76$ mm
Insert Diameter:	$d_{in} = 4.0$ mm
Emission Length:	$L_e = 2.0$ mm
Plasma Density:	$n_e \approx n_i = 1.8x10^{14} cm^{-3}$
Electron Temperature:	$T_e = 0.71$ eV
Plasma Potential:	$V_p = 8.7$ V
Insert Temperature:	$T_s = 1000^oC$
Mass Flow Rate:	$\dot{m} = 67$ mA
Internal Pressure:	$P_o = 4.6$ Torr
Neutral Density:	$n_o = 3.3x10^{16}$ cm^{-3}
Ion Current:	$I_i = 0.9$ A
Electron Emission Current:	$I_e = 2.4$ A
Avg. Effec. Work Function:	$\phi_e = 1.84$ eV

The plasma parameters in Table I are those considered to be typical average values for the region adjacent to the emitting portion of the insert. They are based on the results in Fig. 5. The insert emitting length of 2 mm shown in Table I is a maximum in that all of the tests showed conclusively that for these operating conditions the emission was confined to the first insert segment which was 2 mm long. Based on insert temperature measrements, the actual emitting region of the insert is believed to be between 0.5 and 1.5 mm long for these conditions. The last four parameters in the table (n_o, I_i, I_e, and ϕ_e) are actually results of analysis which will be discussed in the next chapter but are

included here for convenient reference. The total neutral particle density n_o is calculated based on the ideal gas law. The ion current I_i is the estimated ion current for the listed plasma conditions based on the Bohm flux of ions to all cathode surfaces, including the insert. The electron emission current I_e is the current attributed to surface emission from the insert and is just $(I_D - I_i)$. The average effective work function is calculated from the Richardson-Dushman equation based on the insert emission temperature T_s, the insert emission current I_e, and the area of the emitting surface of length L_e.

III. MODEL OF INTERNAL PLASMA PROCESSES

This chapter will present the theoretical model for orificed hollow cathodes that has emerged based on the results of the preliminary experiments described in the previous chapter. The model will first be presented in the form of a general phenomenological description of the important physical processes underlying the operation of the cathode. Processes related to the internal plasma will then be discussed in detail and an analytical model will be formulated which describes these processes.

Phenomenological Model

The preliminary experiments suggest the following description of internal cathode processes. An internal cathode pressure on the order of a few Torr is required for normal operation. This corresponds to a neutral density on the order of a few times 10^{16} cm^{-3}. The function of the cathode orifice is to restrict the propellant flow to a reasonable value, while at the same time maintaining the required neutral density and providing a current path to the downstream discharge. The electrons which exit through the cathode orifice are produced within the cathode both by surface emission and by volume ionization processes. As indicated in the schematic of Fig. 7 the surface electron emission (I_e) comes from a narrow band ($L_e \approx 2mm$) on the downstream end of the insert. The electrons are produced at the surface of the insert primarily by field-enhanced thermionic emission. The very strong electric field is a

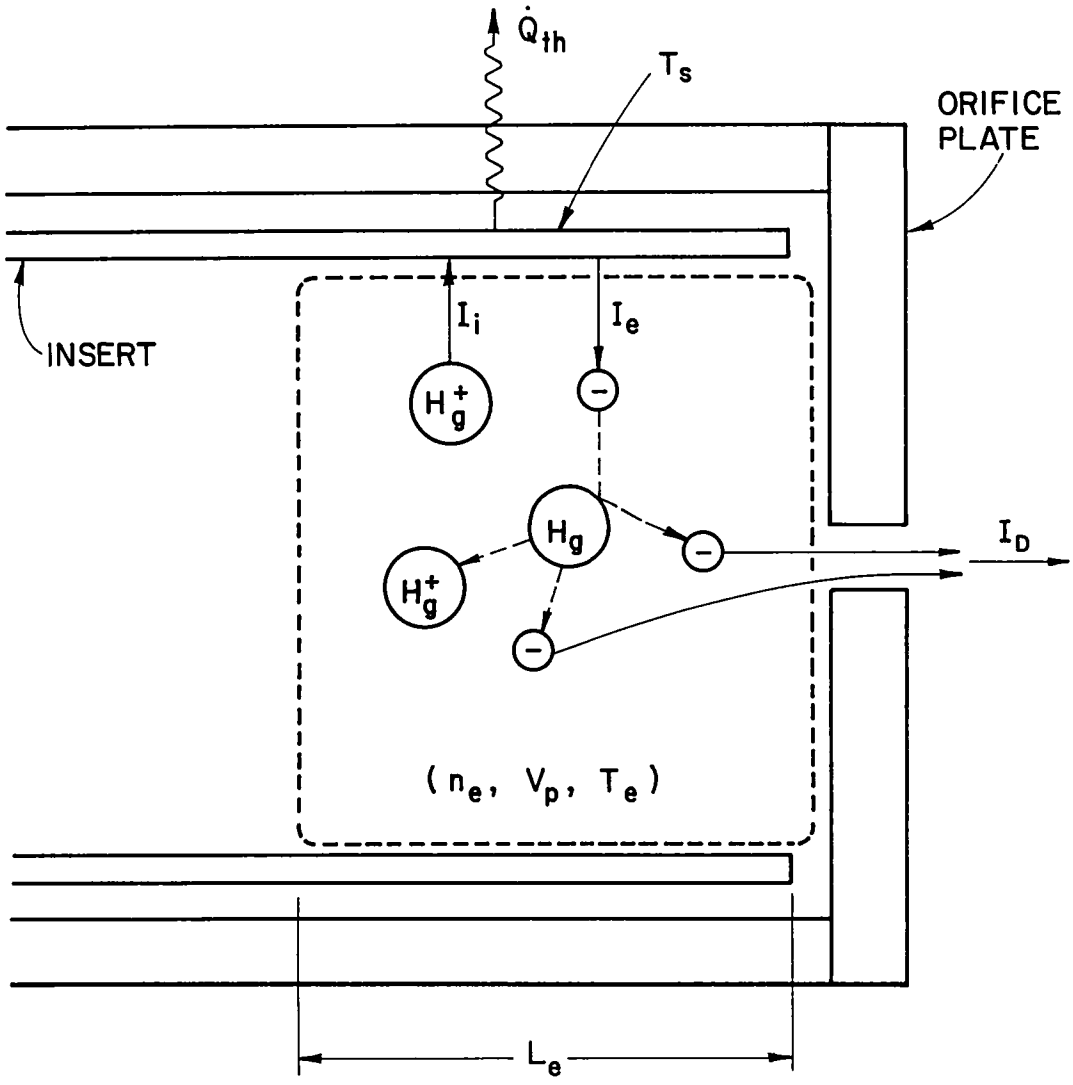

Figure 7. Schematic of Ion Production Region

consequence of the very dense plasma which produces a very thin plasma sheath across which the plasma potential drop occurs. Electrons may also be produced at the insert surface by photoelectric emission and by secondary emission due to ion and metastable bombardment of the surface. The electrons produced at the insert surface are accelerated across the plasma sheath by a potential of ~9v, thereby gaining sufficient energy to produce ion/electron pairs in the bulk plasma. The dense internal plasma is sustained by this ionization. Because of the low electron energies, ionization is predominately a multi-step process, relying heavily on the production of ions from intermediate metastable and resonance states. Since the mean free path for inelastic collisions of the electrons accelerated by the sheath is on the order of the internal cathode radius, the "ion production" region can be idealized as the volume circumscribed by the emitting region of the insert. This is indicated schematically by the dotted area in Fig. 7. Ions produced in this volume diffuse out of it at the Bohm velocity and strike the insert surface with sufficient energy to heat it to the temperature (T_s) necessary to provide the required surface electron emission. These ions are neutralized at the insert surface and thus complete the current path between the cathode surface and electrons produced in the ion production region (current I_i). Energy is also deposited at the insert surface by absorption of line radiation and by de-excitation of metastable and resonance state atoms.

The plasma properties in the ion production region (n_e, V_p, T_e) are coupled into the problem by the energy balance at the insert surface in the following manner. The plasma properties determine the flux of ions and other excited states and, therefore, the energy input to the

emission surface. For a given emission current, the surface temperature (T_s) is determined by the energy balance which requires that the thermal losses from the surface ($\dot{Q}_{th}$) due to electron production, radiation and conduction are balanced by the energy input from the plasma. The plasma properties also affect the required emission temperature because they determine the magnitude of the electric field at the emission surface and, thereby, the degree of field-enhancement in the emission process. Therefore, for a given emission current, the surface temperature and plasma properties must be consistent to the extent that they satisfy the energy balance at the insert surface.

All cathode surfaces which contact the plasma receive ion currents proportional to the Bohm velocity and the plasma density adjacent to the surface. Electron emission, on the other hand, can be assumed to come predominatly from the 2 mm band on the downstream end of the insert. The total discharge current I_D from the cathode is equal to the sum of the ion currents to the various cathode surfaces and the current of the emitted electrons.

The plasma processes described above do not occur uniformly throughout the idealized "ion production region". In the real situation both axial and radial variations of plasma properties, gas and surface temperatures, and gas densities are expected in this region of the cathode. However, a lumped parameter model, which is based on the idea of a well defined "ion production region" characterized by a single set of plasma properties, is analytically simple and is the approach which will be presented here. The discussion which follows will show that this viewpoint provides a useful and qualitatively accurate description of the cathode internal processes. In addition, it

leads to a simple set of analytical relationships which can be used to make reasonable predictions of important cathode operating parameters.

The analytical development of the model will be divided into a discussion of the plasma production processes, which will be presented in this chapter, and a discussion of the surface emission mechanism which is the subject of the next chapter. In this chapter, current continuity and energy balances will also be formulated which link the volume and surface processes together and relate them to such operating parameters as discharge current and discharge voltage.

Neutral Gas Density

A knowledge of the neutral gas density within the cathode is essential in order to model the plasma production processes. The presence of the cathode orifice plate simplifies this problem somewhat because most of the pressure drop is across the orifice and the pressure within the cathode cavity upstream of the orifice is essentially constant. However, predicting this pressure from cathode dimensions, mass flow rate, and operating conditions is, in itself, a complex problem. The problem is made particularly difficult by two factors. For normal cathode dimensions and flow rates, the cathode operates in the transition regime between free molecular and continium flow. In addition, because the gas is ionized, the flow is subject to energy input from plasma processes and is affected by the forces due to the electric fields set up within the plasma. Solution of this complex gas dynamical problem is beyond the scope of the present study. Therefore, a general analytical model for the flow processes will be avoided by using the empirical formulation for predicting the cathode internal pressure that was presented in Chapter II. This pressure can be used to

make a reasonable estimate of the neutral gas density within the cathode.

The total pressure at any point in the cathode is the sum of the partial pressures of each species. Using the ideal gas law this can be expressed as

$$P = n_e kT_e + n_i kT_i + n_o kT_o \tag{3}$$

where k is Boltzmann's constant, n is the density, T is the temperature, and the subscript e, i, o refer to electrons, ions, and neutral atoms respectively. Given the local pressure, each of the temperatures, and the plasma density, Eq. 3 can be solved for the neutral gas density.

For the ion production region, the local pressure P in Eq. 3 can be estimated from the empirical correlation given by Eq. 1 for the desired discharge current, mass flow rate, and orifice diameter. In the region upstream of the cathode orifice, typical mean free paths of the heavy particles (atoms and ions) are less than 0.01 cathode diameters, so it is reasonable in this region to speak in terms of continuum flow properties. The pressure measured in the experiments would, therefore, be the local upstream stagnation pressure P_o. Because the flow velocity along the tube is very low (Mach $\ll 0.1$), the stagnation pressure is nearly constant along the tube and essentially equal to the local pressure P. Even considering a significant increase in stagnation temperature due to heat addition in the ion production region, the pressure is expected to change significantly only very near the orifice. It is, therefore, reasonable to assume that the pressure in the ion production region is constant and is equal to the upstream stagnation pressure determined experimentally, or

$$P \approx P_o = \frac{\dot{m}}{d_o^2} \; (13.7 + 7.82 \; I_D) x10^{-3}. \tag{4}$$

Again the units are P (Torr), $\dot{m}$ (mA equivalent), d_o (mm), and I_D(A).

A reasonable assmuption for the ion and neutral temperature (T_i and T_o) in the ion production region is that they are both equal to the surface temperature T_s of the emitting portion of the insert. This assumption is based on estimates which show that the energy exchange mean free paths for ion-ion, ion-neutral, and neutral-neutral collisions are small compared to the dimensions of the ion production region and that these particles are in much better thermal contact with the insert surface than with the electrons. These arguments will be presented in more detail in the section describing the plasma production processes where the various mean free paths and collisional processes are discussed. In calculating the neutral density from Eq. 3, the electron temperature in the ion production region can be assumed to be 0.71 eV (8240^oK). The electron and ion densities must be approximately equal ($n_e \approx n_i$) since the plasma must be quasi-neutral. Using the above assumptions, Eq. 3 can be solved for the neutral density in the ion production region to give

$$n_o = \frac{P - n_e \; k(T_e + T_s)}{k \; T_s} \tag{5}$$

where n_e is the electron density, T_e is the electron temperature, T_s is the emission surface temperature, k is Bottzmann's constant, and P is the pressure estimated from Eq. 4. It is worthwhile to point out here that the electron density ($n_e \sim 10^{14}$ cm^{-3}) is generally about two orders of magnitude smaller than the neutral density ($n_o \approx 10^{16}$ cm^{-3}).

Therefore, even though the electron temperature ($T_e \approx 8240^oK$) is considerably larger than the ion temperature ($T_i \approx T_s \sim 1300^oK$), the partial pressure of ions and electrons (Eq. 3) is only about 5% of the total pressure; and, at least for a first approximation, the term $n_e k(T_e+T_s)$ in Eq. (5) can usually be neglected.

Although no attempt will be made here to formulate an analytical model for predicting the internal pressure, there are a number of experimental results that provide some insight into the physical processes which cause the internal pressure to rise when the discharge current is increased at a constant flow rate. The important factors affecting this increase appear to be: 1) the increase in the heavy particle stagnation temperature as the current increases, and 2) the backflow of ions through the orifice. The ion backflow is due to a slight electric field which propels ions upstream. This effectively increases the neutral mass flow required and results in a collisional drag force on the neutrals. These factors will be discussed in more detail along with the related experimental results in a section dealing with the orifice region in Chapter VI.

The Internal Plasma

An understanding of the plasma production processes in the hollow cathode is important. The preliminary experiments indicated that volume production of electrons could account for as much as 25% of the total discharge current. Furthermore, the plasma discharge produced by these volume processes is needed to sustain the surface production of electrons. It provides the energy which maintains the insert surface temperatures necessary for thermionic emission and provides the electric field which enhances this emission.

This section will discuss the collisional processes which are responsible for the formation of the plasma and will then present a method for estimating the extent of the ion production region and the number densities of the important particle species in the plasma. Energy balances related to these processes will also be discussed and used to predict the plasma properties in this region.

Collisional Processes

Considerable insight into the nature of the internal plasma processes can be gained by looking at the collision rates associated with various reactions occurring in the ion production region of the cathode. Table II lists energy exchange mean free paths and collision frequencies estimated for the set of typical plasma conditions given in Table I. The first column in Table II lists the reaction followed by the designations which will be used as subscripts on the parameters when they are referred to in the text. The first and second subscripts refer respectively to the projectile and target specie. The mean free paths are expressed in fractions of an insert diameter based on the 4 mm insert diameter of the test cathode. The electron reactions in the table are for the primary (surface emitted) electrons having an energy of 9 eV, which is the energy they would pick up by acceleration across the plasma sheath for a plasma potential of 9 volts. The electron-electron reaction in the first row of the table refers to primary electrons colliding with the background population of thermalized or Maxwellian electrons.

Table II

Energy Exchange Mean Free Paths and Collision Frequencies

Reaction	Type of Energy Exchange	Normalized Mean Free Path (λ/d_{in})	Collision Frequency (ν)
elec*-elec (ee)	elastic	1.6	$3x10^8$
elec*-ion (ei)	elastic	$6x10^5$	$7x10^2$
elec*-atom (eo)	elastic	$1x10^4$	$3x10^4$
ion-ion (ii)	elastic	$6x10^{-4}$	$2x10^8$
ion-atom (io)	elastic	$2x10^{-2}$	$6x10^6$
atom-atom (oo)	elastic	$2x10^{-2}$	$6x10^6$
atom-ion (oi)	elastic	3	$3x10^3$
elec*-effective (e)	elastic	1.6	$3x10^8$
ion-effective (i)	elastic	$6x10^{-4}$	$2x10^8$
atom-effective (o)	elastic	$2x10^{-2}$	$6x10^6$
elec*-inelastic (In)	inelastic	0.20	$2x10^9$

*Primary electron

The three entries between the dashed lines are effective or overall values for the indicated projectile species and are based on the individual reactions shown in the upper part of the table. The last entry in the table is for inelastic collisions of the primary electrons. It is based on the dominant inelastic collision reactions possible for an electron with a mercury atom and is a result of calculations which will be discussed in the next section.

Energy input to the ion production region is mainly through the current of primary electrons. This energy is given up by collisions of these electrons with other electrons and with ions and atoms. The

results of Table II can be used to trace the transfer of the kinetic energy of the incoming primary electrons to other species in the plasma and to ascertain the relative importance of the various reactions.

For primary electrons, the largest collision frequency is that for inelastic collisions ν_{In}. This suggests that much of the initial kinetic energy of the primaries is transferred into potential energy by excitation of mercury atoms in the plasma. Most of the remainder of the primary electron kinetic energy is transferred preferentially into the kinetic energy distribution of the background electron population. This can be seen by comparing ν_{ee} with ν_{ei} and ν_{eo}. The collision rate of primaries with other electrons (ν_{ee}) is at least four orders of magnitude greater than the collision rate with either ions (ν_{ei}) or neutrals (ν_{eo}). In addition, the elastic collision cross-section for an electron-electron collision is proportional to the inverse square of the projectile electron's energy. Therefore, once a primary electron gives up energy, either by small angle elastic or by inelastic collisions its collision rate increases and it is rapidly thermalized, losing its identity as a primary. On the other hand, because of the relatively low collision rate between electrons and heavy particles (ν_{ei} and ν_{eo}), there is little kinetic energy exchange between the electrons and the heavy particles. This means that the bulk of the plasma electrons will be in thermal equilibrium with themselves. The ions and neutrals, however, have very high collision rates among themselves ($\nu_{ii}, \nu_{io}, \nu_{oo}$ are $>10^6 s^{-1}$) and their mean free paths are small compared to the cathode dimensions ($\lambda < 0.02\ d_{in}$). It is a reasonable assumption, therefore, that these heavy particles are locally in thermal equilibrium with themselves. The neutral density analysis presented in the previous

section assumed that their equilibrium temperature was the local wall temperature. This can be justified by looking at the average collision rate with the cathode wall. For typical cathode flow rates, a heavy particle will experience a collision with the wall n the average every 0.005 mm of axial distance as it traverses the cathode. This respresents about 400 collisions over the ~2 mm emitting length of the insert. Since insert temperature gradients in this region are relatively small, it appears that for reasonable values of the accomodation coefficient the assumption of thermal equilibrium between the heavy particles and the wall is valid.

Even though the heavy particles are in equilibrium with themselves at a temperature near the wall temperature, they are influenced by the energy of the primary electrons. This is so because the local plasma conditions such as plasma density and plasma potential influence the local wall temperature. This represents an indirect method of transferring the primary electron energy via potential energy of excitation, into the thermal energy distribution of the heavy particles. This situation in which heavy particles are in thermal equilibrium with the wall while electrons are in equilibrium at a much high temperature is typical of plasma discharges such as the hollow cathode discharge.

Criteria for determining the location and extent of the ion production region are essential for modelling the hollow cathode. Primary electron collisional processes can provide insight into this problem as well. Primary electrons enter the production region with radial trajectories due to their acceleration across the plasma sheath. They would tend to oscillate between opposite walls of the cathode until they had a collision except that there is also a small axial electric

field which accelerates them toward the orifice. Since the plasma is sustained primarily by the excitation reactions of the primary electrons and these electrons are perferentially directed toward the orifice, it is reasonable to expect that the ion production region will establish itself adjacent to the low work function surface closest to the orifice. Therefore, during normal cathode operation with an insert having uniform surface conditions, the emission would be expected to take place on the downstream end of the insert, as found experimentally.

As discussed above, a primary electron is quickly thermalized and loses its identity as a primary once it has had an energy exchange collision. This suggests that the extent of the ion production region might be expected to be on the order of the primary electron mean free path. Primaries can lose energy both by elastic collisions over a mean free path of λ_e and by inelastic collisions over a mean free path of λ_{In}, so the effective mean free path for the loss of a primary electron would be

$$\lambda_{pr} = (1/\lambda_{In} + 1/\lambda_e)^{-1}. \tag{6}$$

From where they are created, primary electrons will be scattered upstream to some extent by elastic collisions. Therefore, a reasonable criterion for the length of the ion production region is probably one to two primary electron mean free paths. Based on the values in Table II, the primary electron mean free path λ_{pr} is ~0.7 mm. This gives an emission length of L_e of 1.4 mm if the ion production region is assumed to have a length of $2\lambda_{pr}$. A length of $2\lambda_{pr}$ was also found to give the best agreement with additional experimental results which will be presented in Chapter VI. The criterion for the emission length L_e is,

therefore, chosen to be

$$L_e = 2\lambda_{pr} \tag{7}$$

For design purposes, it would also be useful to have a criterion for selection of the insert diameter. To most efficiently utilize the cylindrical volume of the ion production region, primary electrons should have a mean free path on the order of the insert radius so that they can reach to the centerline of the cathode before giving up their energy by collision. However, for a primary electron to have a mean free path larger than the insert radius would not be very efficient, because the primary would have a high probability of being lost through the orifice before either exciting a neutral atom or depositing its energy into the Maxwellian electron distribution. Such an argument regarding the loss of primary electrons is similar to the one proposed by Krishnan [1] as an explanation for the location at which the active zone establishes itself in large diameter argon hollow cathodes. It also agrees with experimental results reported by Lidsky, et al. [15] for an open tube cathode. Working with a number of different gases (H_2, H_e, A, N_2), Lidsky determined experimentally that the emission region locates itself where the local pressure-diameter product is ~ 1 Torr-cm. A pressure-diameter product of this magnitude corresponds to a primary electron mean free path on the order of the cathode radius. In the open tube cathode, the local pressure varies significantly along the tube and presumably the active zone locates itself where conditions are most favorable for efficient ion production. In the orificed hollow cathode, on the other hand, most of pressure drop occurs across the orifice plate so that the pressure within the tube is rather constant along the axis

of the cathode and can be adjusted independently without significantly affecting the emission location, which is normally at the downstream end of the insert. While the internal pressure does not affect this location, it is reasonable to expect that efficient operation would be obtained for a pressure-diameter product similar to the one which determines the location of the active zone in the open tube cathode. This is in agreement with experimental results [9] for a mercury orificed hollow cathode which show that a keeper/discharge voltage minimum will occur at a pressure-diameter product of a few Torr-cm. This corresponds to an insert radius of a few mean free paths.

The above discussion suggests that, for design purposes, the insert should be chosen to have a radius on the order of a few primary electron mean free paths. This would correspond to an insert radius which is about the same as the emission length and an ion production region which has an aspect ratio (D/L_e) of approximately two. Such an aspect ratio is also convenient with regards to application of the model since it should result in an ion production region with fairly uniform plasma properties (a basic assumption of the model).

The primary electron mean free path criterion as well as the concept of an ion production region are clearly idealizations. The extent of the ion production region in reality will not be sharply defined; properties will not be uniform throughout the region and ionization will occur upstream of the boundary. In addition, ions produced in the region will diffuse upstream, heating the insert in the region upstream of the boundary. So far the diffusion of ions upstream has not been discussed; although to be consistent with the proposed model, the plasma density must fall off rapidly upstream of the

boundary. If this were not the case, significant ion heating of the insert and related electron emission would be expected to occur upstream of the boundary defined by the mean free path criterion. Experimental plasma density profiles show that, in fact, the axial plasma density drops off exponentially in the upstream direction. This suggests that ion heating will not extend far upstream of the ion production region and is consistent with the rapid fall off in surface temperature upstream of the emission region.

Excited State Densties and the Primary Electron Mean Free Path

In order to estimate the primary electron mean free path λ_{pr}, it is necessary to know not only the collision cross-sections but also the species density for each of the important inelastic reactions which are probable in the ion production region. These species densities will also be needed for the energy balances discussed at the end of this chapter and for estimating secondary electron emission currents in Chapter IV. Peters [16] has compiled the necessary collision cross-section data and developed a computer model which calculates excited state densities for a mercury discharge. Peters' model was originally developed for predicting double ion densities in ion thruster discharge chambers. However, the general analytical method which he used is also applicable to the ion roduction region of the hollow cathode and appears to yield reasonable results for this application. The model is used here to estimate excited state densities and the primary electron mean free path in the hollow cathode ion production region. Peters' original work contains a detailed description of his analytical model and a complete listing of his computer program, so only a brief summary of his method and the required input to the model will be presented here.

The various reactions which are considered in the model are shown schematically in Fig. 8 which is taken from Peters' paper. The species included in the model were selected because they have substantial electron impact cross-sections of formation over the electron energy range of interest and, therefore, would be produced in relatively large numbers. The symbols used in Fig. 8 represent the following species:

H_g^o - neutral ground state mercury

H_g^m - metastable neutral mercury (6^3P_o and 6^3P_2 states)

H_g^r - resonance state neutral mercury (6^3P_1 and 6^1P_1 states)

H_g^+ - singly ionized ground state mercury

H_g^{m+} - singly ionized metastable mercury ($6^2D_{3/2}$ and $6^2D_{5/2}$ states)

H_g^{++} - doubly ionized ground state mercury

The general scheme of the model is to equate the production and loss rates of each species and then solve the resulting set of equations. Excited species are produced by electron impact involving electrons from both the background Maxwellian population at temperature T_e and from the monoenergetic population of primary electrons. An excited state can be lost by de-excitation at the boundary or by excitation to a higher state by another electron impact. A resonance state is also assumed lost whenever a photon diffuses to the boundary. (A photon produced by de-excitation of a resonance state in the bulk of the plasma is readily absorbed by a nearby ground state neutral atom so does not represent a loss until it diffuses to a boundary.) Volume recombination of ions is neglected. The model assumes that the loss rate of the neutrals is the random thermal flux based on the heavy particle temperature T_s, while ions are lost at the Bohm velocity. Since production of excited states is a volume process and their loss to the walls is a surface phenomenon,

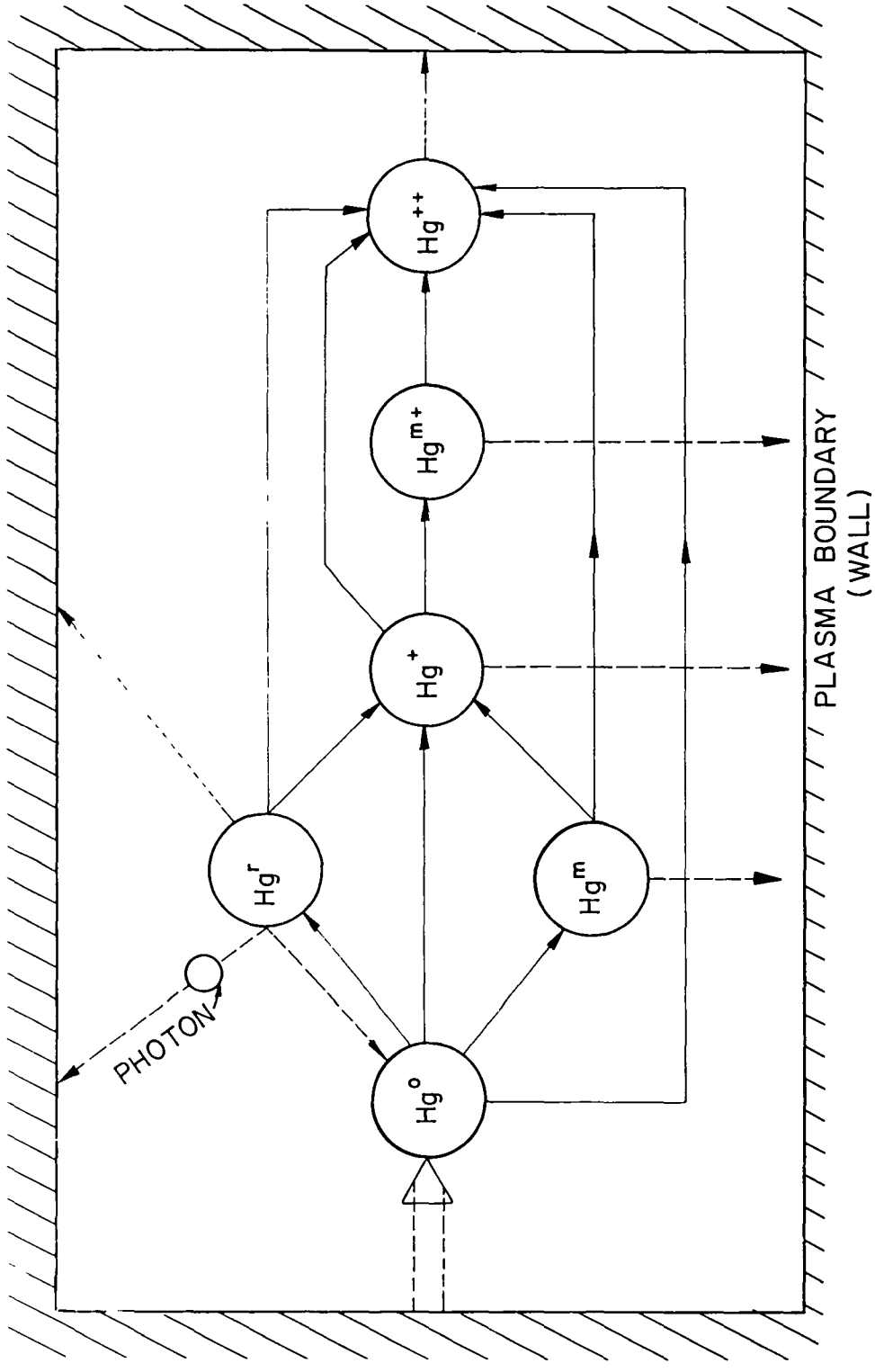

Figure 8. Ion Production Region Reaction Schematic

the production rate is determined by integration over the volume while the wall loss rate is determined by integration over the surface of the ion production region. In order to reduce the integral equations to algebraic equations, the equations are expressed in terms of volume averaged properties; and uniformity factors are introduced which relate the volume to surface averaged properties for each of the excited states. These factors are unity if the temperature and density of the excited states are uniform throughout the volume.

Peters' computer program uses an algorithm based on the above assumptions. Input required by the program are the volume and surface area of the ion production region, the electron temperature of the Maxwellian electrons T_e and their density n_e, the primary electron energy ε_{pr} and density n_{pr}, the heavy particle temperature T_s, and the uniformity factors. Rate factors, which are the collision cross-section times the electron velocity integrated over the electron energy distribution, are also required for each reaction but are contained in a data file included in the program listing. With the above input, the program can calculate the density of each of the excited species considered in the model and the corresponding total neutral atom density. Once the neutral densities are known the inelastic mean free path for primary electrons λ_{In} can also be easily calculated (See Appendix B).

A very useful and rather unexpected result was obtained when the computer program discussed above was used to calculate inelastic mean free paths λ_{In} over a wide range of input parameters typical of hollow cathode conditions. The results of the computations are shown in Fig. 9 where λ_{In} is plotted as a function of total neutral density n_o using

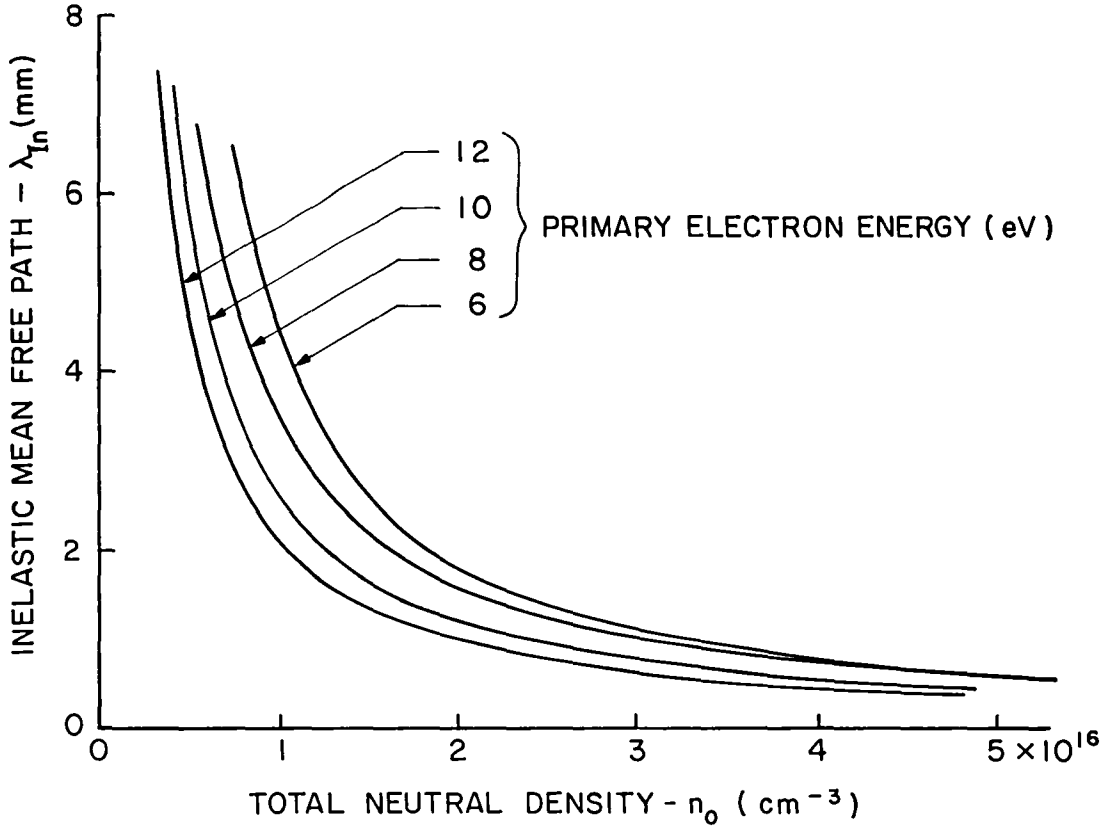

Figure 9. Effect of Total Neutral Atom Density on Primary Electron, Inelastic Mean Free Path

primary energy as a parameter. Although all of the input parameters were varied over a considerable range, the mean free path for inelastic collisions was found to be sensitive only to total neutral density and to primary electron energy. That the mean free path varies with neutral density and primary energy is not surprising since the collision frequency for a reaction is proportional to the target particle density and the collision cross-section (in turn, dependent on the projectile particle energy). However, the effective inelastic mean free path is not dependent simply on the total neutral atom density n_o but on the individual densities of all of the target species, including each of the excited states. To first order, of course, these densities are proportional to the density of the neutral ground state atoms from which they are produced. Since the neutral ground state density is typically 70 to 80% of the total neutral density, it reasonable that the mean free path is most strongly dependent on the total neutral density. However, for a given neutral density, the individual excited state densities and their relative proportions are somewhat sensitive to input parameters besides primary energy. That the mean free path does not reflect this sensitivity is a bit surprising. The reason for this must be due, in part, to the fact that for a given total neutral density, if the density of one neutral excited state increases, then the densities of the ground state and/or the other neutral states must undergo a corresponding decrease. It is believed to be, at least, partially coincidental that these changes precisely compensate one another in calculation of the inelastic mean free path. One minor exception to the above discussion is the Maxwellian electron density n_e which was found to have a slight effect on λ_{In}. However, this effect is rather small amounting to an

increase in λ_{In} of less than 20% when electron density is increased by a factor of five. For our purposes here, this effect can be neglected.

Recognizing that the mean free path varies as the inverse of the neutral density n_o, the results of Fig. 9 can be fit with the following expression

$$\lambda_{In} = \left(\frac{2.83\text{x}10^{23}}{n_o} - 1.5\right) \frac{1}{10^3 \varepsilon_{pr}}. \tag{8}$$

This expression fits the results shown in Fig. 9 over the full range of the parameters within $\pm$ 5% except for values of ε_{pr} equal to 6.0V where λ_{In} is over estimated by ~20% in the intermediate density range. Using Eq. 8 for the inelastic mean free path, the effective primary electron mean free path for energy loss due to both elastic and inelastic collisions can be calculated from Eq. 6, if the elastic mean free path λ_e is known. Since elastic electron-ion and electron-atom collision frequencies (ν_{ei} and ν_{eo} from the previous section) are relatively low, the effective elastic mean free path for energy exchange is approximately equal to the electron-electron mean free path, or

$$\lambda_e \approx \lambda_{ee} = \frac{\varepsilon_{pr}^2}{6.5\text{x}10^{-17} n_e}. \tag{9}$$

Here the expression for λ_{ee} [17] is based on a Coulomb collision between a primary electron with energy ε_{pr} and a low energy Maxwellian electron. Combining Eqs. 6, 8, and 9 the primary electron mean free path for energy exchange λ_{pr} can be estimated as

$$\lambda_{pr} = \left[\frac{6.5\text{x}10^{-17} n_e}{\varepsilon_{pr}^2} + \frac{10^3 n_o \varepsilon_{pr}}{2.83\text{x}10^{23} - 1.5 n_o}\right]^{-1}. \tag{10}$$

These results should prove very useful from the stand point of cathode design calculations. In conjunction, with the criterion presented earlier for determining the length of the ion production region, Eq. 10 provides an easy means of estimating the insert emission length. Of particular importance is the fact that over the normal range of cathode conditions, the results of Eq. 10 are dependent mainly on the neutral density and are not very sensitive to the plasma potential ($\varepsilon_{pr} \approx V_p$ is normally 8-12V) or electron density. This enables one to make a reasonable estimate of λ_{pr} based only on typical plasma conditions and the neutral density.

It is worth pointing out that the curves in Fig. 9 are relatively flat at densities greater than ~2 x 10^{16} cm^{-3} resulting in typical values of λ_{pr} near one millimeter. This is in good agreement with the experiments, which show that for pressures over a few Torr (n_o ~ 2x10^{16} cm^{-3}), the emission is confined to a region ~2 mm long or less on the downstream end of the insert but that the region extends upstream at pressures below a few Torr. Comparison with additional experimental results will be presented in Chapter VI.

In addition to the calculated mean free path λ_{pr}, the other goal of the analysis presented here is an estimate of the excited state densities. All of the input parameters required in order to use the computer program to calculate these densities were determined experimentally except for the primary electron density n_{pr} and the uniformity factors. The primary electron population can be estimated by equating the production and loss rate of primaries, assuming that they are produced by acceleration of surface emitted electrons through the plasma sheath and are lost as soon as they have an energy exchange

collision (See Appendix B). However, at this point, if the uniformity factors are also known, the problem is over specified in the sense that not only the excited state densities but also the total neutral density n_o can now be determined by the computer program. In the present case, the total neutral density can be estimated based on the experimentally determined pressure. Therefore, uniformity factors were simply chosen to give the specified total neutral density n_o. For the typical cathode conditions of Table I and a value of 1.2 for the uniformity factors as input, the computer program yields a neutral density of $3.3 \times 10^{16} cm,^{-3}$ which is the value given in Table I. The corresponding excited state densities calculated by the computer program for these conditions (Table I and uniformity factors equal to 1.2) are shown in Table III. The various species densities are shown in column 2 of Table III followed in column 3 by the density normalized to the total neutral atom density n_o. The designation (m) and (r) following the species designation indicate metastable and resonance states, respectively.

Table III

Excited State Densities for the Operating Conditions Given in Table I.

Species	Density(cm^{-3})	Fraction of n_o
Ground state atom	2.4×10^{16}	0.73
$6^3P_o(m)$	7.2×10^{14}	0.02
$6^3P_2(m)$	3.3×10^{15}	0.10
$6^3P_1(r)$	2.6×10^{15}	0.08
$6^1P_1(r)$	2.1×10^{15}	0.06
Ground state ion (+)	1.8×10^{14}	0.01
$6^2D_{5/2}(+m)$	6.5×10^{11}	~0
$6^2D_{3/2}(+m)$	7.9×10^{11}	~0
Total neutral atom (n_o)	3.3×10^{16}	1.00

It should be noted that uniformity factors equal to 1.2 are reasonable. They correspond to plasma and excited state densities which peak in the center of the production region, or more specifically to a loss rate to the walls which is 0.8 times the rate for a uniform plasma. Higher densities in the center of the plasma are quite possible since ions and excited states can be created anywhere within the volume but are lost mainly at the walls. Additional evidence suggesting a reduced loss rate to the walls will be presented in the energy balance discussion in the next section.

It is, of course, also possible to set the uniformity factors at unity and obtain the specified neutral density by varying one of the other input parameters such as electron temperature. For example, with uniformity factors of unity, an electron temperature of 0.82 eV also results in a neutral density of $3.3 \times 10^{16} cm^{-3}$. This value of the

electron temperature is only slightly outside of the range of the actual measured values shown in Fig. 5. Furthermore, it differs from the value in Table I by only 0.11 eV which is well within the range of uncertainty associated with the data analysis and measurement techniques for the Langmuir probe method used in the experiments. Similar calculations were also made using both the electron density n_e and the primary energy ε_{pr}, separately, as the independent variable while keeping the uniformity factors at unity. In these cases the values required to obtain the specified neutral density were not in reasonable agreement with those in Table I. However, regardless of the parameter chosen as the independent variable (uniformity factor, electron temperature electron density or primary energy), the net results were similar as far as the magnitude of the excited state densities were concerned. Although the relative fractions of the excited states varied somewhat depending on the independent variable chosen, the fraction of the total excited state density to total neutral density was in the range from 0.20 to 0.29 for all of the solutions. The solution based on the uniformity factor of 1.2 was selected for presentation here (Table III) because, of all the input parameters, only the uniformity factors were not experimentally based and were, therefore, somewhat arbitrary.

Energy Balances

Calculations so far have relied on the experimentally determined values of the plasma properties in the ion production region. For a predictive model, it would be desirable to have a means of determining these properties from specified cathode operating conditions. This section will discuss energy balances on the emitting portion of the

insert and on the ion production region and show how in theory these can be used to estimate the electron density and plasma potential.

In order to do the energy balance, it is first necessary to determine the various particle fluxes and currents across the boundaries of the control volume defined by the ion production region. As discussed earlier and shown in Fig. 7, electrons emitted from the insert surface enter the control volume after acceleration across the plasma sheath. In addition, electrons are produced within the volume by ionization reactions. Electrons can leave the volume only through the cathode orifice since they do not have sufficient energy to overcome the adverse potential gradients at the sheath in order to return to the cathode wall. Ions produced in the volume ionization reactions are assumed to leave the volume at the Bohm velocity. There is evidence which will be discussed in Chapter VI that the orifice is also a region of ion production. As such it contributes to the overall discharge current both by ions which are neutralized at the walls of the orifice as well as by ions which are pulled upstream through the orifice into the main ion production region. However, the experiments show that this contribution is small (~5%), and it will be neglected here. Neglecting this component of the current simplifies the analysis considerably since a one to one correspondence can then be assumed between the electrons produced within the control volume and the ions which leave the volume to be neutralized at the wall. This allows the volume production of electrons to be accounted for by the Bohm flux of ions across the control volume surface. Assuming that the plasma properties are uniform throughout the ion production region, the ion current density j_i at the control volume surface is given by

$$j_i = en_i\, v_B$$
$$= en_i(kT_e/m_i)^{1/2} \tag{11}$$

where n_i is the ion density and v_B is the Bohm velocity based on an electron temperature T_e and ion mass m_i. The total discharge current flowing through the cathode orifice is, therefore,

$$I_D = I_e + j_i(A_s) = I_e + I_i \tag{12}$$

where I_e is the electron current emitted from the insert due to all surface emission processes, A_s is the surface area of the ion production region, and I_i is the total ion current crossing the boundary of the region. The surface area of the ion production region is just

$$A_s = A_e + 2A_c \tag{13}$$

where A_e is the insert emission area and A_c is the cross-sectional area of the end boundary of the ion production region.

The Bohm current density j_i can be estimated from an energy balance on the emitting surface. In such a balance, the power due to heating from ion neutralization and de-excitation of excited states is equated to the power conducted and radiated from the surface plus the power removed by emitted electrons. The equation [18] describing this is

$$j_iA_e(V_p + \varepsilon_i - \phi_s) + \dot{q}_{dx}A_e + \dot{q}_{ph}A_e = \dot{Q}_{th} + I_e\phi_e \tag{14}$$

where ϕ_e is the effective work function of the surface, $\dot{Q}_{th}$ is the thermal power transferred away from the surface, V_p is the potential drop across the plasma sheath, ε_i is the ionization potential, ϕ_s is the

work function of the surface material (a material property), and the other terms are as described below. The first group of terms on the left side of Eq. 14 represents the net power deposited at the insert by neutralization of the ion current at the insert surface and assumes that the neutralized ions leave the surface at the insert temperature. The next term $\dot{q}_{dx} A_e$ is the power deposited at the insert surface by de-excitation of the excited states were $\dot{q}_{dx}$ is given by

$$\dot{q}_{dx} = \sum_j \frac{v_{th} n_j \varepsilon_j}{4} . \tag{15}$$

Here v_{th} is the thermal velocity based on the heavy particle temperature T_s, n_j is the density of excited state j estimated in the previous section, ε_j is the excitation energy for state j, and the summation is over all of the excited states. The term $\dot{q}_{ph} A_e$ in Eq. 14 accounts for plasma radiation, such as brehmsstrahlung and resonance radiation, which is absorbed at the insert surface. The term is included for generality, although in most cases it is expected to be negligible. Brehmsstrahlung (due to Coulomb interactions between ions and electrons) is estimated to be very small ($<10^{-5}$ watts); and it will be shown in the section on photoemission that radiation from the decay of resonance states is effectively trapped within the plasma. The terms on the right side of Eq. 14 represent the thermal power lost from the surface $\dot{Q}_{th}$ and the power removed by emitted electrons $I_e \phi_e$. In general, the thermal loss ($\dot{Q}_{th}$ in Eq. 14) is a function of the surface temperature T_s and must be estimated from the specific cathode thermal configuration on the basis of conduction and radiation from the insert. An analysis is presented in Appendix C which estimates $\dot{Q}_{th}$ for the quartz tube test cathode used in the experiments. Equations 12, 13, and 14 can be solved for the Bohm

current density j_1 to give

$$j_1 = \left[\frac{\dot{Q}_{th}-(\dot{q}_{dx}+\dot{q}_{ph})A_e}{\phi_e} + I_D\right]\cdot\left[2A_c+A_e(1+\frac{a}{\phi_e})\right]^{-1} \tag{16}$$

where $a\equiv(V_p+\varepsilon_i-\phi_s)$. Knowing j_1 and assuming the plasma is quasi-neutral ($n_e\approx n_i$), the electron, or plasma density, n_e can be determined from Eq. 11 and is

$$n_e = \frac{j_1}{e[kT_e/m_1]^{1/2}} \tag{17}$$

where T_e is the electron temperature and m_i is the mass of an ion.

The plasma potential can be estimated by a similar energy balance on the control volume which is defined by the ion production region. Energy is convected into and out of this volume by the motion of the various particle species across the boundaries of the ion production region. This particle motion transports not only the random and directed kinetic energy of the particles but also their excitation potential energy. The energy $\dot{U}_{1j}$ transported across surface 1 by particles of type j can be written as

$$\dot{U}_{1j} = (\frac{5}{2}kT_j + \frac{m_1 v_1^2}{2} + e\varepsilon_j)\Gamma_{1j}A_1 \tag{18}$$

where the terms on the right hand side of the equation are respectively, left to right, the enthalpy, the drift kinetic energy, and the excitation potential energy associated with particles of type j having a temperature T_j, a mass m_j, and a drift velocity v_j. In this equation A_1 is the area of a particular surface 1 of the ion production region (e.g., insert emitting area, orifice area, etc.) and Γ_{1j} is the particle flux in one direction across the surface (either into or out of the

volume). The net energy transport associated with a given type of particle is the sum over all of the surfaces i making up the boundary of the ion production region, or

$$\Delta\dot{U}_j = \sum_i (\dot{U}_{ij}(\text{out}) - \dot{U}_{ij}(\text{in})). \tag{19}$$

Using this notation and assuming steady state conditions, the energy balance for the ion production region can be written as

$$\Delta\dot{U}_o + \Delta\dot{U}_i + \Delta\dot{U}_e + \dot{q}_{ph} A_s = 0 \tag{20}$$

where the subscripts (o,i,e) refer to neutral atoms, ions, and electrons, respectively, and A_s is the total surface area of the ion production region. The term $\dot{q}_{ph}$ is the net flux of plasma radiation due to brehmsstrahlung and resonance radiation which leaves the volume. Again the term is included for generality, although it is expected to be negligible.

Before filling in the terms in Eq. 20, it will be useful to discuss Eqs. 18 and 19 for each type of particle, dropping the terms which are small. As a reference for the magnitude of various terms, the electrical power deposited in the ion production region by the primary electrons will be used. This can be estimated as the primary electron current I_e times the plasma potential V_p. The discussion will be based on calculations made for the cathode conditions given in Table I which show a power of ~ 20 watts associated with the primary electrons.

For neutral atoms, including ground state and excited neutrals, the net energy convected into the volume due to the first two terms in Eq. 18 is considerably less than 1% of the total and can can be neglected.

The reason that these terms are small is because the temperature T_j is based on the heavy particle temperature which will in all cases be less than or equal to the insert temperature T_s, resulting in relatively low drift velocities (v_j) and fluxes (Γ_{ij}). This is true even for the sonic region near the orifice where the magnitude of the flow velocity and flux must still be near the thermal quantities based on a temperature of $\sim T_s$. For ground state neutral atoms, the excitation potential energy term is zero. Therefore, only the excitation potential energy term for the excited neutral atoms is of importance, and the net power due to the flux of neutral atoms leaving the volume becomes

$$\begin{aligned} \Delta\dot{U}_o &= A_s \sum_j \frac{v_{th} n_j \varepsilon_j}{4} \\ &= A_s \, \dot{q}_{dx} \end{aligned} \tag{21}$$

where the summation is over all of the neutral excited states and is the same as the one appearing in Eq. 15 where it was represented by the symbol $\dot{q}_{dx}$.

Ions leave the control volume at the Bohm velocity v_B with a corresponding flux based on their density. The enthalpy and drift kinetic energy terms due to this flux of ions are respectively ~0.2 and ~0.3 watts for the conditions of Table I. The ions are neutralized at the surface and return in the ground state. When they return as neutrals, although they have no directed kinetic energy, they have an enthalpy similar in magnitude to that with which they left. This is because they enter and leave at approximately the same temperature. Their net enthalpy flux is, therefore, negligible. Although small, it is convenient to retain in the analysis the drift kinetic energy term

$(m_i v_B^2/2)$ for ions leaving the volume. The potential energy term ε_i for the ions amounts to ~7 watts and must also be retained. The net power associated with the ions leaving the volume can be written as

$$\Delta\dot{U}_i = \left(\frac{kT_e}{2e} + \varepsilon_i\right) j_i A_s \tag{22}$$

where the first term results from the Bohm velocity $v_B = \sqrt{kT_e/m_i}$ and j_i is the Bohm current density. Terms, similar to $\Delta\dot{U}_i$, for excited single ions and for double ions can be neglected because their densities are orders of magnitude lower than the ground state ion density (Table III).

The primary electrons bring into the control volume the kinetic energy that they pick up by acceleration through the plasma sheath $(\dot{U}_e(\text{in}) = I_e V_p)$. Assuming that all of the electrons leaving through the orifice have had sufficient collisions to be thermalized, the power which they remove from the control volume is

$$\dot{U}_e(\text{out}) = \left(\frac{5}{2}kT_e + \frac{m_e v_e^2}{2}\right) \frac{I_D}{e}. \tag{23}$$

The second term in this equation is negligible (~10^{-3} watts) because of the low mass of the electron. The net power due to the electrons is, therefore,

$$\Delta\dot{U}_e = \frac{5}{2}\frac{kT_e}{e} I_D - I_e V_p \tag{24}$$

where I_D is the total discharge current given by Eq. 12, I_e is the electron emission current, and V_p is the plasma potential. Equations 12, 20, 21, 22, and 24 can be solved for the plasma potential V_p to give

$$V_p = \frac{1}{I_D - j_i A_s}\left[\left(\frac{kT_e}{2e} + \varepsilon_i\right) j_i A_s + \frac{5kT_e I_D}{2e} + (\dot{q}_{dx} + \dot{q}_{ph}) A_s\right] \tag{25}$$

where the variables are as previously defined.

Based on the assumptions of the model, Eqs. 16 and 25 provide, at least in theory, a simple means of estimating plasma density and plasma potential. As they stand, however, they do not agree very well with the experimental results. Calculations using the cathode conditions of Table I provide a good example of the difficulties involved and will be used here as a basis for discussing the application of the equations.

For the reasons discussed previously, the radiation term $\dot{q}_{ph}$ in Eqs. 16 and 25 is small and will be neglected. The difficulties in the analysis involve the terms for the power flux associated with the excited states $\dot{q}_{dx}$ and the insert thermal loss $\dot{Q}_{th}$. For example, using the species densities presented in Table III, the power input to the insert due to excited states $\dot{q}_{dx}A_e$ is ~10 watts. The analysis presented in Appendix C estimates the thermal loss $\dot{Q}_{th}$ from the insert to have a probable value of 2.3 W and a maximum conceivable value of 6.7 W. Even using the maximum value of 6.7 W, the Bohm current density j_i calculated using Eq. 16 is negative due to the large value of $\dot{q}_{dx}A_e$. A similar difficulty arises in calculating the plasma potential where the energy loss rate from the volume due to the excited states $\dot{q}_{dx}A_s$ is ~23W which, using Eq. 25, results in a plasma potential of ~14V. This is obviously too large. Similar results are obtained at other operating conditions. These results indicate that the power flux $\dot{q}_{dx}$ associated with the motion of excited states, across the boundaries of the ion production region is probably considerably less than that calculated by the model.

Examination of a number of operating conditions showed that, in general, agreement of Eqs. 16 and 25 with the experimental results required excited atom densities which were 0 to 30% of the values calculated by the computer program. The calculations of the computer

model are believed to be, if not accurate, at least reasonable. The total excited neutral atom fraction of 0.2 to 0.3 calculated with the program is of the order of magnitude expected for this type of discharge; and is supported by the intense line radiation observed spectroscopically in the internal plasma. In addition, the mean free path/emission length agreement based on these densities is reassuring. Much of the cross-section data used in the program was theoretically derived because experimental results were not available. This and other approximations in the computer model could possibly account for calculated densities that are in error by a factor of two or three. It is unlikely, however, that the calculations are in error by much more than this.

Assuming that the calculated densities are, at least, of the right order of magnitude, suggests that either ions and excited neutral atoms do not leave the volume at the rate predicted or, if the particle fluxes are as predicted, the associated potential energy of the particles is either lost at a different rate or is somehow returned to the plasma. Particle fluxes at the boundary could be lower than expected because of density gradients resulting in lower densities near the boundaries. Such gradients have already been accounted for to some extent by the uniformity factor of 1.4 used in the calculations. If the discrepancy in the energy balance is due to such gradients, the uniformity factor would need to be still larger. The net flux of excited atoms across the boundary might also be reduced due to reflection at the cathode surfaces. Although the surface reflection coefficient for excited atoms can take on values greater than 0.5 [19] for light atoms such as helium, it is unlikely that this process is important here. The only data found

for mercury [20] indicate that all mercury excited atoms which collide with a surface are de-excited there. It is also possible that the net flux of potential energy associated with the excited particles does not correspond to the particle loss rate. For example, photons produced by atoms which de-excite near the boundary would be to a large extent reflected back into the volume of the plasma since the reflectivity of tantalum is on the order of 0.8. In this case, the excited atom would be lost but much of its potential energy would be returned to the plasma.

In keeping with the simple nature of the model presented up to this point, the following course is suggested. It will be assumed that the mean free paths and excited state densities predicted by the computer model are reasonably accurate, and that, for whatever reason, the energy loss rate from the volume due to the excited states is less than predicted. Based on these assumptions, the energy flux terms due to the excited states will simply be neglected in Eqs. 16 and 25. This will simplify the analysis considerably, since the densities of the excited states will no longer be required in calculations of the plasma potential and plasma density. The model based on these assumptions will be used as a comparison to the experimental results presented in Chapter VI where it will be seen that, even neglecting these terms, the agreement is reasonably good.

Neglecting the excited state energy flux, the above analysis can provide a rough estimate of the electron density and plasma potential in the ion production region. Of the plasma properties in the ion production region, this leaves only the electron temperature to be determined. The electron temperature is also dependent on the

collisional processes and energy balance. Presumably, one way of determining this parameter would be to select the temperature which gives the specified neutral density and results in excited state densities which are consistent with the energy balances. Considering the uncertainties discussed above regarding the energy and particle fluxes from the ion production region such a method is not expected to be very successful. Fortunately, the model is not very sensitive to the electron temperature over its range of possible variation. It is suggested, therefore, that the experimentally determined value of 0.71 eV be used in the calculations. This value was found to hold within $\pm$ 0.1 eV over a wide range of cathode conditions and should give satisfactory results for calculations based on the proposed model.

The key relationships and assumptions of the model can now be summarized. Electrons are produced both by surface emission from the downstream end of the insert and by volume ionization within the idealized "ion production region". The "ion production region" is defined as the volume circumscribed by the emitting portion of the insert. It is assumed to have a length L_e which is equal to two primary electron energy exchange mean free paths; and all properties (densities, temperatures, etc.) are assumed to be uniform throughout the region. The heavy particles - neutral atoms and ions - are assumed to be in equilibrium at the emission surface temperature and the electrons are in equilibrium with themselves at a higher temperature, which is assumed to be the experimentally determined value of 0.71eV. The plasma density and plasma potential are determined by two energy balances: one on the insert surface and another on the volume of the ion productin region. In performing these energy balances the ions are assumed to leave the

region at the Bohm velocity, and the energy term associated with the thermal flux of excited state atoms is neglected. The neutral atom density is required by the model in order to estimate the primary electron energy exchange mean free path. This density is determined using the ideal gas law and an empirical expression which relates the pressure to the propellant mass flow rate, orifice diameter, and discharge current.

The model described above is complete except for the determination of the emission current from the insert surface. This will be discussed in the next chapter which covers the various possible emission mechanisms. A summary of the important equations which comprise the model will be presented in Chapter V.

IV. SURFACE EMISSION PROCESSES

The electrons required to maintain the internal discharge may be produced at the cathode or insert surface by any one, or a combination, of the five surface emission processes: simple thermionic, field-enhanced thermionic, field, photo electric, and secondary emission (induced ions and excited states). The importance of each of these processes to hollow cathode operation has been a vigorously debated topic and is central to our understanding of the cathode. This section will discuss each of these processes, the extent to which they may be important in hollow cathodes, and how thev can be incorporated into the model. An experiment will then be described which provides additional support for the conclusion that field-enhanced thermionic emission is the dominant surface emission process for this type of cathode.

Simple Thermionic Emission

As a metal is heated, electrons in the conduction band pick up sufficient thermal energy that some of them can overcome the surface potential barrier and escape from the surface. This "boiling off" of electrons from the surface is known as thermionic emission. The current density of emitted electrons is given by the Richardson-Dushman [18] equation

$$J_{th} = a_o T_s^2 \exp\left(-\frac{e\phi_s}{kT_s}\right) \tag{26}$$

where $a_o = 1.2\text{x}10^6$ A/m^2 $^oK^2$ is a theoretical constant, ϕ_s is the surface

work function in eV (a measure of the surface potential barrier), and T_s is the surface temperature in ^oK. It is readily observed with all steady state, hollow cathodes that discharge current increases are accompanied by increases in cathode surface temperatures. Thus, even the earliest work on hollow cathodes suggested that some form of thermionic emission could play a role. The main question has always been whether the surface temperature is consistent with the work function and surface area available for emission. In the present case, since the insert emission current densities and temperatures could be measured, it was possible to estimate the surface work function which would be required to account for all of the emission current by thermionic emission. The preliminary experiments in this study showed that values of the surface work function ranging from 1.7 to 2.0 eV would be necessary for all of the current to be accounted for by thermionic emission. These values, though low, are not unreasonable for tantalum coated with R-500. Fomenko [14] in an excellent summary of work function data gives values ranging from 1.5 eV for tantalum coated with barium oxide to an average value of 2.7 eV for various barium and strontium tantalates. Although it is possible to argue that simple thermionic emission is the dominant surface emission process there is evidence that suggests this process may be enhanced by the presence of strong electric fields at the surface.

Field-Enhanced Thermionic Emission

When a strong electric field is present adjacent to the surface of a material emitting thermionically, its effect is to reduce the work function of the surface; that is, it acts to pull more electrons from the surface than would be expected from the thermionic model for the

prevailing temperature. The average effective work function of the surface then becomes

$$\phi_e = \phi_s - \left[\frac{e|E|}{4\pi\varepsilon_o}\right]^{1/2} \tag{27}$$

and the emitted current density is given by the Schottky equation which is simply Eq. 26 with the surface work function ϕ_s replaced by the effective work function ϕ_e. In Eq. 27, e is the electronic charge, E is the electric field adjacent to the surface, and ε_o is the permitivity of free space.

In the ion production region, the very dense plasma ($\sim 10^{14} cm^{-3}$) results in a very thin plasma sheath ($\sim 10^{-7}$m) which suggests that a very strong electric field should be present at cathode potential surfaces. A first order estimate of this field can be obtained using

$$E = -\frac{dV}{dx} = -\frac{V_p}{\lambda_D} = -V_p\left[\frac{n_e e^2}{\varepsilon_o\ kT_e}\right]^{1/2} \tag{28}$$

where V_p is the plasma potential, T_e is the electron temperature and the sheath thickness is estimated as one Debye length (λ_D). For the plasma conditions in Table I, this would indicate an electric field of 1.9×10^7 V/m and would give an effective reduction of 0.16 eV in the surface work function. A field-enhancement effect of this magnitude is substantial and would result in a four fold increase in the thermionically emitted current for a surface operating at 1000°C.

This order of magnitude calculation indicates that the field-enhancement effect could be significant in the hollow cathode. However, before applying this result, two questions need to be addressed. First, for the very small Debye lengths and low electron temperatures in the

ion production region, are the standard plasma criteria satisfied? These plasma assumptions are implicit for equations such as Eq. 28. Secondly, what is the effect of emitted electrons on the surface electric field?

For a ionized gas to have the collective properties of a plasma two criteria must be met. The Debye length λ_D must be much less than the smallest dimension of the plasma. This criterion is easily satisfied in the hollow cathode where typical dimensions are on the order of a millimeter while the Debye length is ~ 10^{-4}mm. The other criterion is that the plasma parameter or number of particles N_D in a "Debye sphere" must be large, that is

$$N_D \ggg 1 \tag{29}$$

where

$$N_D \equiv \frac{4}{3}\pi\lambda_D^3 n_e$$
$$= \frac{4\pi}{3\, n_e^{1/2}}\left[\frac{\varepsilon_o\, kT_e}{e^2}\right]^{3/2}$$

For plasma conditions typical of the ion production region of the hollow cathode, N_D is approximately seventy. For most plasmas, the plasma parameter N_D is considerably greater than a thousand; so by this criterion the discharge inside of the hollow cathode is borderline for being considered as a plasma. Having said this, it must also be recognized that there is no other reasonable method of approaching the problem except to model the discharge as a plasma which is what has been assumed throughout the development of the model.

At least, in the case of estimating the electric field there is support for making this assumption even in cases where N_D is less than in the present case. Porotnikov and Rodnevich [21], using a statistical

analysis, calculate the average electric field near a cathode surface due to a collection of charged particles. They show that, even for N_D as low as ~ 0.1, the average electric field is approximately the same as that calculated on the basis of plasma assumptions using Poisson's equation.

If the plasma adjoins a cathode surface which is emitting electrons, such as by thermionic emission, a double sheath is formed between the surface and the plasma. This double sheath is characterized by a region of net negative charge close to the emitting surface where the emitted electrons are moving slowly and their density is high. Between this negative charge region of the sheath and the essentially neutral plasma is a region of net positive charge. The negative space charge near the surface acts to reduce the electric field from what it would be for a non-emitting cathode surface. Therefore, the approximation given by Eq. 28 for a non-emitting surface over estimates the field adjacent to the insert emitting surface. Prewett and Allen [22] provide a theoretical treatment of the double sheath at a hot cathode surface in which they calculate the normalized electric field ε_c at the cathode surface as

$$\varepsilon_c = \left[4\,\rho_1\eta_o\left[\left(1 + \frac{\eta_p}{\eta_o}\right)^{1/2} - 1\right] - 8\,J_e\eta_p^2 + 2\,\exp(-\eta_p) - 2\right]^{1/2} . \quad (30)$$

The parameters in this equation are normalized in the following manner. The normalized electric field is

$$\varepsilon = -\frac{e\lambda_D}{kT_e}\,\frac{dV}{dx} , \quad (31)$$

the normalized plasma potential is

$$\eta_p = \frac{eV_p}{kT_e} , \tag{32}$$

the normalized emission current is

$$J_e = j_e \left[n_e e \left(\frac{kT_e}{m_e}\right)^{1/2} (2\eta_p)^{3/2} \right]^{-1} , \tag{33}$$

the normalized positive ion density at the sheath edge is

$$\rho_1 = 1 + 2\eta_p J_e , \tag{34}$$

and the normalized energy of the positive ions at the sheath edge is

$$\eta_o = \frac{1}{2} \left[\frac{1 + 2 \eta_p J_e}{1 - J_e} \right] . \tag{35}$$

The dimensional parameters in these equations are the emission current density j_e, the plasma electron density n_e, the electron temperature T_e, the plasma potential V_p, the Debye length λ_D and the usual physical constants e, k, m_e. For the range of hollow cathode operating conditions covered in the present study, typical values of J_e and η_p are: $J_e \lesssim 10^{-3}$ and $\eta_p \approx 10$. Under these conditions, the electric field can be approximated based on Eqs. 30 through 35, as

$$E \approx \left[\frac{n_e \, kT_e}{\varepsilon_o}\right]^{1/2} \left[2 \left(1 + 2 \frac{eV_p}{kT_e}\right)^{1/2} - 4\right]^{1/2} . \tag{36}$$

This equation gives an electric field of 3.8×10^6 V/m for the same conditions used in the earlier approximation given by Eq. 28. This is only 20% of the value estimated earlier. It does, however, still represent a reduction of the surface work function by 0.073 eV which would effectively double the thermionic current of a surface at 1000°C. Although not as large an effect as indicated by the first approximation,

field enhancement of the thermionic emission current is probably significant for orificed hollow cathodes.

Field Emission

In the presence of very strong electric fields ($>10^7$ v/m), electrons can be "pulled" out of even cold surfaces by the action of the field alone. This form of pure field emission is also known as cold cathode or auto-electronic emission. Fowler and Nordheim [23] developed the following expression based on wave-mechanics theory for this type of emission:

$$J_e = 1.54 \times 10^{-6} \frac{E^2}{\phi s} \exp(-6.8 \times 10^9 \frac{\phi_s^{3/2}}{E}) \qquad (37)$$

where E is the electric field in V/m, ϕs is the surface work function in eV, and the physical constants have been incorporated into the numerical coefficients to give the current density, J_e in A/m^2. It is readily apparent from the exponential term in this equation that electric fields on the order of 10^9 V/m are necessary to provide significant electron emission by this process. Such large electric fields are three orders of magnitude greater than the electric fields estimated in the previous section for the hollow cathode discharge. Equation 37 has been verified experimentally [18] for very carefully cleaned surfaces. However, it has also been found experimentally that cold emission will start from impure mercury surfaces at lower average electric fields on the order of 10^7 V/m [18]; and Müller [18] found that for tungsten surfaces coated with cesium some measurable field emission could be obtained at electric fields as low as 10^6 V/m. While these experimental values for the onset of cold cathode emission are in the upper range of the surface electric fields estimated for the hollow cathode, it is unlikely that this

emission process is important for steady state, hollow cathode operation.

Photoelectric Emission

Electrons can be emitted from the surface of a metal due to the impingement of photons having energies greater than the work function of the surface. The current density of electrons produced by this photoelectric process depends on the quantum yield, which is the number of electrons emitted per incident photon, and on the photon flux to the surface. An estimate of the magnitude of the photoemission current in the hollow cathode will be presented in the discussion which follows.

The quantum yield is strongly dependent both on the photon energy and on the surface material and its condition. For the electron energies found in the hollow cathode discharge, the only excited states expected in any quantity are those of mercury atoms (Hg I) and single ions (Hg II). Photon energies associated with transitions from these states are all less than 10 eV (wavelength ~ 1200Å). The quantum yield for clean metallic surfaces due to photons with energies less than 10 eV is generally accepted to be less than 10^{-2} [24]. Metals with contaminated surfaces can have higher yields, on the order of a few percent for energies below 10 eV; and BaO and SrO , both of which may be present in cathode inserts, have shown yields reaching 0.1 electron per photon for energies in the 5-6 eV range [24] . It turns out, however, that the quantum yield makes little difference in the present case because the photon fluxes at the cathode surfaces can be shown to be very small.

Only the two optical transitions of mercury between the 6^2P_1 and 6^3P_1 resonance levels and the Hg I ground state need be

considered in in determining the photon flux for the following reasons. Excited states of single ions (Hg II) can be neglected because the single ion density is at least two orders of magnitude less than the neutral density. The density of excited states of ionic species will, therefore, be relatively low compared to those of the atom (see Table III). Of the excited states of the atom (Hg I), only the first four lowest energy levels need to be considered for two reasons. First, most of the discharge energy which goes into excited states of mercury can be accounted for by these four states [25] which is just an indication that their population densities are relatively large (Table III). Secondly, the energies associated with transition from each of these states back to the neutral ground state are larger than for any allowable transition from higher excited states. These states are only ones with energies (4 to 7 eV) sufficiently greater than the work function to give significant quantum yields. Of the first four Hg I energy levels, two are metastables (6^3P_o and 6^1P_2) and can be neglected in photo processes because of their long average lifetimes. This leaves only the two resonance levels (6^3P_1 and 6^1P_1) to be accounted for.

Photons released by de-excitation of resonance levels are quickly re-absorbed. The transport of photons through the plasma can, therefore, be modeled as a diffusion process. From diffusion theory the flux of photons across a plasma boundary can be determined using Fick's Law,

$$\Gamma_p = -D \frac{dn_p}{dx} , \tag{38}$$

where n_p is the photon density and D is the diffusion coefficient for photons given by

$$D = \frac{1}{\left[3\ \tau(n_{gs}\ \sigma_c)^2\right]} \tag{39}$$

Here, τ is the average lifetime of the resonance state atom, n_{gs} is the neutral ground state atom density, and σ_c is the cross section for absorption of the photons by neutral ground state atoms [26]. Using Equations 38 and 39, Peters [16] develops the following expression for the photon flux

$$\Gamma_p = \frac{n_r}{3C}\left[\frac{1}{\tau\ n_{gs}\ \sigma_c}\right]^2 \tag{40}$$

where n_r is the resonance state atom density and C is the speed of light. In developing this equation, Peters assumes that the photon density is uniform in the plasma and decays linearly to zero at the boundary over a distance of one photon mean free path $1/(n_{gc}\ \sigma_c)$. He also assumes that in the plasma the photon density is proportional to the resonance state density and that the constant of proportionality can be expressed as the ratio of the average lifetime of a free photon $1/(C\ n_{gs}\ \sigma_c)$ to the resonance state atom lifetime τ. Using Eq. 40 for the photon flux, the photoemission current from a cathode surface is

$$I_p = \gamma e \Gamma_p A_e = \frac{\gamma e A_e n_r}{3C}\left[\frac{1}{\tau\ n_{gs}\ \sigma_c}\right]^2 \tag{41}$$

where γ is the quantum yield, e is the electronic charge, and A_e is the emission surface area. Equation 41 can be used to estimate an upper bound for the photoemission current from the hollow cathode insert due to photons produced in the ion production region of the cathode. Using the resonance and ground state atom densities from Table III and the known cross sections and lifetimes for mercury [27], Eq. 41 gives

photoemission currents of ~ $10^{-8}\gamma$ for both the 6^3P_1 and the 6^1P_1 resonance states. It is apparent that, even for quantum yields on the order of one, photoemission is not an important process in the orificed hollow cathode. The reason that the photon fluxes and, therefore, possible photoemission currents are so low in the hollow cathode is that the neutral atom density is quite high. This combined with large absorption cross sections ($\sigma_c \sim 10^{-13} cm^2$) causes the photons from the resonance state transitions to be effectively trapped within the plasma. Even, if as suggested by the discussion of excited state energy fluxes, many of the resonance state atoms were to de-excite preferentially very near the surface, the photon flux would not be expected to be large enough to produce a significant photoemission current.

Secondary Emission

The final surface emission process which is possibly of significance in hollow cathodes is that of secondary emission. This process is similar in nature to photoemission in the sense that the emission results from particles colliding with the surface and giving up sufficient energy to free electrons. Secondary emission can result from the impacts of electrons, ions, excited atoms, and ground state neutral atoms. The energy which is given up by the particles in this process can be either their kinetic energy or their potential energy of excitation, or both. The extent to which each of these categories of particles can contribute through secondary electron emission to the hollow cathode discharge current will be discussed in this section.

Secondary electron emission due to the impact of both electrons and ground state atoms can be readily neglected. Generally, plasma electrons cannot make it back to cathode potential surfaces because they

do not have sufficient energy to overcome the adverse potential of the sheath. The number of electron impacts with cathode surfaces and the secondary emission due to these impacts is, therefore, negligible. Ground state neutral atoms arrive at cathode surfaces at a rate determined by their thermal velocities. Although the flux of these particles to the surface is large, they have no excitation potential energy to give up and their kinetic energy for typical cathode temperatures is much too low to produce secondary electron emission.

On the other hand, the flux of ions to cathode surfaces is significant, as is the amount of potential and kinetic energy with which they arrive. Ions have a high probability of being neutralized at the surface, so will pick up at least one electron upon impact. This neutralizing electron leaves the surface bound to the atom and is best considered as the final step of the volume ionization process which had previously produced a free electron in the plasma in creating the ion. However, in addition to completing the circuit for what is essentially a volume electron production process, the ion can also produce unbound or secondary electrons at the surface. This is possible because the ion deposits in the surface both its kinetic energy from falling through the cathode sheath and the potential energy in excess of its neutralization energy. The yield for this process, that is the number of secondary electrons per incident ion, is dependent on both the available energy and the surface material. As with most surface processes the difficulty in estimating the magnitude of the secondary emission current is highly dependent on a knowledge of parameters such as yield coefficients, which often are not available for the material or combination of materials of interest. Yield coefficients for mercury ions on BaO coated tantalum

surfaces are not available but an order of magnitude estimate can be made based on the coefficients for similar materials. For ions with kinetic energies less than a few hundred electron volts, kinetic ejection is negligible and secondary electron emission is predominantly due to potential ejection [19]. The potential ejection yield coefficient for low energy, singly-charged, mercury atoms bombarding a tungsten surface are on the order of 0.01 for surface temperatures typical of hollow cathode operating conditions (~1300°K). Potential ejection of electrons is most strongly dependent on the potential energy of the ion and the work function of the surface. Empirical correlations [28] show that as a first order approximation the yield coefficients for potential ejection increase linearly with the potential energy in excess of that needed to neutralize the ion. For ground state ions, this excess potential energy $\Delta\varepsilon_p$ is the difference between the ionization energy ε_i and twice the surface work function ϕ_s,

$$\Delta\varepsilon_p = \varepsilon_i - 2\,\phi_s. \tag{42}$$

For the R-500 coated tantalum emitting surfaces used in the cathode experiments, a reasonable value for the surface work function is ~ 2.0 eV. This would give an excess potential energy $\Delta\varepsilon_p$ of ~ 6.4 eV for mercury ions for the R-500 coated surface. This is about five times the excess potential energy for Hg^+ on a clean tungsten surface ($\Delta\varepsilon_p$ = 1.4 eV) and suggests that a reasonable value of the yield coefficient γ_i for the emitting surfaces in the hollow cathode would be ~ 0.05 electrons per incident ion. The ion collision rate with cathode surfaces can be calculated based on the Bohm velocity and the plasma density. For typical cathode conditions, this amounts to an ion current (I_i) to cathode surfaces of less than ~ 30% of the total discharge

current. The secondary emission due to ions would, therefore, be approximately five percent of this or less than 2% of the total discharge current.

In the hollow cathode discharge, excited atomic states of mercury (Hg I) have negligible kinetic energy but may have sufficient potential energy to cause secondary electron emission. As discussed in the section on photoemission, only the first four excited levels of the mercury atom (two resonance and two metastable states) are present in sufficient numbers or have sufficient energy associated with them to make them important for surface emission processes. While we have shown that photon fluxes to the cathode surface are negligible because the resonance radiation is effectively trapped in the plasma, both resonance state and metastable state atoms arrive at the wall at significant rates because of their high number density (Table III). Their arrival rate is just their random thermal flux ($nv_{th}/4$), so that the secondary emission current due to excited state atoms is

$$I_{sec} = \frac{v_{th} e A_e}{4} \sum_j \gamma_j \, n_j \tag{43}$$

where v_{th} is the average velocity, n_j is the number density of the excited state, γ_j is the electron yield per excited atom, and the summation is over the four excited states being considered ($6^3P_1, 6^1P_1, 6^3P_o, 6^3P_2$). In Eq. 43, it has been assumed that all of the excited species are at the same temperature and, therefore, have the same thermal velocity v_{th} and that their density is uniform throughout the production region.

In order to estimate the magnitude of emission current using Eq. 43, it is necessary to know the yield coefficient and the number density

of each of the excited states. Again, yield coefficients for this process for the materials used in the cathode insert are not available in the literature but reasonable estimates can be made. The closest applicable data is by Sonkin [29] who found that, for the 6^3P_o mercury metastable on a tungsten surface, the maximum yield for the normal surface conditions of his experiment was one or two electrons per hundred incident metastable atoms. Sonkin found that the yield was highly dependent on the presence of a stable complex of mercury and oxygen atoms on the surface and that, for temperatures of 1000^oC and above, the surface film of mercury was evaporated and yield fell to approximately ten percent of the normal value (i.e., $\gamma_m \sim 0.001$). Assuming that the work function of the surface operating at 1000^oC was approximately that of pure tungsten, the yield coefficient for R-500 coated tantalum used in our experiments can be estimated based on an excess potential energy argument similar to that used for incident ions. For metastables, the excess potential energy is the difference between the excitation energy ε_{ex} and the surface work function ϕ_s, or $(\varepsilon_{ex} - \phi_s)$. For the 6^3P_o metastable state, the excitation energy is 4.68 eV and the ratio of the excess potential energy for a surface with a work function of 2.0 eV to that of clean tungsten (4.52 eV) is $(4.68 - 2.00)/4.68 - 4.52) \approx 17$. Using Sonkin's result of $\gamma_m = 0.001$ for tungsten at 1000^oC gives a yield coefficient of ~ 0.017 electrons per incident metastable atom for our conditions. It is a reasonable assumption that the yield coefficient for resonance states which de-excite at the insert surface can be estimated in a similar manner from the above data. The 6^1P_1 state has the largest excitation energy (6.7 eV) of the Hg I resonance states and would give an estimated yield

coefficient of ~ 0.03. Recognizing that the above arguments are only intended to give an order of magnitude estimate for the maximum value of the yield coefficient, a value of 0.03 will be assumed to hold for potential ejection due to each of the four excited states of mercury being considered here.

Equation 43 can now be used to estimate the secondary emission current due to excited states if the number density of each of the excited species is known. Using the densities from Table III, an average thermal velocity based on a temperature of 1000°C, and a yield of 0.03 electrons per incident excited atom, the maximum secondary emission current due to all excited atomic states is estimated to be of the order of 0.1 A or approximately 3% of the total discharge current.

In summary, it appears that for the orificed hollow cathode most of the surface emitted electrons are a result of thermionic emission probably enhanced to a significant degree by the effect of the strong electric field present at the plasma-surface interface. The only other surface emission process that appears to be of any significance in these devices is that of secondary electron emission due to impacting ions, metastable and resonance state atoms. The potential ejection of electrons associated with this process is expected to account for less than 5% of the total surface emission current. Field emission and photoelectric emission were both shown to be negligible in this type of hollow cathode.

The results discussed above can be used to estimate the total surface emission current I_e which was required in equations such as Eq. 12 in Chapter III. The total surface emission current I_e for the cathode insert will be

$$I_e = I_{th} + I_{sec} \tag{44}$$

where I_{th} is the field-enhanced thermionic emission current based on Equations 26, 27, and 36; and I_{sec} is the total secondary emission current due to both ions and excited neutral atoms. Since the secondary emission current was shown to be small, it will be neglected in future calculations. This is consistent with other approximations made in developing the model and means that calculation of the excited state densities will not be required anywhere in the model.

Surface Work Function and the Emission Mechanism

In the discussion above, the hypothesis that field-enhanced thermionic emission is the dominant surface phenomenon producing electrons is based mainly on calculations showing that the other emission processes play only a minor role. Verification of this hypothesis is important to the proposed model. Direct experimental evidence supporting the suggested emission mechanism has been based primarily on the ability of the model to predict reasonable values of the surface work function (ϕ_s). Based on the results of the preliminary experiments using a cathode with two millimeter long insert segments, the model was used to calculate average surface work functions which were found to be on the order of 1.9 eV and showed a clear linear increase with surface temperature. More extensive work function tests completed subsequent to these experiments gave similar results with surface work functions ranging from 1.8 to 2.2 eV and also increasing linearly with temperature. A surface work function of ~ 2.0 eV is quite reasonable for tantalum coated with R-500 and agrees with tabulated values for these materials. Further, a surface work function which is a

linearly increasing function of the surface temperature is, in fact, expected when the theoretical constant for $a_o(1.2x10^6\ A/m^{2o}K^2)$ is used to calculate ϕ_s from the Schottky equation. In this case ϕ_s is known as the "true" work function as opposed to the "Richardson" work function which is not a function of temperature but relies on an empirically determined value for the constant a_o. The relationship between these two work functions is discussed in Ref. [30].

The experimental results discussed above indicate that the field-enhanced thermionic emission process is, in fact, characterized by a work function that is reasonable because of its magnitude and its linear dependence on temperature. However, these were average results based on a relatively large surface area. Because of this and because the emission current shows an exponential sensitivity to the work function, this evidence alone was not considered sufficient to permit one to state conclusively that field-enhanced thermionic emission was the predominant emission mechanism. It was felt that such a judgement might be made, however, if the actual work function were accurately known for the emitting surface. One method of determining this work function would be to make an independent measurement of the work function of a small sample of the emitting surface without the discharge present. This work function could then be compared with the surface work function of the same sample area calculated using the hollow cathode model based on data from the operating cathode. Because of the extreme sensitivity of the surface work function to contamination and operating history, it was considered imperative that this measurement be made without having to remove the insert from the cathode. An experiment to perform such an in-situ measurement was designed and the basic features of the apparatus

used in the test are illustrated schematically in Fig 10. The sample area for the test was a tantalum "patch" ~ 2 mm square and 0.125 mm thick coated with R-500. The patch had three, 0.25 mm dia. leads including a platinum/platinum-13% rhodium thermocouple pair and a lead for measuring the emission current. The patch was electrically isolated from the insert and the rest of the cathode. The basic procedure for the experiment was to operate the cathode in the normal manner while making measurements of patch temperature, emission current, and plasma properties. The discharge and flow were then turned off and a conventional surface work function test was performed in which the cathode was heated using the external heater and the patch emission current was collected using the auxiliary anode.

This experiment was attempted a number of times without much success because it was very difficult to establish electron emission reliably from the patch while the cathode was operating. This was due to difficulty in maintaining a sufficiently low work function at the patch surface for a long enough period to conduct a complete experiment. The assumption of uniform surface work function and emission current density are idealizations. Apparently the work function of the insert surfaces show rather strong local variations with the emission tending to take place predominantly from sites having the lowest work function. There were occasions when the patch was apparently a low work function site and would emit. However, when this occurred the tendency was for most of the cathode emission to come from the patch. This caused a rather high patch temperature which resulted in a gradual depletion of barium from the patch causing the emission site to shift eventually to another location. It was impossible to complete an experiment with

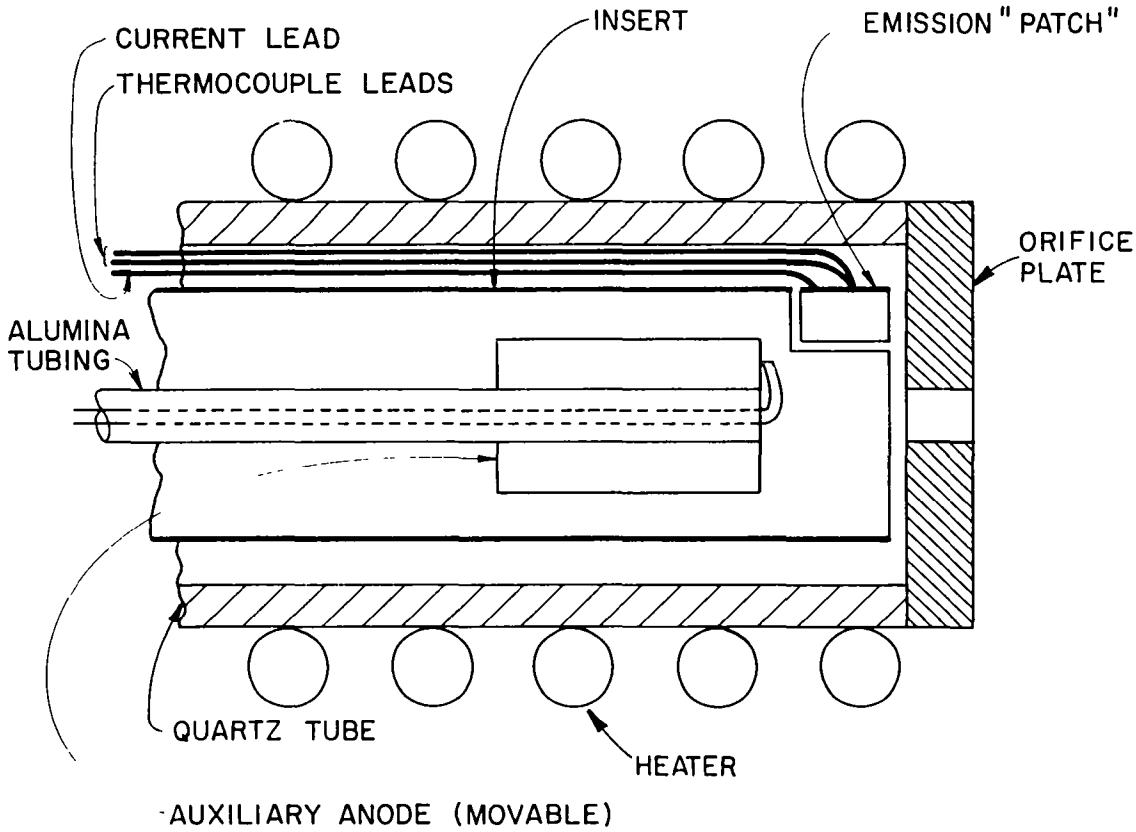

Figure 10. Apparatus for In-Situ Measurement of Patch Work Function

consistent results under these conditions. This problem was finally circumvented by using a separate power supply to bias the patch negative with respect to cathode potential and, thereby, establish electron emission from the patch. The emission process was stimulated when this procedure was followed because the power supply increased the sheath potential drop at the patch. This raised the patch temperature due to increased ion heating and also increased the electric field adjacent to the patch, thereby, increasing the field-enhancement of the emission process. The fact that the patch would not emit under normal conditions is now seen as beneficial because when this occurs the patch can be used both as a probe to sense plasma conditions at the cathode wall (these are necessary inputs to the model) and as a test surface from which electron emission can be measured. The experiment was conducted by operating the cathode in the normal manner and recording a current-voltage characteristic while the patch was biased from -35 v to +5 v above cathode potential. The procedure and data analysis for this are discussed in Appendix D. Using data collected from the patch in the field-enhanced thermionic emission mode, the work function of the surface was computed based on Eqs. 26, 27, and 36. These work function results are shown as the open symbols in Fig. 11. As the figure suggests, this test was conducted three times and at two separate discharge current levels. The solid symbols in Fig. 11 correspond to a conventional surface work function test in which the Richardson-Dushman equation was used to compute the surface work function.

The results shown in Fig. 11 indicate that the test patch had a work function of approximately 2.5 eV with the discharge present and approximately 2.7 eV without the discharge. Considering the exponential

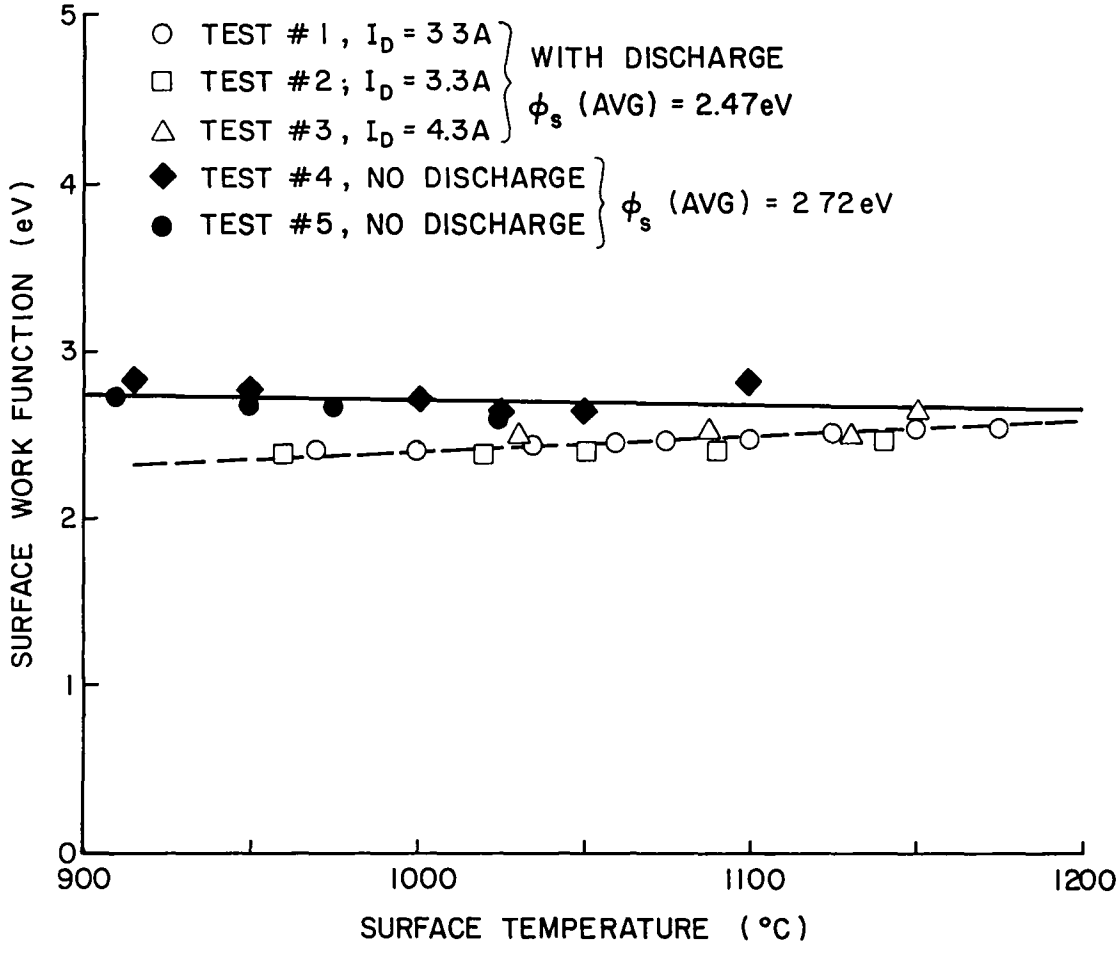

Figure 11. Comparison of Surface Work Function With and Without Discharge Present

sensitivity of the emission current to the work function, the 0.2 eV difference between the work functions for the two cases is quite large. However, some of this difference is probably due to experimental variation in work function. The data in fact show that the work function varied both during the course of an individual test as well as from one test to the next. It was observed for example that the electron emission current at the higher temperatures decreased during the time it took to make a temperature measurement. (See Fig. D.1, Appendix D.) This change became increasingly significant as the negative bias, and therefore, the patch temperature were increased. This decrease in emission current with time indicates an increase in work function probably due to increased sputtering and evaporation of barium caused by higher ion bombardment energies at the higher negative bias. In the extreme case, the barium was apparently depleted to the point where there was negligible electron emission from the patch even if the patch was biased to -35 V, thus indicating a substantial increase in surface work function. This situation is discussed in Appendix D. It was found, when the patch would not emit, that by heating the entire cathode to ~ 1250°C using the external heater the patch surface could be reactivated, presumably by forcing a redistribution of barium from other, normally cooler, surfaces within the cathode. After such a heating cycle the experiment could be continued although the surface work function would be somewhat different than that in the previous test. Such a reactivation procedure was performed between Test #1 (open circles) and Test #2 (open squares). A similar redistribution of barium apparently took place during Test #4 when the cathode was heated to 1100°C by the end of the test and is responsible for lowering the

surface work function from Test #4 to Test #5. The point of this discussion is that the magnitude of the surface work function results in Fig. 11 is seen to vary significantly from one test to the next and that this variation, due to actual surface condition changes occurring between tests, is nearly as great as the variation between the discharge case (open symbols) and the no discharge case (solid symbols).

The fact that the work function with the discharge present was less than the case without the discharge may be attributable in part to the procedure used in running the experiment and analyzing the data. Biasing the patch negative with respect to the other cathode surfaces in order to induce emission may locally increase the plasma density adjacent to the patch. The work function is calculated based on the increase in electron current from the patch as the patch is biased negative. The analysis (Appendix D) treats all of this increase as being due to electron emission while, if the local plasma density is also increasing, then the measured current increase would also be due to the increased ion flux to the surface. There is no way of accounting for this effect in analyzing the data. A local increase in plasma density would also increase the electric field at the surface and, thereby, contribute to an estimate of the surface work function which was lower than its actual value. Finally, the presence of the discharge may truly decrease the surface work function by its interaction with the surface. For example, some barium that would normally evaporate and diffuse to cooler surfaces is probably ionized by electron impact and attracted back to the hot cathode surface, tending to keep the work function of the surface lower than for a surface at the same temperature but not exposed to the discharge.

The purpose of the experiment embodied by Fig. 11 was to compare the surface work function of the test patch calculated using the hollow cathode model with an independently determined value measured when no discharge was present. Consistent agreement between the two values of the work function for a number of such tests could have been considered sufficient evidence to conclude that field-enhanced thermionic emission is the dominant surface emission mechanism for the hollow cathode. The actual agreement obtained between the discharge and no discharge case is not close enough to warrant such a statement. However, it is possible to explain the discrepancy between the two cases on the basis of the experimental considerations discussed above. It is suggested, therefore, that the results support the hypothesis that field-enhanced thermionic emission is the most likely emission process for this type of cathode.

It should be mentioned that the work function of 2.5 to 2.7 eV applies to the test patch which is probably somewhat depleted and, therefore, not representative of the larger tantalum insert surfaces which are coated with R-500. Values in this range (2.5 to 2.7 eV are typical of barium tantalate compounds which are probably present on the surface even after the oxide coating is depleted. It is considered likely that most of the emission in the cathode takes place from regions of the insert where the work function is on the order of 2.0 eV. This average surface work function is typical of the larger surfaces such as the 2 mm long insert segments discussed previously and probably reflects the presence of barium oxide coating. In fact, considering the observed experimental variation in work function and its extreme sensitivity to surface condition, it is probable that average surface work functions of

2.0 eV are obtained as a results of small, localized regions where the work function is even lower.

V. SUMMARY OF MODEL

Before presenting the results of an additional experiment which was performed to test certain assumptions of the model, it will be helpful to present the collection of equations which comprise the analytical model. The equations are shown in Table IV where the first column indicates the physical basis of the equation and the second column notes important assumptions. Table V lists the symbols and units used for the parameters in the equations in Table IV. It should be noted that all of the equations in Table IV are in MKS units EXCEPT for the parameters in the empirical expression for the pressure (Eq. IV.1).

Given the mass flow rate $\dot{m}$, the orifice diameter d_o, the total discharge current I_D, the surface work function ϕ_s, the insert thermal power loss $\dot{Q}_{th}$, and the physical constants (e, k, m_i, ε_o, ε_i, a_o), the equations in Table IV can be solved for all of the other parameters except the electron temperature. As discussed in Chapter III, a value of 0.71 eV is a reasonable assumption for the electron temperature. Because Eq. IV.10 can not be solved explicitly for the surface temperature T_s, the solution of these equations is necessarily iterative. However, the equations generally converge to five place accuracy in six or seven iterations. The results of calculations based on this set of equations will be compared with experimental results in Chapter VI.

Table IV

Summary of Equations Used in Model

Physical Basis	Comments	Equation	No.
Empirical	Neglects orifice plate thickness effect.	$P = \frac{\dot{m}}{d_o^2}\,(13.7 + 7.82\ I_D)\times 10^{-3}$ (Torr) where $\dot{m}$(mA) and d_o(mm).	IV.1
Ideal gas law	Assumes heavy particle temperature equal to insert temperature.	$n_o = \frac{P - n_e\ k(T_e + T_s)}{k\ T_s}$	IV.2
Semi-empirical	Energy exchange mean free path based on results of computer model. Assumes $\varepsilon_{pr} = V_p$.	$\lambda_{pr} = \left[\frac{6.5\times 10^{-17} n_e}{V_p^2} + \frac{10^3 n_o V_p}{2.83\times 10^{23} - 1.5 n_o}\right]^{-1}$	IV.3
Existence length for primary electron	Criterion for emission/ion production region length.	$L_e = 2\lambda_{pr}$	IV.4
Current balance	Thermionic electron emission from insert only; ion flux based on Bohm criterion.	$I_D = I_e + I_i = J_{th}A_e + J_i A_s$	IV.5
Insert energy balance	Neglects energy input due to excited states and plasma radiation.	$J_i = \left[\frac{\dot{Q}_{th}}{\phi_e} + I_D\right]\cdot\left[2A_c + A_e\left(1+\frac{a}{\phi_e}\right)\right]^{-1}$ where $a \equiv (V_p + \varepsilon_i - \phi_s)$.	IV.6

Table IV (cont.)

Summary of Equations Used in Model

Physical Basis	Comments	Equation	No.
Bohm criterion	Assumes uniform or average plasma properties.	$n_e = \frac{J_1}{e[kT_e/m_1]^{1/2}}$	IV.7
Energy balance on ion production region	Neglects energy loss due to excited states and plasma radiation.	$V_p = \frac{1}{I_D - J_1 A_s}\left[\left(\frac{kT_e}{2e}+\varepsilon_1\right)J_1 A_s + \frac{5kT_e I_D}{2e}\right]$	IV.8
Double sheath analysis	Approx. based on theoretical analysis in Ref. [22]. Holds for $J < 10^{-3}$ (J from Eq.33)	$E \approx \left[\frac{n_e\, kT_e}{\varepsilon_o}\right]^{1/2}\left[2\left(1 + 2\frac{eV_p}{kT_e}\right)^{1/2} - 4\right]^{1/2}$	IV.9
Field-enhanced thermionic emission	Model neglects all surface emission mechanisms, except this one.	$J_{th} = a_o T_s^2 \exp\left(-\frac{e\phi_e}{kT_s}\right)$	IV.10
Effective work function	Based on electric field at emission surface	$\phi_e = \phi_s - \left[\frac{e\lvert E\rvert}{4\pi\varepsilon_o}\right]^{1/2}$	IV.11

Table V

List of Symbols and Units

a_o - theoretical constant (1.2×10^6 A/m^2 $^oK^2$)

A_c - area of end boundary of ion production region (m^2)

A_e - insert emission area (m^2)

A_s - total surface area of ion production region (m^2)

d_o - orifice diameter (mm)

e - electronic charge (Coulombs)

E - electric field at insert surface (V/m)

I_D - total discharge current (A)

I_e - insert electron emission current (A)

I_i - total ion current to cathode surfaces (A)

J_i - Bohm current density (A/m^2)

J_{th} - field-enhanced thermionic emission current density (A/m^2)

J - normalized emission current (Eq.33)

k - Boltzman's constant (1.38×10^{-23} J/^oK)

L_e - insert emission length (m)

$\dot{m}$ - propellant mass flow rate (mA equivalent)

m_i - ionic mass (kg/ion)

n_e - electron density in ion production region (m^{-3})

n_o - total neutral atom density in ion production region (m^{-3})

P - internal cathode pressure

$\dot{Q}_{th}$ - insert thermal power loss (W)

T_e - electron temperature in ion production region (^oK)

T_s - insert emission temperature (^oK)

V_p - plasma potential in ion production region (V)

ε_i - ionization potential (10.4V for Hg)

ε_0 - permittivitity of free space (8.85×10^{-12} F/m)

ε_{pr} - primary electron energy, equivalent to plasma potential V_p(eV)

λ_{pr} - primary electron, energy exchange mean free path (m)

ϕ_e - average effective work function (V)

ϕ_s - average surface work function (V)

VI. COMPARISON WITH EXPERIMENT

One of the major assumptions of the model presented here is that most of the hollow cathode current can be accounted for at the boundaries of the ion production region either as electrons produced at the emission surface circumscribing the region or as ions produced within the region and returning to the cathode surfaces at the Bohm velocity. To determine the magnitude and origin of the various hollow cathode currents, an experiment was set up to perform a current balance on all of the cathode surfaces which could contribute to the total emission current. The purpose of this experiment was to account for the current to each surface of the cathode and to determine for each surface the fraction of the current that was due to ion current. The experiment also provided a means of testing other assumptions of the model related to the ion production region such as the emission length criterion, the applicability of the Bohm velocity, and the use of the energy balances for predicting plasma density and plasma potential. In this chapter, the results of this experiment are compared to the predictions of the model and discussed in the context of the assumptions of the model regarding the ion production region and the cathode current distribution.

Current Accounting

The test cathode designed and built to facilitate the measurement of the currents necessary to perform the overall current balance is

shown in Fig. 12. The cathode was fabricated from a quartz tube such that all of the internal surfaces were covered with tantalum foil and each surface of interest was isolated as a separate electrode. The insert was made 2.2 mm long to test the assumption regarding the location and extent of the emission region. Both the insert and the cathode tube were coated with the low work function chemical R-500. This cathode had an inner diameter of 3.9 mm and an orifice diameter of 0.96 mm. The cathode discharge was coupled to a cylindrical anode which was completely enclosed within a stainless steel ground tube covered on its downstream end by a fine mesh screen. The current from each of the surfaces shown in Fig. 12 was measured separately for total discharge currents I_D of 1.3, 2.3, 3.3 and 4.3A at a mercury flow rate ($\dot{m}$) of ~100mA. Data were also collected for an emission current of 3.3 A at internal cathode pressures P ranging from 1.3 to 5.5 Torr. The internal pressure and insert temperature were measured using the procedures described in Chapter II. The ammeters used in making the current measurements were carefully calibrated to the same reference prior to the experiment.

The results of these experiments are shown in Table VI where the currents - I_1, I_2 etc. - are those from the surfaces identified in Fig. 12. The current I_T is the sum of these numbered currents. The results are normalized with respect to the total emission current I_D. It appears that all of the currents necessary to perform the overall cathode current balance are accounted for, because the total of the currents (I_T) agrees with the total emission current ($I_D = I_A + I_K$) within a few percent.

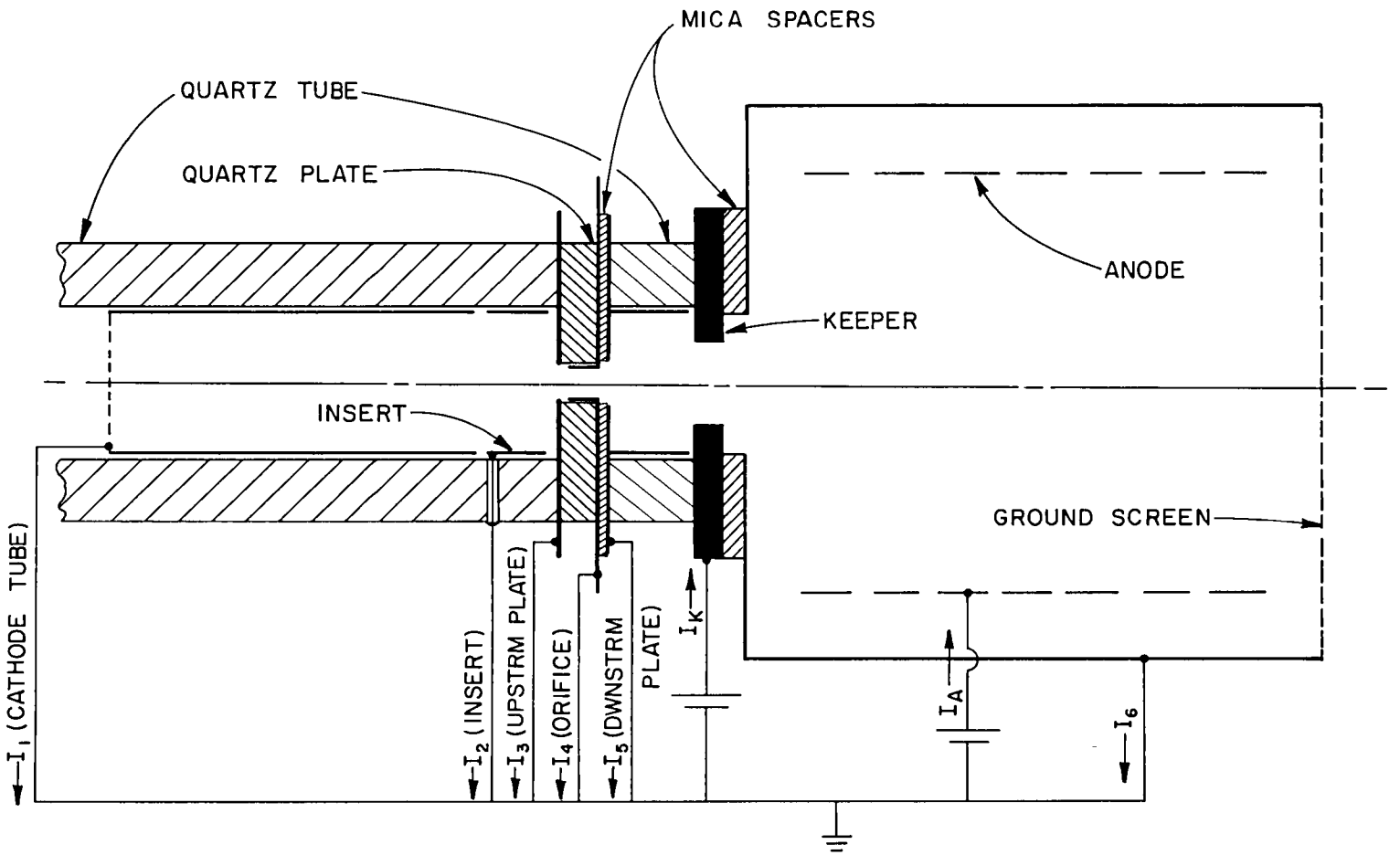

Figure 12. Test Cathode for Current Accounting

TABLE VI

Cathode Current Accounting

$\dot{m}$(mA)	P(torr)	I_D(A)	I_1/I_D (Cathode tube)	I_2/I_D (Insert)	I_3/I_D (Upstm Orifice Plate)	I_4/I_D (Orifice)	I_5/I_D (Downstm. Orifice Plate)	I_6/I_D (Ground Screen	I_T/I_D (Total	T_{insert} (°C)
102	3.6	1.3	0.023	0.846	0.077	0.031	0	0.002	0.980	965
102	4 6	2.3	0.022	0.865	0.070	0 039	0.004	0.002	1.000	1009
106	5.5	3 3	0 021	0.854	0.070	0 052	0.006	0.002	1.003	1039
105	6.2	4.3	0 021	0.844	0.067	0.060	0 006	0.003	1.000	1070
110	5.8	3 3	0.015	0 854	0.073	0 052	0.005	0.002	1.000	1039*
78	4.1	3 3	0.042	0.842	0.073	0 033	0.003	0 002	0.997	1051*
62	3 2	3 3	0.076	0.824	0 070	0.027	0.003	0 002	1.003	1057*
35	1.8	3 3	0.379	0.533	0.054	0 015	0 003	0.002	0.988	1067*
25	1.3	3 3	0.576	0 373	0.042	0.012	0	0.002	1.006	1071*

* These temperatures were estimated from an earlier experiment under similar conditions

TABLE VII

Calculated Ion and Electron Currents to Insert

P(torr)	I_D(A)	$I_2(e)/I_D$ (Insert Electron Current)	$I_2(i)/I_D$ (Insert Ion Current	$I_T(i)/I_D$* (Total Cathode Ion Current)	$n_2(10^{14}cm^{-3})$
3.6	1.3	0.68	0.16	0.30	0 8
4.6	2 3	0 73	0 14	0.28	1.2
5.5	3.3	0.73	0.13	0.28	1.6
6 2	4.3	0 72	0.12	0 28	2.0
5.8	3.3	0.73	0.13	0 27	1 6
4.1	3.3	0.72	0.13	0 28	1.6
3.2	3.3	0 70	0.13	0 31	1.6
1 8	3 3	0.48	0.10	--	1.2
1 3	3.3	0.29	0.08	--	1.0

* $I_T(i) = \sum_J I_J(i)$

One purpose of this test was to determine the origin and relative importance of the various current components of the cathode. The data presented in Table VI indicates that for internal cathode pressures above ~3 Torr the 2.2 mm long insert provided ~85% of the total emission current (I_2/I_D, column 5) which is in agreement with the earlier experiments. Most of the remaining current was accounted for by the upstream surface of the orifice plate (~7%), which forms the downstream boundary of the ion production region, and the wall of the orifice canal (3 to 6%).* In all cases the surfaces upstream of the orifice were responsible for at least 93% of the total discharge current. This supports the assumption of the model that most of the current can be accounted for by considering only the boundary of the ion production region. Note that while the results of Table VI indicate that the insert current (I_2/I_D) decreases for pressures below ~ 3 Torr that the current to the cathode tube (I_1/I_D) undergoes a corresponding increase. This indicates that the emission region is extending upstream along the cathode tube. However, even at these lower pressures where the emission surface extends to cover both the 2.2 mm insert segment and a portion of the cathode tube, the emission surfaces account for 85% or more of the total emission current (I_D).

Ion Currents

The data of Table VI indicate how much of the total emission current is attributable to each of the cathode surfaces but do not show

---

* The fact that the very small surface area of the orifice canal accounts for as much as 6% of the total emission current is felt to be significant. Evidence will be presented and discussed shortly which will suggest that the orifice region is itself an ion production region.

whether these currents are ion currents or electron currents. The proposed cathode model assumes that electron emission takes place only at the low work function insert surface and that the current contribution of the other cathode surfaces is due solely to ion currents to those surfaces. This assumption was tested experimentally by biasing each of the electrode surfaces (except the insert) with respect to cathode potential and observing the effect on the collected current. A typical current-voltage trace obtained from these tests is shown as the solid curve in Fig. 13. This characteristic is essentially the same as the ion saturation region of a Langmuir probe trace. That the curve is approximately horizontal where it crosses the y-axis (i.e., at a cathode potential), indicates that the current is primarily a collected ion current. The current-voltage trace at negative potentials for a surface such as the insert which is emitting electrons thermionically is substantially different than a non-emitting surface and takes the form suggested by the dotted curve in Fig. 13. For a relatively large emitting surface, this response is observed because negative biasing of the surface effectively increases the discharge voltage and, thereby, the discharge current. For smaller surfaces, the effect is due to increased heating of the surface as the potential difference between the surface and plasma potential is increased.

The test described above demonstrates that the surfaces, except for the insert, are neither emitting thermionically nor collecting electron currents in any significant amounts. It does not prove whether or not electrons are being emitted from the surfaces due to photo or secondary emission processes. However, these secondary emission currents for surfaces other than the insert should be less than the secondary current

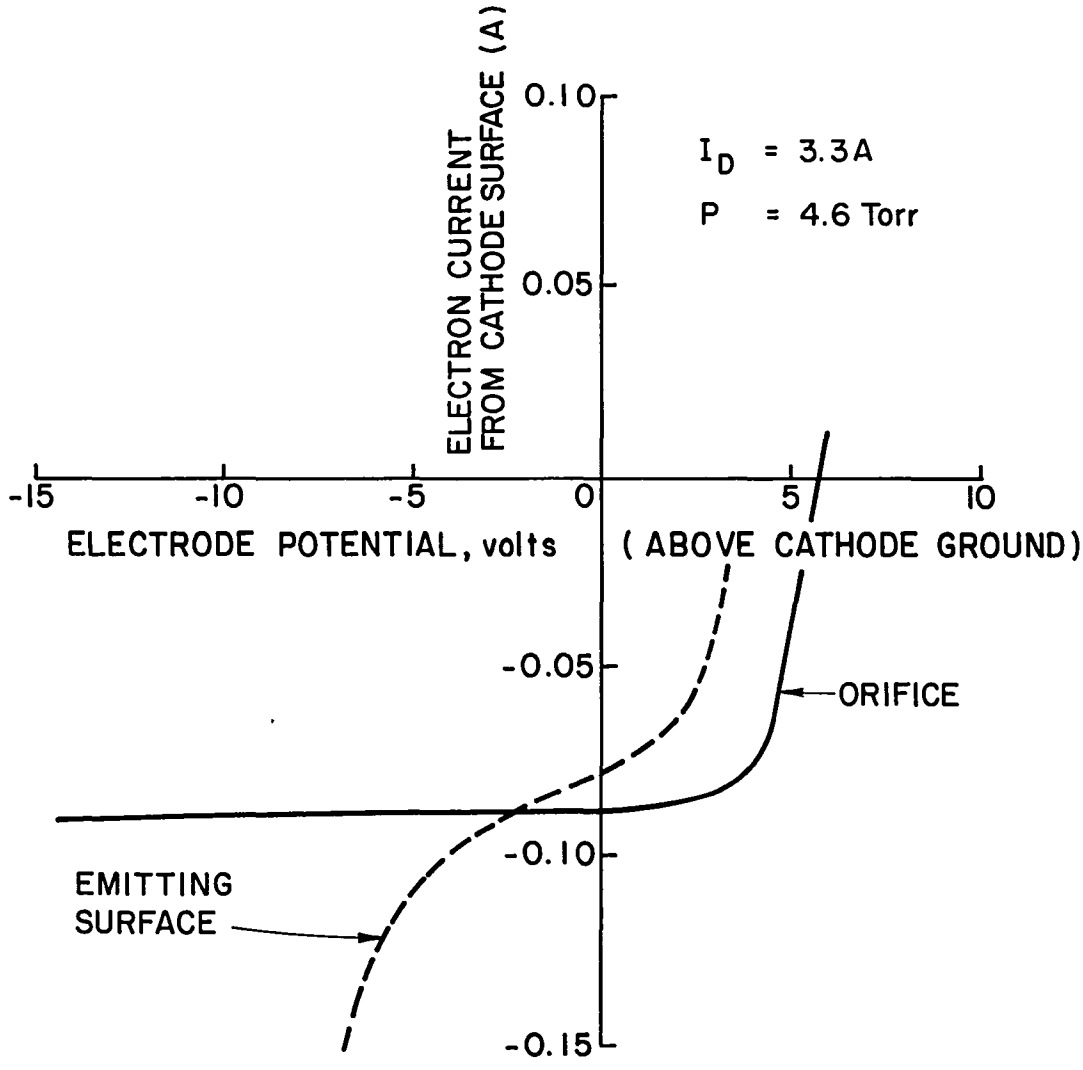

Figure 13. Typical Voltage-Current Characteristic for a Cathode Surface

estimated in Chapter IV for the insert because the work functions of these surfaces are expected to be significantly greater than the insert work function and, therefore, their yield coefficients considerably less. The secondary emission current from the relatively low work function insert was already shown in Chapter IV to be negligible. On the basis of these considerations, currents I_1, I_3, I_4, I_5, and I_6 can be assumed to be ion currents to each corresponding cathode surface.

The data of Table VI can also be used to determine that fraction of the total discharge current due to volume processes (i.e., ion production) and that due to surface electron emission. To do this it is first necessary to separate the collected ion current component of the measured insert current (I_2) from the emitted electron component. The ion current $I_2(i)$ to the insert can be estimated from Eq. 16 based on the insert energy balance. In making this calculation, the thermal power $\dot{Q}_{th}$ was taken from the solid curve of Fig. C.1 in Appendix C based on the insert temperature shown in Table VI. In addition, the other power terms ($\dot{q}_{dx}A_e$ and $\dot{q}_{qh}A_e$) were neglected and the surface work functions (ϕ_e and ϕ_s) were both assumed to be 1.9 eV. The results in the next section, which deals with the model predictions, will show that this is a reasonable value for the work function; furthermore, the calculations are not very sensitive to this parameter over its possible range of variation. The plasma density n_2 adjacent to the insert surface can also be calculated using the value of $I_2(i)$, estimated above, and Eq. IV.7, which is based on the Bohm current density. The results of these calculations are shown in Table VII (on p.109) where the currents are again normalized with respect to the total discharge current I_D. With the estimates of insert ion current $I_2(i)$ shown in the

table, the fraction of the total discharge current which is due to ions collected at cathode surfaces can be calculated. This is shown in the fifth column of the table. The important point to be drawn from this analysis is that the volume production of electrons (as indicated by $I_T(i)/I_D$, column 5) amounts to ~30% and is relatively constant over the rather broad range of cathode conditions in the experiment. The estimates of the plasma density n_2 are also of interest and will be discussed in the next section.

Ion Production Region

The results of this experiment can also be used to check other aspects of the model regarding the ion production region. The model assumes that the ion production region is a region of rather uniform plasma density circumscribed by the emission surface. On the test cathode where the insert is the electron emission surface, the upstream surface of the orifice plate also forms a boundary of the ion production region. Since ions are assumed to leave this region with the Bohm velocity, the plasma density can be calculated from Eq. IV.7 for any surface for which the ion current and the surface area are known. This means that if, in fact, the plasma density in the ion production region is fairly uniform and if the energy balance used to calculate the ion component of the insert current is valid, then the plasma density computed using the ion current to the insert ($I_2(i)$) should be the same as that computed using the ion current to the orifice plate (I_3). Figure 14a shows the plasma density adjacent to the insert (n_2 from Table VII) plotted (circles) as a function of total discharge current for the cathode operating at a mass flow rate of ~ 100 mA. The plasma density based on the ion current to the upstream surface of the orifice

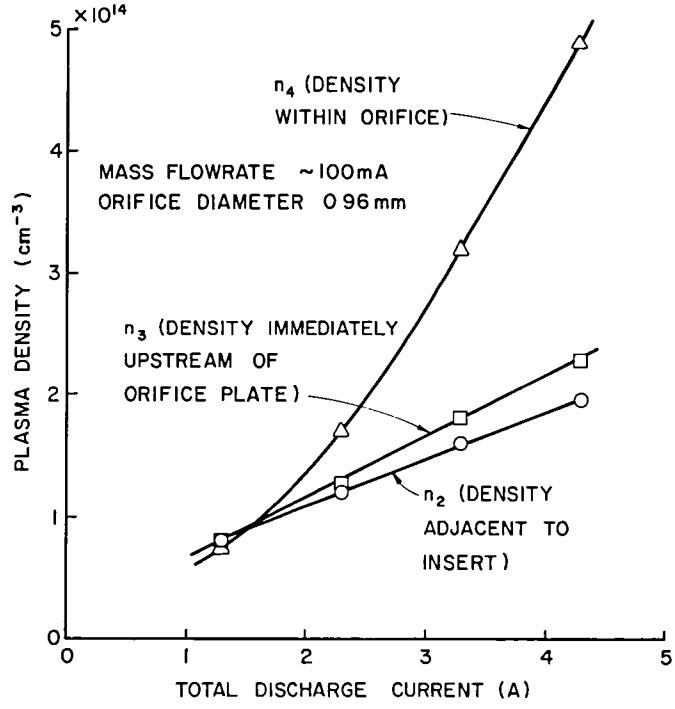

Figure 14a. Effect of Total Discharge Current on Plasma Densities

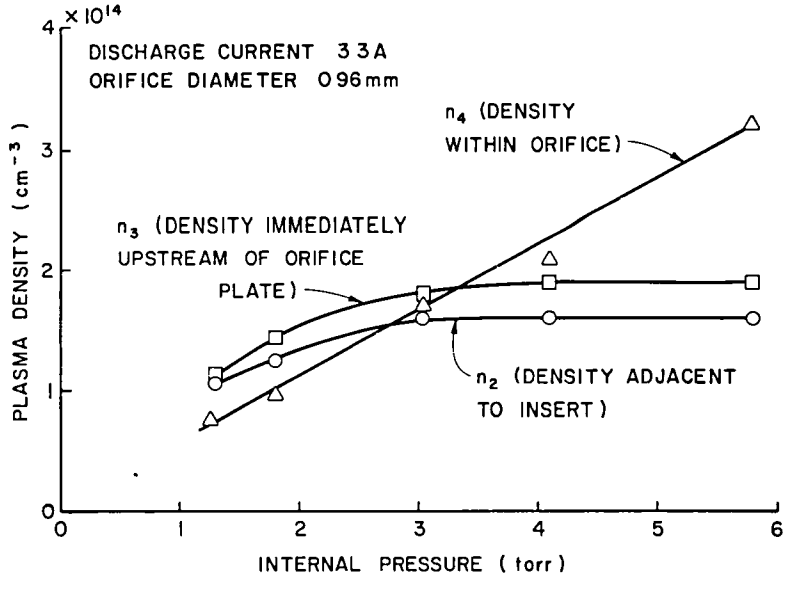

Figure 14b. Effect of Internal Pressure on Plasma Densities

plate (n_3) and to the orifice (n_4) are also plotted in Fig. 14a as the squares and triangles respectively. Fig. 14b shows the same sort of data plotted as a function of internal cathode pressure for a total emission current of 3.3A. In both Figs. 14a and 14b the plasma density adjacent to the insert (n_2) and the plasma density adjacent to the orifice plate (n_3) agree reasonably well both in magnitude and in their dependence on the independent variable. This supports the assumptions discussed above regarding the ion production region and suggests that the energy balance provides self-consistent results for the ion current to the insert. It should also be noted that the plasma densities near the insert (n_2 and n_3) are in agreement with those presented in Fig. 5a based on Langmuir probe measurements made under similar conditions.

Predictions of the Model

A critical test of the model is its ability to predict the length of the insert emission region as this parameter strongly affects the predicted insert surface temperature for a given discharge current and surface work function. The model assumes that the insert emission length is of the order of the primary electron mean free path. The primary electron mean free path λ_{pr} can be calculated with Eq. IV.3 assuming a primary electron energy of 8.7 eV and a neutral density estimated from the measured cathode pressure. The results of this calculation are plotted as the solid curve ($2\lambda_{pr}$) in Fig. 15. Insert emission lengths determined from the experimental results are indicated in the figure as circles. The agreement between the experimental data points and the calculated curve is quite good and supports the assumption of the model that L_e/λ_{pr} is approximately two. The data points above a pressure of four Torr would have been in even closer

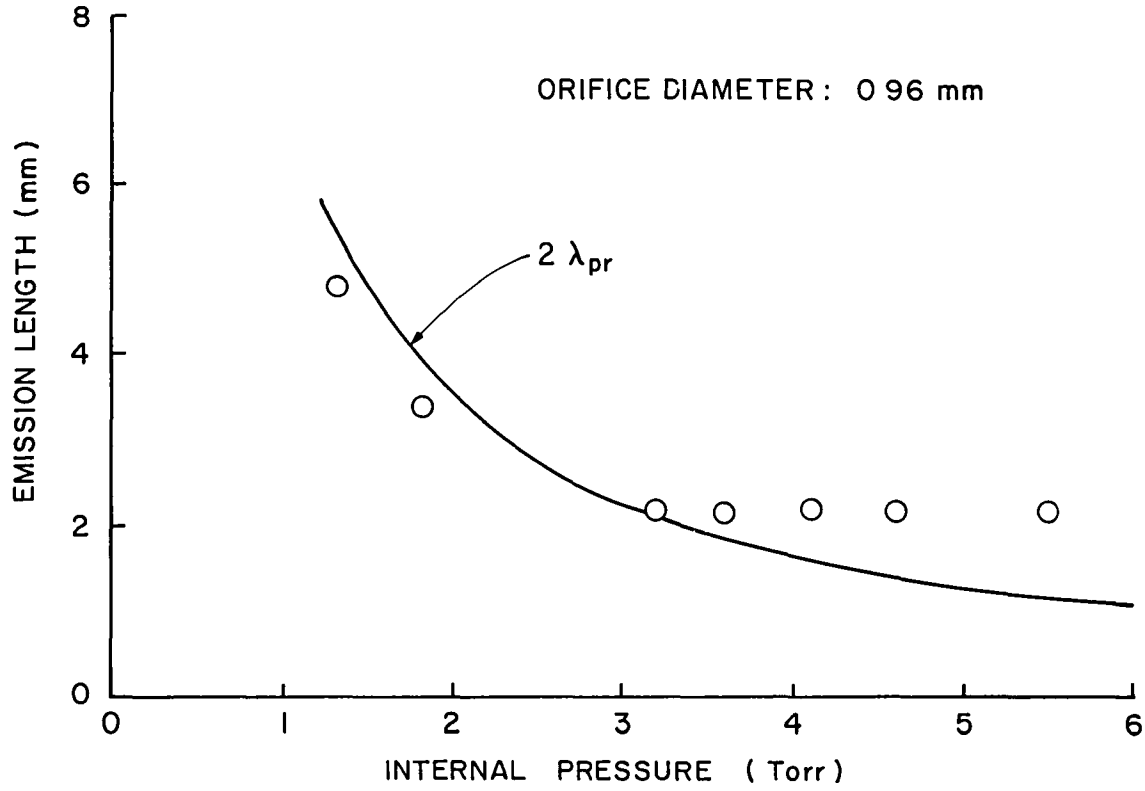

Figure 15. Comparison of Emission Length with Primary Electron, Energy Exchange Mean Free Path

agreement with the curve except that there was no way of discriminating emission lengths shorter than the 2.2 mm long insert segment. (Temperature profiles were not measured in this experiment.) Insert emission lengths, for conditions where emission was taking place from the cathode tube (surface 1), were estimated from the fraction of the current to that surface.

If controllable operating parameters (discharge current and mass flow rate) $\dot{m}$ and the cathode physical configuration (dimensions, surface work function, and thermal characteristics) are specified, the equations of the model as summarized in Chapter V can predict cathode operating conditions such as insert temperature and plasma potential. The experiment described above provides a good opportunity to compare measured operating conditions with the predictions of the model. Calculations using the model were performed based on the following considerations.

1. The measured pressures were used as input to the model rather than the mass flow rate. Equation IV.1 could have been used to determine the pressure from the flow rate and orifice diameter, but in this case it underestimates the pressure by about 20%. A probable explanation for this discrepancy is that the effective diameter of the tantalum, foil-lined orifice was slightly smaller during operation than its measured diameter when cold. A small error in the orifice diameter results in a large error in pressure because it appears in Eq. IV.1 as an inverse square.
2. The surface work function ϕ_s for the insert was not known. The value used in the calculation was arbitrarily chosen as 1.94 eV to give agreement between the measured and the calculated temperature

at the operating conditions where I_D is 3.3 A, and $\dot{m}$ is 100 mA. The comparison between calculated and measured temperatures will, therefore, be a relative one valid mainly for checking the functional dependence on discharge current and pressure predicted by the model.

3. The thermal power loss used for the calculations was taken from the dashed curve of Fig. B.1 in Appendix B.
4. The electron temperature was assumed to be 0.71 eV.
5. The ratio of emission length to mean free path L_e/λ_{pr} was assumed to be two.
6. Because Eq. IV.10 cannot be solved explicitly for the surface temperature T_s, the equations in the model were solved in an iterative manner.

The results of calculations using the model based on the assumptions discussed above are shown in Figs. 16 through 18. Figures 16a and 16b show the effect of discharge current and pressure on the emission temperatures predicted by the model based on the assumed average surface work function of 1.94 eV. It should be recalled here that agreement with the experimental temperature at a current of 3.3A was assured by selecting a value of 1.94 for ϕ_s. The significant feature of Fig. 16a, therefore, is that the model accurately predicts the effect of discharge current on the emission temperature.

Such good agreement is not obtained for the effect of pressure on the emission temperature. Fig. 16b shows emission temperatures plotted as a function of pressure for a discharge current of 3.3 A. Unfortunately, at the pressure conditions indicated by the solid circles, insert temperatures were not measured because the original

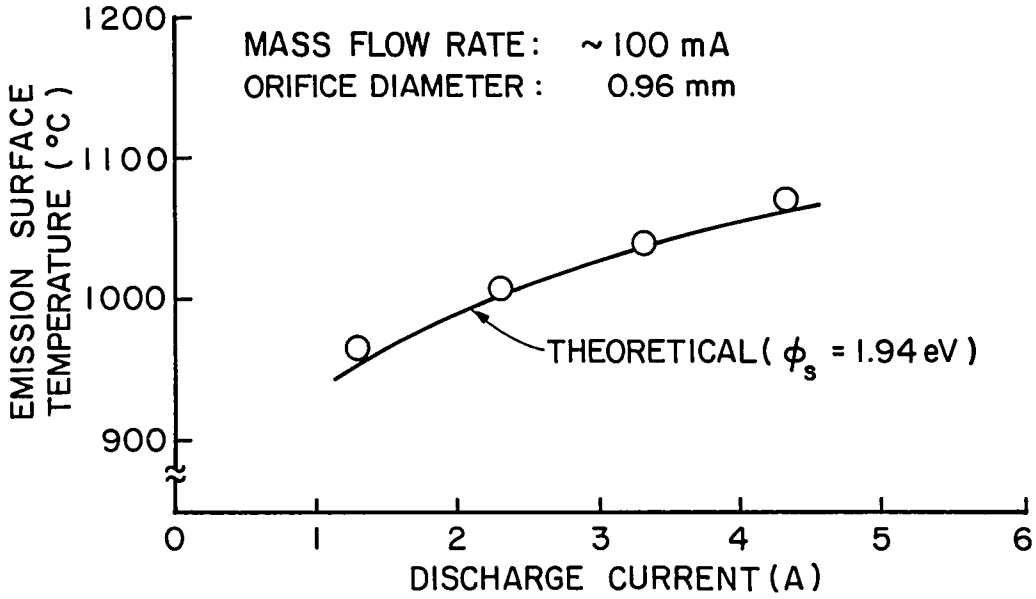

Figure 16a. Effect of Discharge Current on Calculated and Measured Emission Surface Temperatures

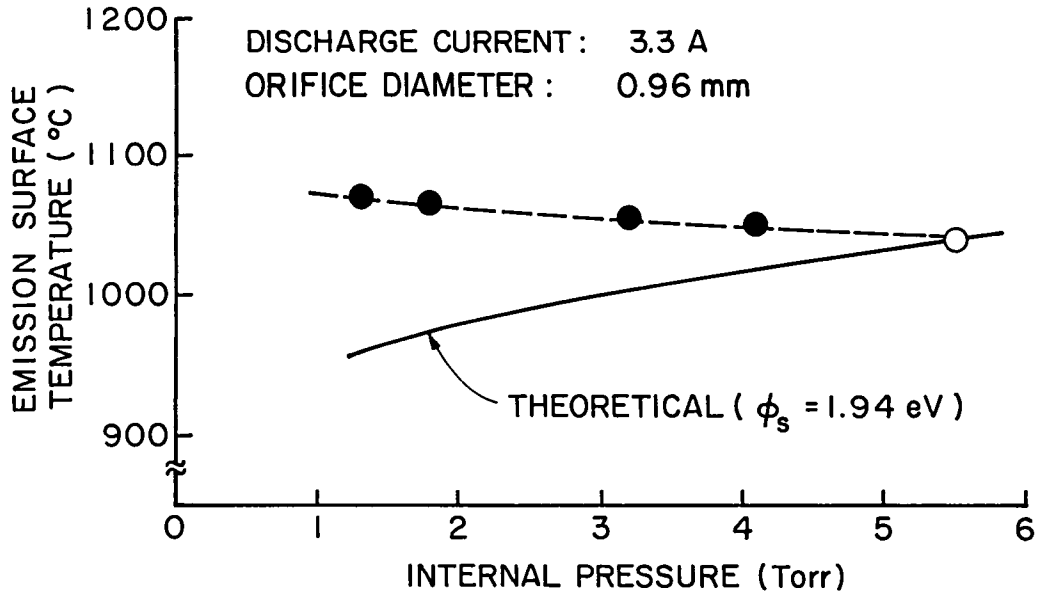

Figure 16b. Effect of Internal Pressure on Calculated and Measured Emission Surface Temperatures

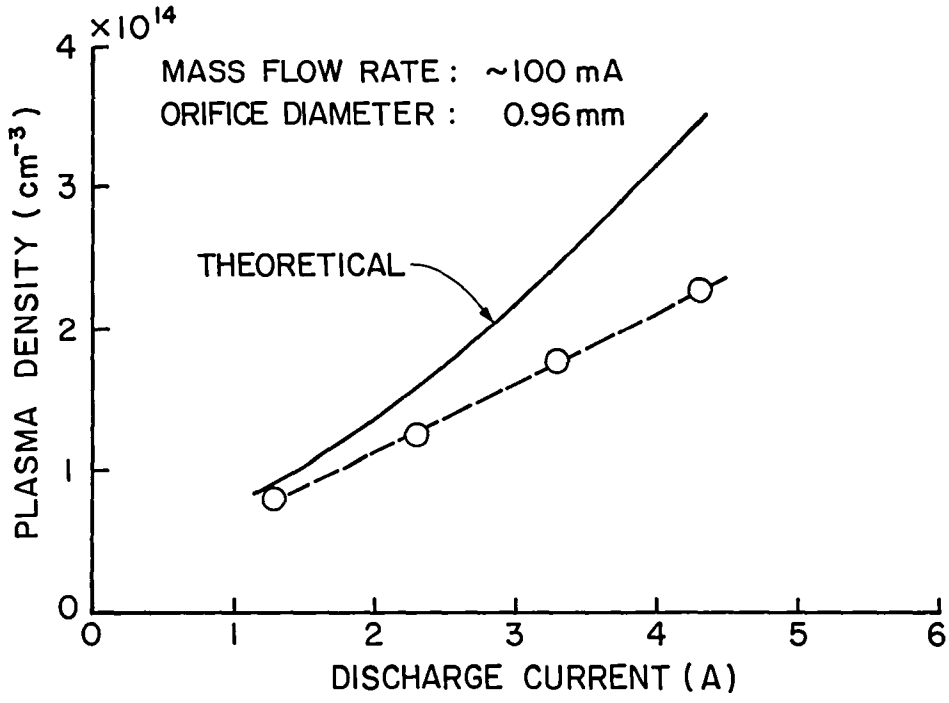

Figure 17a. Effect of Discharge Current on Calculated and Measured Plasma Densities

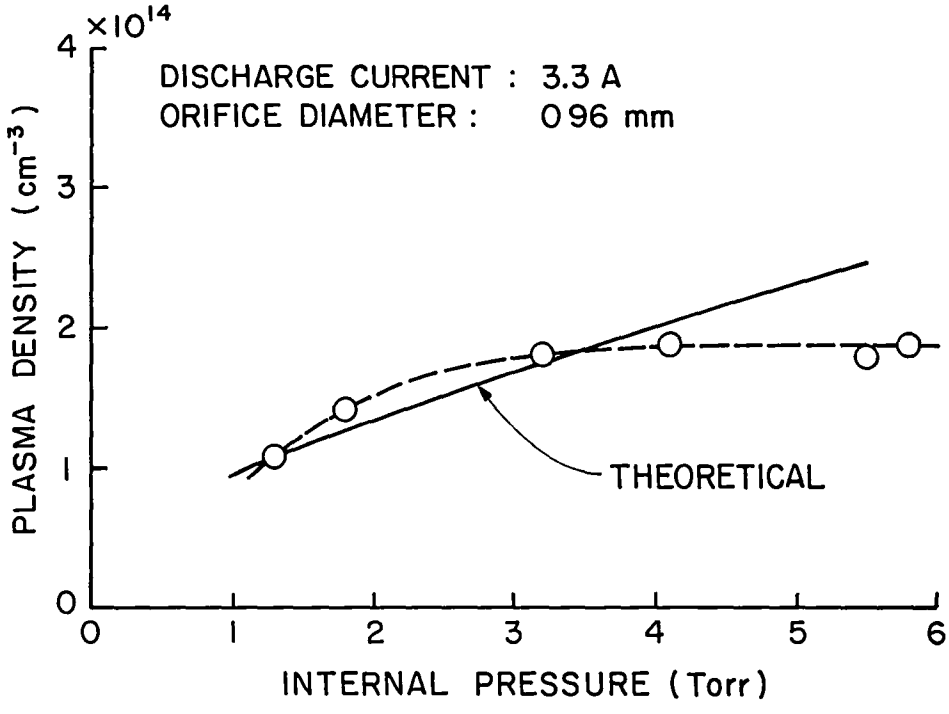

Figure 17b. Effect of Internal Pressure on Calculated and Measured Plasma Densities

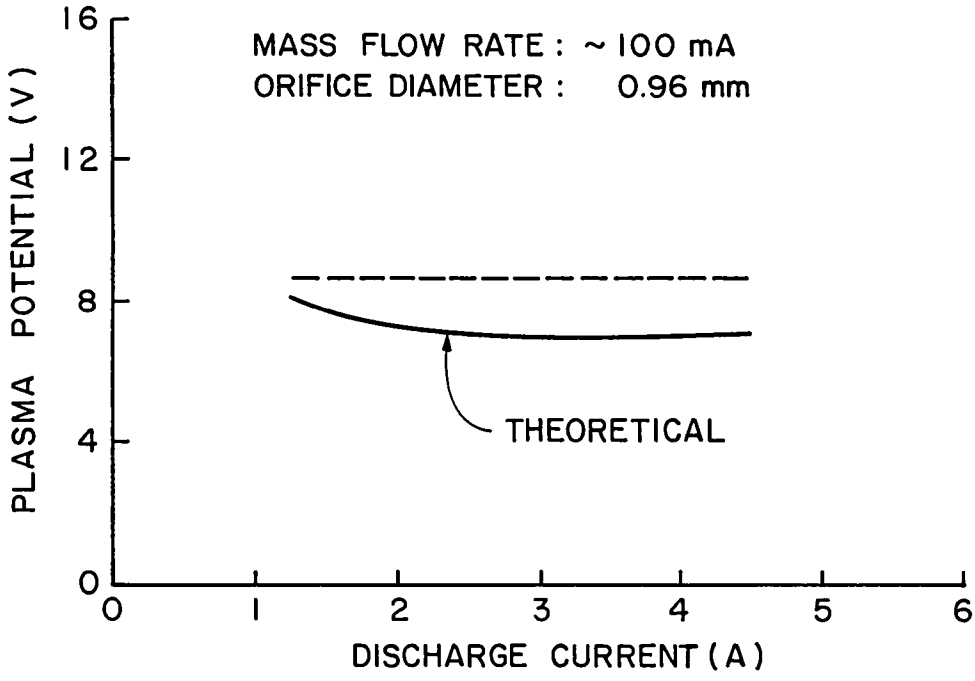

Figure 18a. Effect of Discharge Current on Calculated and Measured Plasma Potentials

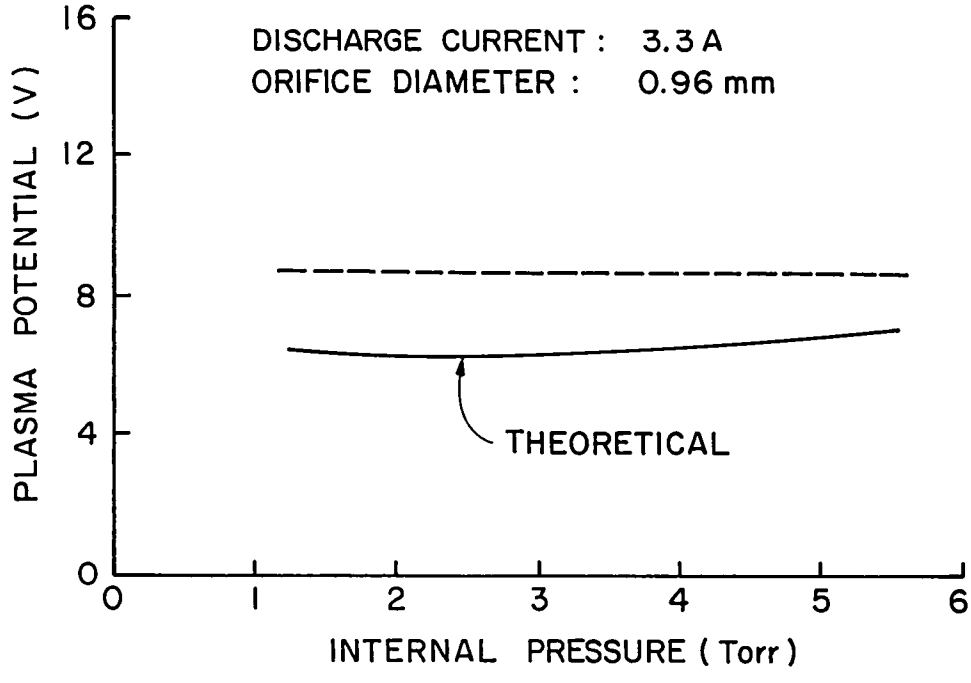

Figure 18b. Fffect of Internal Pressure on Calculated and Measured Plasma Potentials

objective of the experiment required only measurement of the cathode currents. The data indicated by the solid symbols were, therefore, estimated using the results of Fig. 4c which showed that for a cathode of similar construction operating at a discharge current of 3.3A the maximum insert temperature decreased with internal pressure by ~ $7^{o}C$ per Torr. However, it is believed that this estimate is reasonably reliable, so it would not account for the differences between the two curves in Fig. 16b. The main reason for the differences between the two curves is that the temperatures indicated by the circles are the maximum emission temperature while the calculated temperatures (solid curve) are average values based on the assumption of uniform emission over the entire emitting length. The calculated emission temperature increases with internal pressure because the emission length L_e and, therefore, the emission surface area predicted by the model decreases as the pressure is increased. While for short emission lengths, the uniform emission assumption is probably valid, the assumption apparently breaks down as the length of the emission region increases. This suggests that, for low pressures, emission temperature gradients become important and the simple, lumped parameter model does not provide an accurate description of the emission temperature.

The ion production region plasma density predicted by the model is plotted in Fig. 17a as a function of discharge current (solid curve). For comparison, the plasma densities n_3 adjacent to the upstream side of the orifice plate are plotted as the circles. These data points (n_3) were estimated from the measured current I_3 based on the Bohm criterion and are repeated here from Table VII and Fig. 4a. They represent the average plasma density adjacent to the downstream boundary of the ion

production region. Plasma densities are shown in Fig. 17b plotted as a function of internal pressure for a discharge current of 3.3A. In both cases (Figs. 17a and 17b), the agreement between experimental values and those predicted by the model is reasonably good although in Fig. 17b the curve shapes for the measured and calculated values are different. This difference may be attributable, at least partially, to the assumption in the model of a uniform ion production region. This assumption is expected to hold best for operation at conditions where the primary electron mean free path is on the order of the insert radius. As the internal pressure is increased beyond this point (a few Torr), the primary electrons have a lower probability of reaching the centerline of the cathode, so that ion production is increasingly confined to an annular region bounded by the emission surface (as opposed to the assumed cylindrical volume). Such a reduction in volume could account for the fact that the average measured values of the plasma density adjacent to the orifice plate are nearly constant for pressures above a few Torr (Fig. 17b).

The fraction of the total discharge current that is due to volume processes depends mainly on the plasma density. For the plasma densities predicted by the model this fraction ranged from 0.30 to 0.34. This is in good agreement with the values in column 5 of Table VII which were based on measured currents.

Finally, the plasma potential predictions of the model are shown in Figs. 18a and 18b where they are plotted, respectively, as a function of discharge current at a constant mass flow rate (~100 A), and as a function of internal pressure at a constant discharge current (3.3A). The plasma potential was not measured in this experiment so the average

value of 8.7V determined from Langmuir probe measurements for a cathode operating under similar conditions is indicated in the figures as a dashed line. The value is shown as a constant (horizontal line) because the probe measurements showed no clear correlation of the plasma potential in the ion production region with either current or pressure.

It should be recalled that the plasma potential prediction is based on the energy balance for the ion production region and neglects the energy lost from the region due to the the flux of excited atoms. Including the excited state power term would increase the predicted plasma potential by 8 to 10 volts in most cases. In view of this, the results shown in Fig. 18 indicate that the model predicts plasma potentials of approximately the right magnitude when the excited state power term is neglected but, as suggested in Chapter III, would provide better agreement if a power which is 20 to 30% of the calculated excited state power were included.

The energy balance used for predicting the plasma potential is useful from the standpoint of a qualitative understanding of the important internal physical processes, but is not very useful for accurately predicting the plasma potential. It is, therefore, suggested that, since the measured plasma potential does not vary much from its average value of 8.7V, that this experimentally determined value should be used when making calculations with the model.

In summary, for a cathode operating on mercury, the model represented by the equations of Table IV (Ch. V) provides reasonably accurate predictions of emission length, emission surface temperature, plasma density and fraction of discharge current due to volume ionization, particularly at pressures above the critical pressure of a

few Torr. It will be worth reviewing at this point the important assumptions which went into the model used for making these predictions. The model assumed that plasma properties and surface temperatures were uniform throughout the ion production region and that the region was two primary energy exchange mean free paths in length. It neglected the energy loss associated with the thermal flux of excited state atoms across the boundary of the region and assumed a value of 0.71 eV for the electron temperature. In addition to the above assumptions, the comparison with experimental results suggested that when applying the model to cathodes operating on mercury that a plasma potential of 8.7 V should be assumed for the ion production region. Finally, the model is believed to be most accurate for conditions where the primary electron mean free path is on the order of the insert radius. Such an operating conditon is expected to result in relatively uniform plasma properties in the ion production region in addition to providing efficient cathode operation.

The Orifice Region

Though the main thrust of this paper is the model and experimental results dealing with the internal cathode processes, the experiments have also produced some interesting results providing insight into processes taking place in the orifice region. Processes taking place in that region are important to cathode operation because they provide the link between the internal discharge and the downstream anode collection region. The results of Fig. 14 are particularly interesting because they suggest that the plasma in the orifice may be somehow separated from the internal discharge. This can be seen by examining the curves

for the plasma density within the orifice region (n_4, triangles). These curves display a different dependence on the emission current and internal pressure than do the curves for the densities in the ion production region adjacent to the insert (n_2, n_3).

Two other experiments were performed which also suggested that the plasma processes in the orifice region are somewhat independent of the internal discharge. One experiment involved moving the insert back ~ 2mm from the orifice plate and examining the effect on local plasma densities. This experiment showed that while moving the insert back decreased the plasma density adjacent to the upstream side of the orifice plate by a factor of four it hardly affected the density in the orifice canal. The plasma density adjacent to the insert was also unaffected by the upstream movement of the insert. The other experiment involved biasing the upstream surface of the orifice plate (surface #3) as an anode to collect all of the emission current. In this case, not driving the emission current through the orifice bore decreased the discharge voltage by ~2.5V from what it was when the current was collected on the downstream side of the orifice (surface #4). The internal cathode pressure was also reduced by almost a half. These experiments and their results are discussed in more detail in Reference [31] but are mentioned briefly here because they help to explain a couple of important aspects of cathode operation.

In both of the experiments discussed above, the results suggest that the internal discharge may be separated from the plasma in the orifice region by the double sheath which normally forms just upstream of a discharge constriction such as the orifice [32]. A sheath of this kind is characterized by a potential drop which provides to electrons

crossing the sheath sufficient energy to form an ion production region within the constriction, in this case the orifice canal. The resulting increased plasma density in the orifice region is essential for maintaining current continuity in the presence of the large change in cross sectional area of the conduction path. Since the experimental results indicate that the orifice walls are not emitting thermionically, the higher electron densities found in the orifice region (n_4, Figs. 14a and 14b) are considered evidence of the presence of such a double sheath.

These experimental results also help to explain the effect of the orifice on the overall discharge voltage. It is ultimately the discharge voltage, not the internal plasma potential, which is of interest from the standpoint of cathode design and performance. The discharge voltage drop is made up of three components: 1) the potential drop across the cathode sheath, indicated by the plasma potential in the ion production region, 2) the potential drop across the orifice, and 3) the potential drop occurring between the orifice and the anode. The last is highly dependent on downstream conditions such as background pressure, anode surface area, and the presence of magnetic fields. It is, therefore, very application specific and will not be discussed here. The plasma potential in the ion production region was shown to be normally ~8.7 volts. This value was seen to be fairly constant and probably reflects the large excitation cross-sections for mercury near this voltage. As for the orifice, there are believed to be two processes which contribute to the potential drop in that region. One is the double sheath which is believed to form at the orifice upstream boundary. The other is the ohmic drop associated with the

plasma conductivity in the orifice. The double sheath analysis [33] is quite sensitive to the relative magnitudes of the plasma densities in the ion production region and within the orifice. This makes a reasonable estimate of the potential drop associated with the double sheath difficult. On the other hand, a reasonable estimate can be obtained for the ohmic potential drop across the orifice. The ionization fraction in the orifice region is sufficiently large that the conductivity can be estimated using Spitzer's formula [34]:

$$\sigma = \frac{T_e^{3/2}}{65.3 \ \ln\Lambda} \qquad \text{(mho/m)} \tag{45}$$

where T_e is the electron temperature in the orifice in ^oK and $\ln \Lambda$ is the coulomb logarithm. The value of $\ln \Lambda$ is a weak function of the electron density so that the conductivity is virtually independent of the electron density. For plasma conditions typical of the hollow cathode, $\ln \Lambda$ is ~6. In one dimension, Ohm's law is

$$j = \sigma E = -\sigma \frac{dV}{dx} \tag{46}$$

and the potential drop across the orifice can be estimated as

$$\begin{aligned} \Delta V &= \frac{1}{\sigma} t \\ &= \frac{65.3 (\ln\Lambda) t \ I_D}{T_e^{3/2} A_o} \end{aligned} \tag{47}$$

where t is the orifice plate thickness and A_o is the cross-sectional area of the orifice, I_D is the discharge current, and T_e is the electron temperature in the orifice region in ^oK. The electron temperature in the orifice region can be estimated from the voltage-current

characteristic for the orifice surface (Fig. 13, solid curve) and was found to be 0.86 eV at a discharge current of 3.3A. The orifice diameter and length were respectively 0.96 mm and 1.8 mm. Using Eq. 47 these conditions result in a potential drop across the orifice of 3.2V, which is in fair agreement with the experimental value of ~2.5V discussed above.

It is worth noting that Eq. 47 is in qualitative agreement with cathode design experience which has shown that the operating voltages increase with increasing orifice length and decreasing orifice diameter. It is also significant that the plasma conductivity is proportional to $T_e^{3/2}$. This indicates that small changes in electron temperature should have a significant affect on the operating voltage. Since the double sheath, if it exists, would control the acceleration of electrons into the orifice, it could have a significant effect on the electron temperature in the orifice and, thereby, on the discharge voltage. However, the fact that the ohmic drop can account for the observed potential drop across the orifice would suggest that the potential drop across the double sheath may be rather small.

The experiment described above in which the internal pressure was reduced by one half when the discharge was collected at the upstream side of the orifice helps to explain the pressure-flow rate results (Fig. 6) of Chapter II. Those results showed that for a given mass flow rate, the cathode pressure increased substantially with discharge current. This increase is certainly due in part to the plasma heating upstream of the orifice region, but cannot be accounted for entirely on that basis. Electric field effects on the ions also appear to contribute to the pressure increase. Because of the electric fields,

the ions produced in the orifice region migrate to the orifice walls or in the upstream direction but cannot readily travel downstream except as propelled by collisions. The effect of this on the pressure is twofold. First, ions created in the orifice and returning to the interior of the cathode represent a net flux of atoms upstream which does not occur in the absence of the discharge. This flux of ions has the same effect as increasing the mass flow rate because the same net mass flux through the orifice now requires a greater flow of neutral atoms downstream across the orifice plane. In other words, some of the neutral atoms which entered the orifice and would normally pass through are ionized and then accelerated back upstream. This motion of ions in the upstream direction is also the basis for the second effect on the pressure. This effect is related to collisions. The orifice region is highly collisional because of the high particle densities. As ions produced in the orifice move upstream under the influence of the electric field there, they have collisions which transfer their momentum in the upstream direction to the neutral atoms which are trying to exit the cathode. This represents an effective collisional drag force. Based on plasma conditions in the orifice, rough estimates were made for the magnitude of both of these effects. The calculations indicated, that together with plasma heating, the effects could easily account for the pressure increases observed when the discharge current is increased.

VII. CONCLUSIONS

A phenomenological model has been presented which describes the physical processes underlying the operation of mercury orificed hollow cathodes of the type used in ion thrusters. That this descriptive model is in good qualitative agreement with the experimental results indicates that our basic understanding of the important physical processes for these devices is essentially correct. Further, by assuming an idealized ion production region within which most of the plasma processes are concentrated, this phenomenological model has been expressed analytically as a simple set of equations which relate cathode dimensions and specifiable operating conditions, such as mass flow rate and discharge current, to such important parameters as insert temperature and plasma properties. A comparison between the results calculated using this model and the experimental results described in this study has lead to the following conclusions.

1. Approximately 70% of the cathode discharge current is due to surface emission of free electrons from a localized region on the downstream end of of the insert. The dominant surface emission process is field-enhanced thermionic emission which is estimated to account for more than 97% of the surface emitted electrons. Volume ionization of mercury vapor accounts for ~30% of the total discharge current.
2. Because of the low primary energies and low electron temperatures the volume ionization process in the cathode is a multi-step

process in which ions are produced predominately from intermediate metastable and resonnance state atoms.

3. The ion production region in the cathode is adjacent to the emitting region of the insert where the primary (surface emitted) electrons are produced. Its length is approximately two primary electron mean free paths, where the mean free path is that for energy exchange due to both inelastic and elastic collisions. The mean free path is easily determined using the simple relation given in Eq. IV.3.

4. The plasma density and plasma potential in the ion production region determine the emission surface temperatures by their effect on the energy input to the surface from the plasma. One energy balance on the emission surface and another energy balance on the control volume, represented by the ion production region defined in the model, are used to estimate these two plasma properties. The best agreement between measured and calculated values of the plasma density and plasma potential is obtained when the energy transport associated with the excited atomic states are not included in the energy balances. However, the results indicate that the true situation is one in which the excited state energy flux is probably significant but is considerably over estimated based on the assumptions made in the present model. Based on these results it is concluded that using the emission surface energy balance and neglecting the excited state energy flux allows a reasonable estimate of the plasma density and emission surface temperature, while the plasma potential is better taken as its average measured

value of 8.7V. This value of plasma potential was found to hold within ± 0.5V over a wide range of operating conditions.

5. No provision is made in the model for calculation of the electron temperature. However, the calculations in the model are not very sensitive to this parameter and, like the plasma potential, its measured value is rather constant over the normal range of operating conditions. Based on the experimental results, a reasonable value for the electron temperature in the ion production region of mercury hollow cathodes is the average measured value of 0.71 ± 0.1 eV.

6. The model predicts emission surface temperatures which are believed to be reasonably accurate and show excellent agreement with measured values in their functional dependence on the total discharge current.

7. The primary function of the cathode orifice is to restrict the propellant flow to a moderate value, while at the same time maintaining a relatively high neutral density (a few times 10^{16} cm^{-3}) in the ion production region and providing an electron conduction path between that region and the downstream anode.

8. The total neutral density within the cathode is an important parameter because it affects the primary electron mean free path and, thereby, affects the length of the emission region and the ion production region. Based on a correlation of results from the measurement of internal cathode pressures, the total neutral density can be estimated for a given orifice diameter, mass flow rate, and discharge current from the simple empirical relationship given in Eq. IV.1.

9. The overall discharge voltage drop is the sum of the plasma potential in the ion production region, the potential drop across the orifice, and the potential drop between the orifice and the anode. As noted above, the experimental results indicate an internal plasma potential of ~8.7 eV. The potential drop across the orifice is determined experimentally to be on the order of a few volts and can be estimated from the ohmic drop across the orifice region. The matter of the potential drop between the orifice and the anode has not been addressed in the present study.

The analytical model presented here should be a useful tool for designing new hollow cathodes and improving the design of existing cathode configurations. Probably more important, however, than the estimates of cathode operating parameters that can be obtained with the simple analytical model, is the physical understanding of critical cathode processes that is reflected by the general agreement between the phenomenological model and the results of the experimental portion of this investigation.

Future Work

Currently, there is considerable interest in the development of ion thrusters which operate on an inert gas such as argon. The present study has dealt specifically with cathodes which use mercury vapor as the propellant gas. The analytical model presented here can easily be extended to cathodes operating on other propellants such as argon or other inert gases by simply using the appropriate values for parameters such as atomic mass and collision cross-sections. However, the applicability of this extension of the model to cathodes operating on other propellants needs to be checked experimentally. Of particular

interest would be an experimental determination of the location and extent of the emission region, and the dependence of these on mass flow rate and discharge current for the propellants of interest. In addition, a determination for these propellants of the ratio of volume to surface production of electrons and of the extent to which field-enhanced thermionic emission contributes to the surface emission process is a matter of critical importance to applying the present model to other propellants. Measurements of the internal plasma properties would also be of interest to determine if the plasma potential and electron temperature are relatively constant over a wide range of operating conditions as they were for operation with mercury.

One factor which was not included in the present investigation was the effect of insert diameter on cathode operating parameters. In the development of the present model, it was suggested that for efficient operation the insert diameter should be on the order of the primary electron mean free path. In addition, the experimental results indicated that the model will be most accurate when this condition holds, because such a condition is expected to result in relatively uniform plasma properties in the ion production region, a basic assumption of the model. The insert diameter is obviously an important parameter and the effect of varying it should be investigated in future studies.

Another area that has not been addressed here is that of plasma processes taking place downstream of the orifice, between the orifice and the anode. An earlier investigation [7] indicated that conditions in that region, such as background pressure and anode configuration/spacing are important in determining the overall discharge

voltage and strongly affect whether the cathode operates in the so called plume or spot discharge mode. Understanding of the processes taking place in the region downstream of the orifice and the interaction of the cathode with these processes is of considerable interest and could easily be the goal of a separate investigation.

REFERENCES

1. Krishnan, M., Jahn R. G., von Jaskowsky, W. F., and Clark, K. E., "Physical Processes in Hollow Cathodes," AIAA Journal, Vol. 15, No. 9, Sept. 1977, pp 1217-1223.

2. Delcroix, J. I. and Trindade, A. R., "Hollow Cathode Arcs," Advances in Electronics and Electron Physics, Vol. 35, ed. L. Marton, Academic Press, New York, 1974, p. 158.

3. Ernstene, M. P., James, E. L., Purmal, G. W., and Worlock, R. M, "Surface Ionization Engine Development, "J. Spacecraft and Rockets, Vol. 3, No. 5, May 1966, pp. 744-747.

4. Hall, D. F., Kemp, R. F., Shelton, H., "Mercury Discharge Devices and Technology," AIAA Paper no. 67-669, Sept. 11-13, 1967.

5. Fearn, D. G. and Philip, C. M., "An Investigation of Physical Processes in a Hollow Cathode Discharge," AIAA Paper No. 72-416, April 17-18, 1972.

6. Rawlin, V. K., and Kerslake, W. R., "Durability of the SERT II Hollow Cathode and Future Applications of Hollow Cathodes," NASA TM X-52532, 1969.

7. Siegfried, D. E. and Wilbur, P. J., "An Investigation of Mercury Hollow Cathode Phenomena," AIAA Paper No. 78-705, April 25-27, 1978.

8. Wilbur, P. J., "Visual Observations of the Interior of an Operating Hollow Cathode," appears in "15 CM Mercury Ion Thruster Research - 1975," NASA CR-134905, December 1975.

9. Siegfried, D. E. and Wilbur, P. J., "Studies on an Experimental Quartz Tube Hollow Cathode," AIAA Paper No. 79-2056, Oct., 1979.

10. Groh, K. H., and Walther, S. E., "Operation Modes of Hollow Cathode Arcs with Reduced Gas Flow," Journal de Physique, Vol. 40, No. C-7, July 1979.

11. Bessling, H., "Theorie de Hochtemperatur-Hohlkathode, ein Modell fur den Kathodenmechanismus," DFVLR Report DLR-FB 76-50, Stuttgart, West Germany, 1976.

12. Brunet, A., "Experimental Study of the Interior of the Cathode of a Hollow Cathode Arc," Proc. of 4th International Conference on Gas Discharges, Swansea, Wales, Sept. 7-10, 1976.

13. Ferreira, C. M. and Delcroix, J. L., "Theory of the Hollow Cathode Arc," Journal of Applied Physics, Vol. 49, No. 4, April 1978, pp. 2380-2395.

14. Fomenko, V. S., Handbook of Thermionic Properties, Plenum Press Data Division, New York, 1966.

15. Lidsky, L. M., Rothleder, S. D., Rose, D. J., Yoshikawa, S., Michelson, C. and Macken, Jr., R. J., "Highly Ionized Hollow Cathode Discharge," Journal of Applied Physics, Vol. 33, No. 8, August 1962.

16. Peters, R. R., "Double Ion Production in Mercury Thrusters," NASA CR-135019, April 1976.

17. Jahn, R. G., Physics of Electric Propulsion, McGraw-Hill, New York, 1968, Ch. 4.

18. Cobine, J. D., Gaseous Conductors: Theory and Engineering Applications, 1st ed., Dover Publications, Inc., New York, 1958, Chaps. 5,8,9.

19. Massey, H. S. W. and Burhop, E. H. S., Electronic and Ionic Impact Phenomena, Oxford at the Clarendon Press, London, 1956.

20. Coulliett, J. B., "The Diffusion of Metastable Atoms in Mercury Vapor," Physical Review, Vol. 32, Oct. 1928, pp. 636-648.

21. Porotnikov, A. A. and Rodnevich, B. B., "Average Electric Field at a Cathode," Sov. Phys. Tech. Phys., Vol. 21, No. 4, April 1976, pp. 525-526.

22. Prewett, P. D. and Allen, J. E., "The Double Sheath Associated with a Hot Cathode." Proc. R. Soc. Lond. A, Vol. 348, No. 1655, April 1976, pp. 435-446.

23. Fowler, R. H. and Nordheim, L. W., "Electron Emission in Intense Electric Fields," Proc. Roy. Soc. Lond. A, 119, 1928, p. 173.

24. Sommer, A. H., Photoemissive Materials, John Wiley and Sons, Inc., New York, 1968.

25. Rockwood, S. D., "Elastic and Inelastic Cross Sections for Electron-Hg Scattering from Hg Transport Data," Phys. Rev. A., Vol. 8, No. 5, Nov. 1973, pp. 2348-2358.

26. Mitchell, A. C. G., Resonance Radiation and Excited Atoms, Cambridge at the University Press, London, 1961.

27. von Engel, A., Ionized Gases, 2nd ed., Oxford at the Clarendon Press, London, 1965.

28. Abroyan, A., Eremeev, M. A., and Petrov, N. N., "Excitation of Electrons in Solids by Relatively Slow Atomic Particles," Soviet Physics USPEKHI, Vol. 10, No. 3, Nov.-Dec. 1967, pp. 332-367.

29. Sonkin, S. "The Action of Mercury Metastable Atoms on a Tungsten Surface," Phys. Rev., Vol. 43, May 15, 1933, pp. 788-803.

30. Hensley, E. B., "Thermionic Emission Constants and their Interpretation," Journal of Applied Physics, Vol. 32, No. 2, Feb. 1961, pp. 301-308.

31. Siegfried, D. E., "A Phenomoenological Model Describing Orificed Hollow Cathode Operation," appears in "Ion and Advanced Electric Thruster Research," P. J. wilbur, ed., NASA CR-165253, Dec. 1980.

32. Crawford, F. W. and Freestone, I. L., "The Double Sheath at a Discharge Constriction" Proceedings of the 6th International Conference of Ionization Phenomena in Gases, Paris, July 1963.

33. Levine, J. S. and Crawford, F. W., "A Fluid Description of Double-Layers," J. Plasma Physics, Vol. 28, No. 23, 1980, pp. 223-247.

34. Spitzer, L. Jr., Physics of Fully Ionized Gases, Interscience Publishers, 1972.

35. Huddlestone, R. H. and Leonard, S. L., Plasma Diagnostic Techniques, Academic Press Inc., New York, 1965, Ch. 4.

36. Waymouth, J. F., "Perturbation of a Plasma by a Probe," The Physics of Fluids, Vol. 7, No. 11, Nov. 1964, pp. 1843-1854.

37. Self, S. A. and Shih, C. H., "Theory and Measurements for Ion Collection by a Spherical Probe in a Collisional Plasma," The Physics of Fluids, Vol. 11, No. 7, July 1968, pp. 1532-1545.

38. Wehner, G., and Medicus, G., "Reliability of Probe Measurements in Hot Cathode Gas Diodes," Journal of Applied Physics, Vol. 23, No. 9, Sept. 1952, pp. 1035-1046.

39. Siegfried, D. E., "Plasma Probing in Orificed Hollow Cathodes," appears in "Advanced Space Propulsion Thruster Research," P. J. Wilbur, ed., NASA CR-165584, Dec. 1981.

APPENDIX A

Probe Analysis

In the early stages of this investigation, probe measurements made within the cathode were made using a cylindrical Langmuir probe with a very fine 0.076 mm diameter tungsten electrode [7]. This gave reasonably good results in regions where the plasma density was less than $10^{14}cm^{-3}$. However, in regions where the emission is taking place, which are of greatest interest, the plasma densities are greater than $10^{14}cm^{-3}$. Biasing the probe to plasma potential in the regions where the plasma density is very high causes the fine wire probe to burn up. In order to alleviate this problem, a technique using a spherical probe having a larger surface area and an analysis based on the ion saturation region of the probe trace was developed. (Details of the construction of the 0.75 mm diameter spherical probe used in the experiments are discussed in Chapter II. See Fig. 2c.) The large surface area of the spherical probe makes it sensitive to the ion saturation current over the wide range of plasma densities found inside the cathode. The ion saturation current is normally only a very small fraction ($\sim 10^{-5}$) of the electron saturation current so that the larger area is necessary to get a measurable signal in regions of low plasma density. Figure A.1 shows a sketch of a typical voltage-current characteristic for a Langmuir probe biased to a potential above plasma potential. For the experimental results reported in this investigation, the spherical probe was only biased to a potential just above floating potential and the

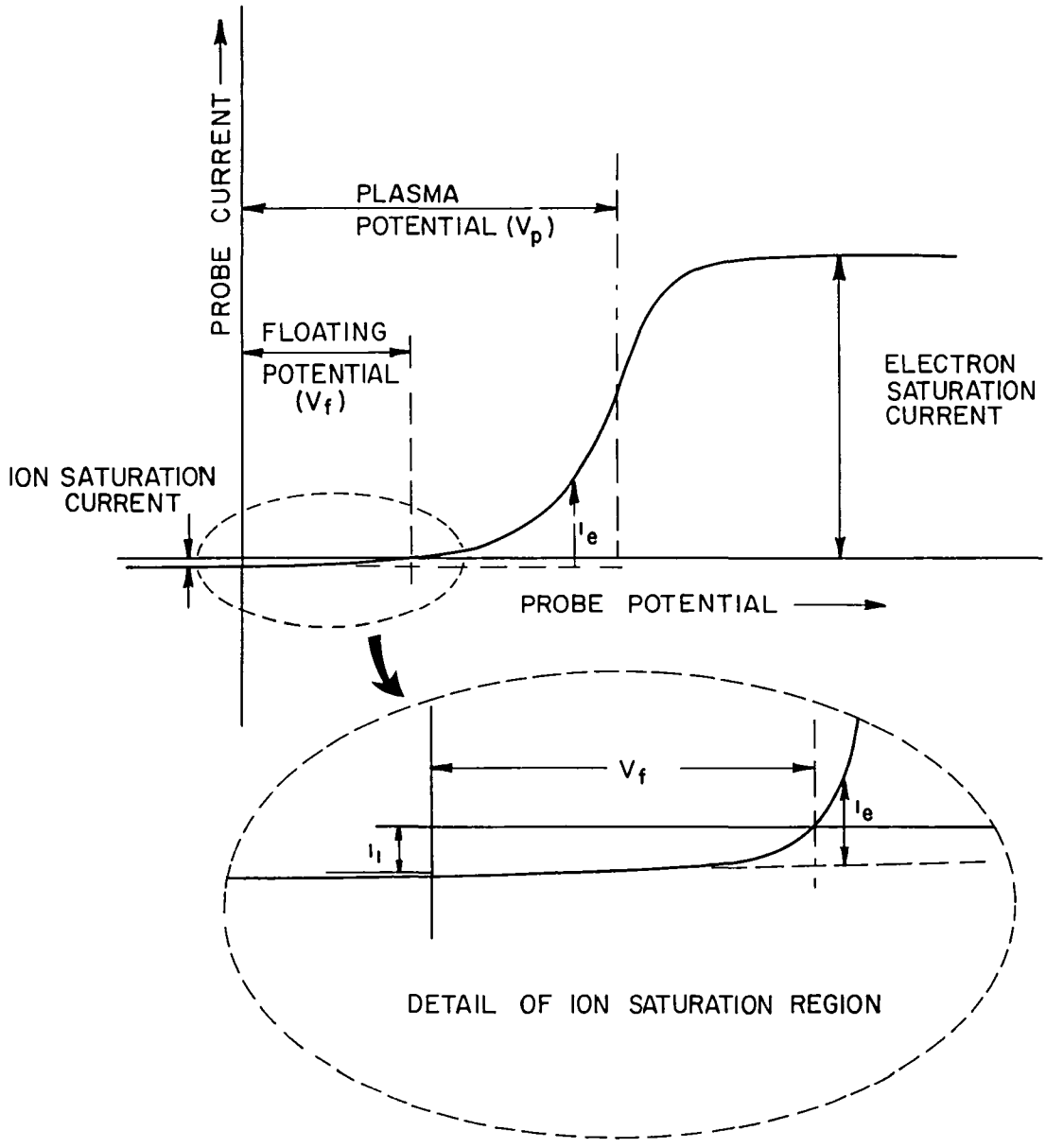

Figure A.1. Typical Langmuir Probe, Current-Voltage Characteristic

resulting trace of the ion saturation current (shown enlarged in the detail of Fig. A.1) was used to determine the plasma properties. Operation at floating potential or below has the additional advantage of causing less of a perturbation to the plasma than does the large electron current drawn to a probe at plasma potential. The use of the ion saturation region of the probe current-voltage characteristic requires a different method of analysis than does the usual Langmuir probe trace. A method for performing this analysis will be presented, but first it will be useful to discuss some considerations which affect the type of analysis used.

Previously, characteristics taken from probes inside of the hollow cathode have been analyzed based on Langmuir's theory [35]. This analysis applies in the limit where the sheath is collisionless and is thin with respect to probe size. This implies a low pressure, slightly ionized plasma. The hollow cathode plasma, however, is a relatively high pressure (a few Torr) plasma with a high plasma density (10^{11} to $10^{15}cm^{-3}$). Even though the pressure is high, it has been assumed in the past that because of the very thin Debye length (due to the high plasma density) the normal analysis could be applied with reasonable results. It still appears that this is the case, based on the argument contained in the following paragraphs.

The conditions found in the hollow cathode are such that, although the sheath is thin compared to the probe dimensions, the high neutral density within the cathode results in particle mean free paths which are of the same order as or smaller than the probe dimensions. This usually causes a presheath to be established between the bulk plasma and the sheath itself. In this presheath, particles approaching the probe

undergo numerous collisions. These collisions would normally result in significant gradients in the plasma density and plasma potential. When the presheath is present, the conventional Langmuir analysis is inaccurate in that it significantly underestimates both the plasma potential and the plasma density of the undisturbed bulk plasma. A survey of the literature has shown that there are a number of theories [36,37] which are available for analyzing the probe data in a situation where the sheath is thin and the high neutral density causes a significant presheath. In the case of the hollow cathode, however, the region surrounding the probe is also one in which the ion production rate is large compared to the rate of ion loss to the probe. Further, the probing technique being proposed here involves the use of only the ion saturation portion of the characteristic probe curve so that large electron currents are not drawn to the probe. Under these conditions, it is believed that the presheath plasma gradients discussed above cannot be established.

Under typical hollow cathode operating conditions it is estimated that the production rate of ions in a volume on the order of the presheath volume is considerably greater than the loss rate of ions to the probe. Where this is the case it is considered justifiable to assume that no significant plasma gradients can be sustained and the conventional thin sheath analysis can be applied. This is almost certainly the situation in the high plasma density (10^{13} to $10^{15}cm^{-3}$) region of the cathode where electron emission and ion production are concentrated. Upstream of this region where more moderate (10^{11} to $10^{13}cm^{-3}$) plasma densities are expected some intermediate situation probably occurs in which the ion production rate is not great enough to

compensate for the plasma gradients set up as ions diffuse to the probe. However, in order to standardize and simplify the analysis, and because the method of approach in the intermediate situation is uncertain, all of the probe results obtained inside of the hollow cathode were analyzed using the relatively simple, thin sheath, collisionless type of analysis.

Given the ion saturation portion of the probe characteristic shown in the detail of Fig. A.1, the analysis for the thin sheath probe in an unperturbed plasma (i.e. no presheath) is quite simple. First, the electron temperature is determined in the standard manner from the exponential portion of the trace. This is done by making a semilog plot of the electron current measured above the extrapolated ion saturation current (i_e shown in the detail of Fig. A.1) against probe potential. The electron temperature is then proportional to the inverse slope of this line. The plasma density is determined from the ion saturation current (i_i) based on the assumption that the ions enter the sheath with the Bohm velocity. This can be expressed as

$$n_e = \frac{i_i}{\alpha A_p e v_B} = \frac{i_i}{\alpha A_p e \left[\frac{kT_e}{m_i}\right]^{1/2}} \tag{A.1}$$

where A_p is the probe surface area, e is the electronic charge, k is Boltzmann's constant, T_e is the electron temperature, and m_i is the ion mass. The parameter α is dependent on the ratio of ion temperature to electron temperature and also on the size of the probe in relation to the extent of the plasma but usually as a value of ~0.6 [35] for small probes. Since the probe used here was relatively large compared to the

extent of the plasma, a value of 1.0, which is also the appropriate value for a plasma confining surface, was used for α. The plasma potential is estimated from the floating potential based on the condition that the ion and electron currents to the probe must be equal when the probe is floating. This leads to the following expression for the plasma potential [35]:

$$V_p = V_f - \left[\frac{kT_e}{e}\right] \ln \left[4\alpha \left[\frac{\pi m_e}{8m_i}\right]^{1/2}\right] \tag{A.2}$$

where V_f is the floating potential, m_e is the electron mass, and the rest of the symbols are as previously defined. The analysis described above is actually applicable to any non-emitting surface in contact with the plasma and was used for determining plasma properties from current-voltage characteristics like that shown in Fig. 13 of Chapter VI.

Probe Contamination

A common problem with probe traces taken in an oxide cathode environment is that the probe will be contaminated by the low work function compounds [38]. This can cause two problems: 1) the formation of resistive oxide coatings, and 2) a reduction in the probe work function. The resistive coatings cause a change in the shape of the characteristic, and thereby, give a false indication of the velocity distribution of the electrons in the plasma. The probe work function affects the position of the probe characteristic with respect to the reference potential and can, therefore, affect the value determined for the plasma potential. Because barium oxide compounds are used to reduce the surface work function in the hollow cathode, probe contamination was a concern. In order to minimize the effect of probe contamination,

probe circuitry was developed which incorporated a probe cleaning bias and allowed a rapid sweep of the probe potential. Preliminary tests using the circuitry showed that contamination could affect the probe traces if the traces were recorded slowly (5-10 seconds). However, by using the cleaning bias and then rapidly recording the probe traces, this effect was shown to be minimal. The rapid sweep circuitry with cleaning bias was, therefore, used for making the probe traces in the experiments reported here. Details of the design of the probe circuitry and of the preliminary tests mentioned above are discussed in Ref. [31].

The probe traces that were recorded using the spherical probe and the procedure described above indicated electron energy distributions within the cathode which appeared to deviate somewhat from a Maxwellian distribution. That is they did not plot as a straight line on a semilog plot. Extensive tests were performed to determine whether this was an inadequacy of the probing technique or if it was a true reflection of the electron energy distribution. The tests, which are discussed in detail in Ref. [31], did not indicate any obvious problem with the experimental procedure. Indeed, in the region adjacent to the insert, a non-Maxwellian population might even be expected due to the surface electron emission. However, for typical cathode conditions the density of primary or wall emitted electrons is estimated to be only ~0.2% of the Maxwellian population (see Appendix B) and is, therefore, difficult to detect. For this reason a computer program [39] using a numerical curve fitting technique was developed to fit the recorded data to a Maxwellian (exponential) plus mono-energetic (straight line) energy distribution. The results of this analysis did not show a clearly defined mono-energetic or primary population, although for a number of

conditions the curve fit indicated primary electron concentrations in the range 0.01 to 0.2%. The electron temperatures determined by separating out the primary portion of the electrons, determined with the curve fitting procedure were not very consistent. However, they also were not significantly different ±15% than temperatures determined by fitting the data to a purely Maxwellian distribution. The results reported here (Fig. 5c) were, therefore, based on the simple Maxwellian fit of the data.

APPENDIX B

Determination of the Primary Electron Inelastic Mean Free Path and Density

The primary electron energy exchange mean free path λ_{pr} can be easily calculated from the excited state densities which are the normal output of Peters' computer model for a mercury plasma discharge [16]. The calculation of the mean free path λ_{pr} is given by Eq. 6 which is repeated here

$$\lambda_{pr} = (1/\lambda_{In} + 1/\lambda_e)^{-1}. \tag{B.1}$$

The elastic mean free path for primary electrons λ_e can be calculated from the primary electron energy and Maxwellian electron density using Eq. 9. The inelastic mean free path λ_{In} is given by the following expression

$$\lambda_{In} = \frac{1}{\sum_j n_\alpha \sigma^j_{\alpha\beta}} \tag{B.2}$$

where $\sigma^j_{\alpha\beta}$ is the collision cross-section for production of excited state β from a target particle of type α having a density n_α. The summation in Eq. B.2 is over all of the possible reactions accounted for in the model. The collision cross-sections used in Eq. B.2 are easily determined from the tabulated rate factors in the data file of Peters' computer program simply by dividing the rate factor for the reaction by the velocity of of the primary electron. The calculation of λ_{pr}

described here was incorporated into Peters' computer program and the program was run for a wide range of input parameters typical of hollow cathode plasma conditions. The results of these computer calculations form the basis of Eq. 10 presented in Chapter III.

The excited state densities specific to the cathode conditions given in Table I were also used in the development of the cathode model. As discussed in Chapter III, the use of Peters' computer model to calculate these densities required an estimate of the primary electron density n_{pr}. The primary electron density is estimated by equating the production and loss rate of primaries, assuming that they are produced by acceleration of surface emitted electrons through the plasma sheath and are lost as soon as they have an energy exchange collision. The production rate P_{pr} is

$$P_{pr} = \frac{I_e}{eV} \tag{B.3}$$

where I_e is the current of surface emitted electrons and V is the ion production volume given by

$$V = \frac{\pi d_{in}^2 L_e}{4} \tag{B.4}$$

Here d_{in} is the insert inner diameter and L_e is the eission length of the insert. Assuming that primaries are lost only by collision (i.e, not lost through the orifice), the loss rate is the primary electron collision frequency ν_{pr} times the density of the primary electrons n_{pr}, or

$$R_{pr} = \nu_{pr} n_{pr}$$
$$= (n_{pr} v_{pr})/\lambda_{pr} \tag{B.5}$$

where v_{pr} is the velocity of the primary electrons. The density n_{pr} can be determined by combining Eqs. B.3, B.4, and B.5 to give

$$n_{pr} = \frac{4\ I_e \lambda_{pr}}{\pi d_{in}^2\ e\ L_e} \ . \tag{B.6}$$

Calculations based on Eq. B.6 result in typical values of the primary density which are on the order of a few tenths of a percent of the Maxwellian electron density. For example, assuming a value of two for the ratio of emission length to mean free path, the primary density for the set of typical cathode conditions of Table I is 3.4×10^{11} cm^{-3}, which represents a primary electron fraction of 0.0019. This small primary fraction is in qualitative agreement with the experimental results. While no clearly identifiable primary electron population was obtained in analyzing the Langmuir probe traces, the probe traces were found to be distorted from a Maxwellian distribution at energies near the expected primary energy. Such a distortion is consistent with the presence of a small population of essentially monoenergetic electrons having energies spread about the primary energy.

APPENDIX C

Thermal Power Loss from Emission Surface

The rate of heat transfer ($\dot{Q}_{th}$) away from the emitting portion of the insert due to conduction, convection and radiation is required for the energy balance calculations discussed in Chapter III. An accurate value for the power loss $\dot{Q}_{th}$ for the experimental cathode is not easily determined, although bounds can be placed on its value and a reasonable estimate can be made. A maximum value can be determined by assuming that end of the quartz inner bushing which holds the insert segment is at the same temperature as the segment (perfect thermal contact). The power loss is then calculated based on conduction down the quartz tube and radiation from its outer surface to ambient ($T_a \approx 25^{o}C$). The quartz tube would then be analogous to a cylindrical fin one end of which was at the insert temperature. The results of this analysis are plotted in Fig. C.1 as a function of insert temperature and are indicated by the upper curve. The minimum value of $\dot{Q}_{th}$ is calculated by assuming radiation from both outer and inner surfaces of the insert to surfaces at $700^{o}C$ and neglecting all losses due to conduction and convection from the insert. A temperature of $700^{o}C$ was selected because the adjacent surfaces - non-emitting portion of insert, start-up heater, etc. - were at a temperature less than the minimum temperature detectable with the optical pyrometer ($\sim 700^{o}C$). The minimum value for $\dot{Q}_{th}$ calculated in this way is plotted as the lower curve in Fig. C.1. Finally, a more probable value for $\dot{Q}_{th}$ is calculated by assuming direct

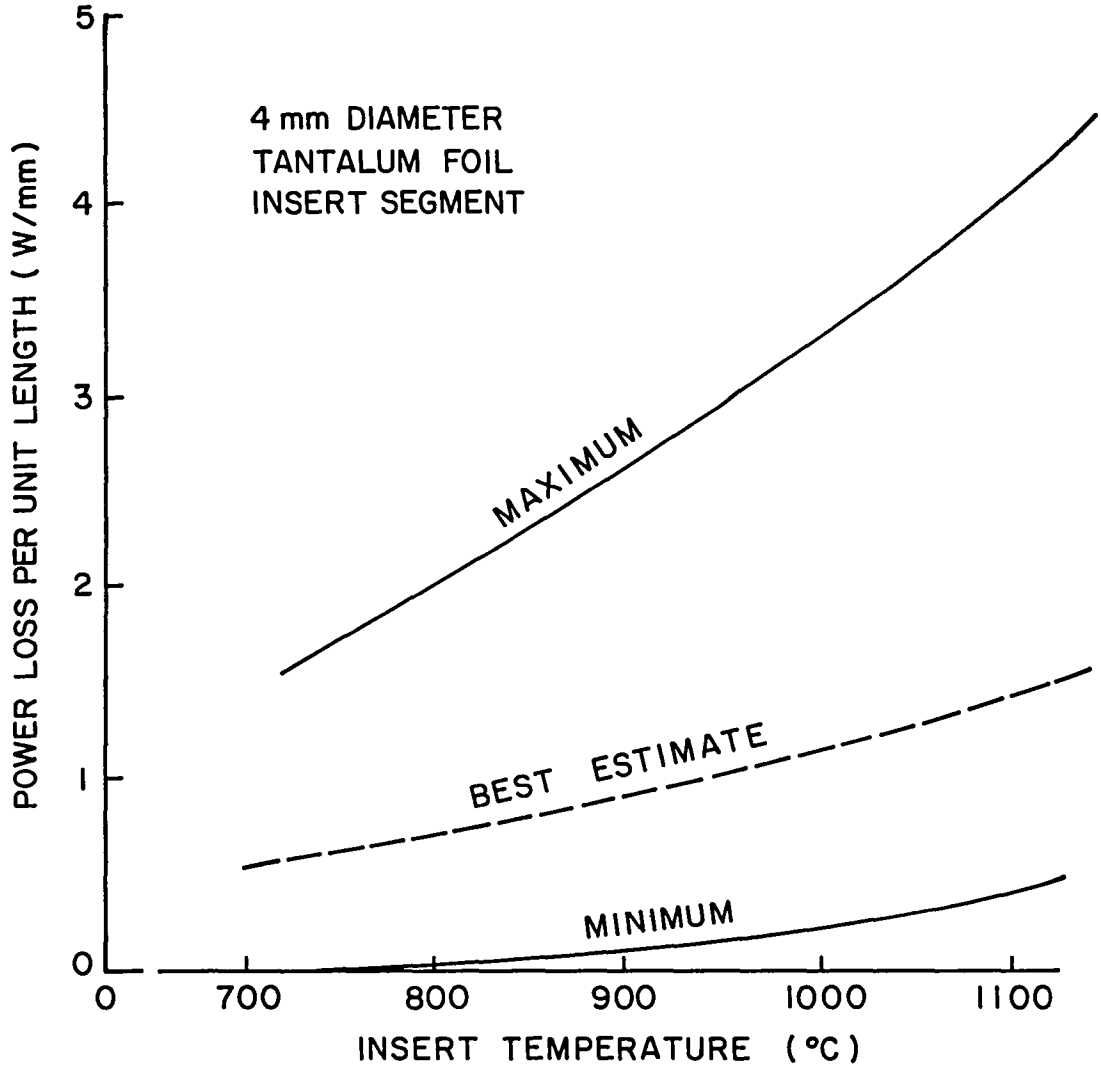

Figure C.1. Thermal Power Loss for Tantalum Foil Insert Segment

radiation from the insert in addition to some contact between the insert and the quartz bushing. The heat transfer between the insert and bushing is estimated to be due to a combination of direct contact and transfer via the intervening mercury vapor. The heat transferred to the bushing is then assumed to be conducted down its length and radiated from its median diameter to surfaces at $T_a \approx 25^{\circ}C$. The results of this analysis are plotted in Fig. C.1 as the dashed curve.

APPENDIX D

Determination of the Work Function of an Emitting Patch in a Hollow Cathode Insert

A small patch of tantalum foil isolated from and adjacent to a rolled foil, tantalum insert was connected to a power supply that could be used to bias the test patch (Fig. 10) with respect to the remainder of the insert and the orifice plate (both at cathode potential). Figure D.1 shows the characteristics of this patch for a typical test (#1 of Fig. 11) in the form of a plot of electron current to the patch vs. patch potential. At potentials above cathode potential, this figure shows that the patch behaves as a Langmuir probe operating in the ion saturation region of the probe current-voltage characteristic. The electron temperature of the plasma adjacent to the patch can be obtained in the normal manner from the exponential rise in collected electron current (I_{ce}) in this region of the probe trace. The ion saturation current ($I_p(i)$) and floating potential (V_f) can then be used to estimate the plasma density and plasma potential (See Appendix A). The emission portion of the trace (that portion at potentials below cathode potential) gives the electron emission current ($I_p(e)$) from the patch as a function of negative patch potential at various patch temperatures. The negative portion of the curve is obtained by reducing the patch voltage, measuring its temperature and then reducing the voltage again and repeating the procedure. Down to potentials of about -15v the curve looks relatively smooth. However, at about -20v (~1100°C)

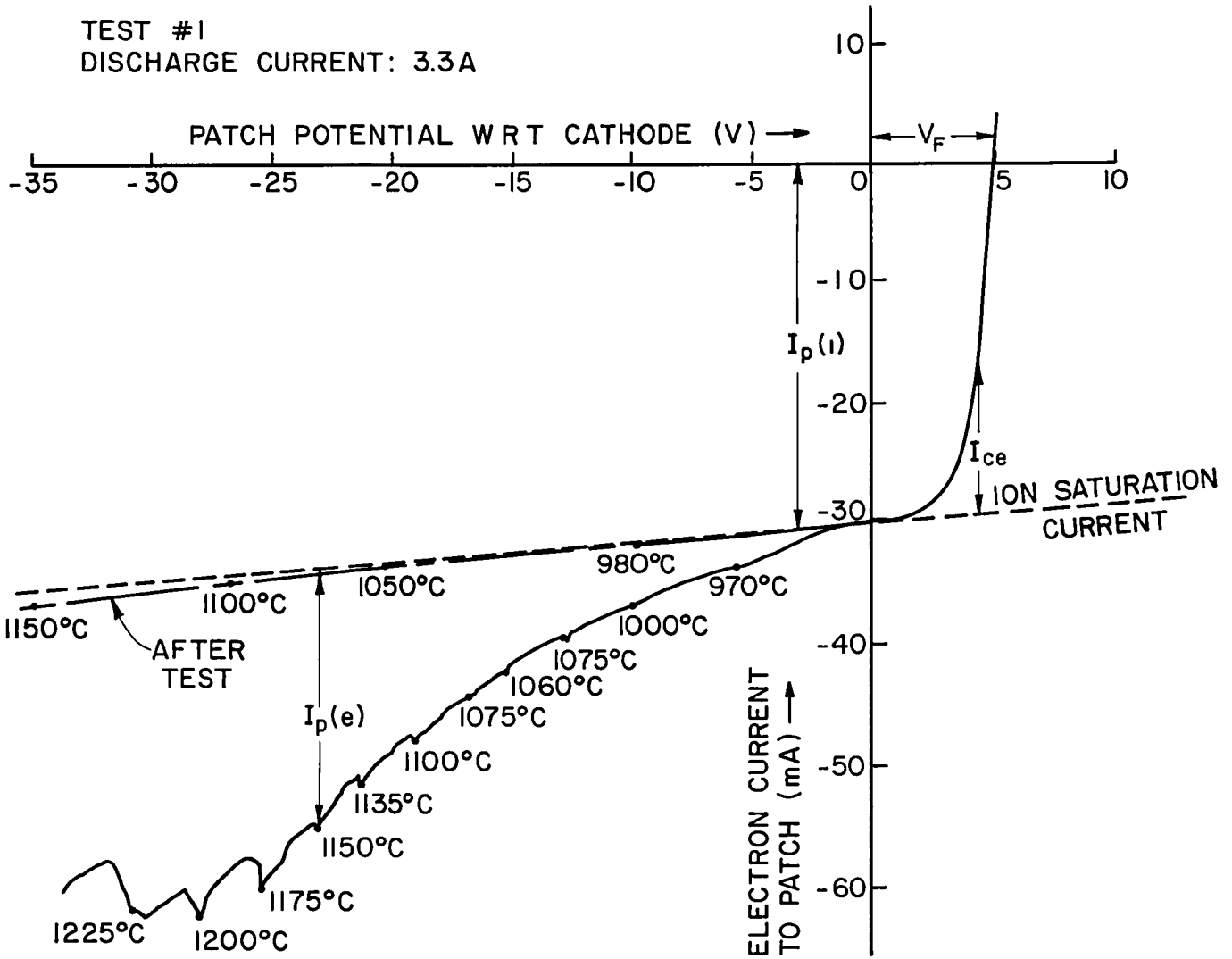

Figure D.1. Patch Current-Voltage Characteristic

irregularities in the curve appear and they become more pronounced as one goes to greater negative biases. These irregularities were introduced because of the procedure used in obtaining the data. This procedure involved slowly reducing the patch potential to a given voltage and then measuring the patch temperature. During the time interval when this temperature measurement was being made the insert was bombarded by ions which probably tended to drive off some of the barium on its surface. This caused the work function to increase, thereby, causing the emission current ($I_p(e)$) to decrease and the hump to appear on the I-V curve. A further reduction in the patch potential caused its temperature to increase and with it the associated electron emission. The cycle was then repeated and at the lower bias values the sizes of the humps became progressively larger. If one went back to zero bias and repeated the test, the positive bias portion of the curve was unchanged but the negative bias portion would be shifted upward (lower electron emission currents). After several tests a substantial amount of the barium would be driven off and the patch would exhibit the curve labelled "After Test" on Fig. D.1. The dotted "ion saturation" curve shown in Fig. D.1 is extrapolated from the cathode (zero) potential region of the characteristic. It represents the limiting current-voltage characteristic curve for the case of zero electron emission. It was found that when the patch became depleted of barium, as in the curve labelled "After Test" that it could be reactivated by heating the entire cathode to ~ 1250°C using the external heater. This reactivation was presumably caused by a redistribution of barium from other normally cooler, surfaces within the cathode. After reactivation, emission from the patch could be re-established, although usually at a

somewhat different level. Work functions were obtained from the data by using the plasma properties (obtained from the positive bias portion of the curve) together with the electron emission current ($I_p(e)$), the patch surface temperature, the patch surface area and the patch bias potential in the Schottky Equation for field-enhanced thermionic emission.

End of Document